The Damaging Nature of Extracellular RNA in Cardiovascular Diseases

Héctor Alejandro Cabrera Fuentes

INAUGURALDISSERTATION zur Erlangung des Grades eines
Doktors der Humanbiologie
des Fachbereichs Medizin der Justus-Liebig-Universität Gießen

édition scientifique
VVB LAUFERSWEILER VERLAG

1. Auflage 2014

1st Edition 2014

Printed in Germany

édition scientifique
VVB LAUFERSWEILER VERLAG

STAUFENBERGRING 15, D-35396 GIESSEN
Tel: 0641-5599888 Fax: 0641-5599890
email: redaktion@doktorverlag.de

www.doktorverlag.de

The Damaging Nature of Extracellular RNA in Cardiovascular Diseases

INAUGURALDISSERTATION

zur Erlangung des Grades eines Doktors der Humanbiologie

des Fachbereichs Medizin

der Justus-Liebig-Universität Gießen

vorgelegt von

Héctor Alejandro Cabrera Fuentes

aus

El Espinal, Oaxaca, Mexiko

Gießen 2014

Aus dem Institut für Biochemie

des Fachbereichs Medizin der Justus-Liebig-Universität Gießen

Leiter/Direktor: Prof. Dr. Lienhard Schmitz

Gutachter: Prof. Dr. Klaus T. Preissner
Gutachter: Prof. Dr. Saverio Bellusci

Prüfungsmitglied: Prof. Dr. Raimund Schäffer
Prüfungsvorsitz: Frau Prof. Dr. Susanne Rohrbach

Tag der Disputation: 06.08.2014

“Science is the soul of the prosperity of nations and the living source of all progress”

“La ciencia es el alma de la prosperidad de las naciones y la fuente de vida de todo progreso”

- Louis Pasteur.

I. Table of contents

II. List of figures

II. List of tables

IV. List of abbreviations

α-Sma	= α-smooth muscle actin
8SPT	= 8-sulfophenyltheophylline
ADAM17	= A disintegrin and metalloprotease 17
AF	= Atrial fibrillation
ApoB-LPs	= Apolipoprotein B-containing lipoproteins
Arg	= Arginase
AS	= Aortic stenosis
ATP	= Adenosine triphosphate
AVR	= Aortic valve replacement
BMDM	= Bone marrow-derived macrophage
BSA	= Bovine serum albumin
CABG	= Coronary artery bypass grafting
Cd115/Csf1r	= Colony stimulating factor 1 receptor
Cd206	= Macrophage mannose receptor-2
CAD	= Coronary artery disease
Cd31/PECAM-1	= Platelet endothelial cell adhesion molecule-1
CS	= Coronary sinus
CsA	= Cyclosporin A
CSF	= Colony-stimulating factor
DAPI	= 4',6-diamidino-2-phenylindole
eDNA	= Extracellular deoxyribonucleic acid
EDTA	= Ethylenediaminetetraacetic acid
Elane	= Neutrophil elastase
ELISA	= enzyme-linked immunosorbent assay
eRNA	= Extracellular ribonucleic acid
FBS	= Fetal bovine serum
GAPDH	= Glyceraldehyde-3-phosphate dehydrogenase
GM-CSF	= Granulocyte-macrophage colony-stimulating factor
HFD	= High-Fat-Diet
Hprt	= Hypoxanthine-phophoribosyl-transferase
IL	= Interleukin
Inf	= Interferon
iNOS	= Inducible nitric oxide synthase
kDa	= kiloDalton
I/R	= Ischemia/Reperfusion
LAD	= Left anterior descending artery
LDH	= Lactate dehydrogenase

LV	= Left ventricular pressure
LVdevP	= Left ventricular developed pressure
LVEDP	= Left ventricular end-diastolic pressure
$Ldlr^{-/-}$	= Low density lipoprotein receptor-deficient mice
Maze	= Atrial ablation
MCP1	= Monocyte chemoattractant protein-1
Mcpt6	= Tryptase beta-2
M-CSF	= Macrophage colony-stimulating factor
MMP	= Matrix metalloproteinase
mPTP	= mitochondrial permeability transition pore
MR	= Mitral regurgitation
MVR	= Mitral valve reconstruction
NF-kappa B	= Nuclear factor-kappa B
PBS	= Phosphate buffered saline
Prdx3	= Peroxiredoxin 3
RA	= Radial artery
RI	= RNase inhibitor
RNase	= Ribonuclease
ROS	= Reactive oxygen species
SOD	= Superoxide dismutase
SDS	= Sodium dodecyl sulfate
Serca2a	= Cardiac sarcoplasmic reticulum Ca^{2+} -ATPase2a
STEMI	= ST-segment elevation myocardial infarction
TACE	= TNF-α converting enzyme
TAPI	= TNF-α processing inhibitor (TACE-inhibitor)
TBS	= Tris buffered saline buffer
TBS-T	= Tris buffered saline buffer + 0.1% Tween 20
Tcf21	= bHLH transcription factor
TEMED	= N,N,N',N'-tetramethyl-ethane-1,2-diamine
TLR	= Toll-like receptor
TMRE	= Tetramethyl-rhodamine-ethylester
TNF-α	= Tumor necrosis factor - alpha
TRITC	= tetramethylrhodamine isothiocyanate
TTC	= Tetrazoliumchlorid
VEGF	= Vascular endothelial growth factor

V. Summary

After vessel damage or injury, atherosclerosis and vascular remodeling are driven by inflammation and mononuclear cell infiltration. Macrophages respond to external stimuli with rapid changes in their expression of many inflammation-related genes to undergo polarization towards the M1 (pro-inflammatory) or M2 (anti-inflammatory) phenotype. This unique property of macrophages allows these cells to modulate chronic inflammatory processes such as atherogenesis. Cardiomyocyte death occurs during acute myocardial infarction under situations of cardiac ischemia/reperfusion resulting in a major impact on the quality of life and survival of patients suffering from coronary artery disease. Despite optimal therapy, the morbidity and mortality of patients presenting with an acute myocardial infarction (MI) remain significant. Self-extracellular RNA (eRNA) has recently been implicated by our group to become enriched at sites of tissue damage, and to act as a pro-inflammatory mediator.

In thus study, (a) the role of eRNA in high-fat-diet (HFD)-induced atherosclerosis in mice was documented. Given the association of eRNA with macrophages within atherosclerotic lesions, it was assessed whether eRNA generated by the macrophages themselves may induce inflammatory responses within these cells, independent of Toll-like receptor signaling. Moreover, (b) the role of eRNA as a novel therapeutic target for protecting the heart against the detrimental effect of acute ischemia/reperfusion (I/R) injury was observed.

(a) The presence of eRNA was revealed in atherosclerotic lesions from HFD-fed low density lipoprotein receptor-deficient (*Ldlr*$^{-/-}$) mice in a time-progressive fashion. RNase activity in plasma increased more than 50% within the first 2 weeks of HFD, followed by a decrease to levels below baseline after 4 weeks. Recombinant mouse macrophage CSF–driven bone marrow-derived macrophage (BMDM) differentiation was skewed towards the M1 phenotype by exposure of cells to eRNA. This was reflected by the overexpression of inflammatory markers such as *Tnf-α, Arg2, Il-1β, Il-6,* or *Ifn-γ* together with *Il-12* and *iNOS,* whereas anti-inflammatory genes such as *Il-10* and *Il-4* together with *Arg1* and macrophage mannose receptor-2 (Cd206) were significantly down-regulated by eRNA. Accordingly, the release of TNF-α and IL-6 proteins into the cell supernatant was significantly elevated by eRNA stimulation. Moreover, the capacity of granulocyte macrophage CSF–driven BMDM differentiation (already representing M1 phenotype) towards further M1 polarization in response to eRNA was moderate. Nevertheless, a significant down-regulation of M2 markers

was found. (b) In patients subjected to acute global I/R during cardiac bypass surgery, significant elevation in plasma levels of eRNA and TNF-α were found. Moreover, following *in vivo* myocardial I/R in mice or I/R induced in the isolated Langendorff-perfused rat heart, both, eRNA levels and cardiac injury markers were increased. Similarly, in cardiomyocytes subjected to hypoxia, eRNA was released resulting in TNF-α liberation through the activation of TNF-α converting enzyme (TACE). Conversely, TNF-α promoted further eRNA release especially under hypoxia, feeding a vicious cell-damaging cycle during I/R with the massive production of oxygen radicals. The administration of RNase1 or TAPI (a TACE-inhibitor) prevented cell death and reduced myocardial infarction. Likewise, RNase1 significantly reduced I/R-mediated energy exhaustion, opening of the mitochondrial permeability transition pore as well as oxidative damage in cardiomyocytes. Mechanistically, a major cellular response of eRNA is the liberation of TNF-α from its membrane-anchored proform into the highly active diffusible cytokine, which in turn may amplify this process reciprocally by inducing further release of eRNA, finally resulting in massive production of oxygen radicals. This uncovered cell-damaging vicious cycle for the situation of cardiac I/R injury could be interrupted or prevented by administration of RNase1 or an inhibitor of TNF-α-converting enzyme (TACE). These treatments revealed cytoprotection and suppressed energy exhaustion as well as oxidative damage in cardiomyocytes by maintaining expression of antioxidant enzymes.

In conclusion, eRNA is associated with atherosclerotic lesions and contributes to inflammation-dependent plaque progression in atherosclerosis-prone mice. Its targeting with RNase1 may serve as a new treatment option against atherosclerosis. It, was further showed that eRNA and TNF-α, are released by the myocardium in response to I/R, and both contribute to cardiomyocyte death. Therefore, RNase1 and TACE-inhibition provide novel therapeutic strategies for counteracting the adverse eRNA-TNF-α interplay which occurs during I/R, thereby preventing cell death, limiting myocardial infarct size and preserving cardiac function. This newly discovered fundamental pathogenic mechanism of I/R injury is likely to operate in other organs and tissues as well.

VI. Zusammenfasung

Die Atherosklerose und der nach Schädigung auftretende Gefäßumbau werden durch Entzündungen und die Infiltration mononukleärer Zellen verursacht. Makrophagen reagieren auf äußere Stimuli mit kurzfristigen Veränderungen durch die Expression vieler entzündungs-spezifischer Gene und polarisieren in den M1- (proinflammatorischen) oder den M2- (anti-inflammatorischen) Phänotyp. Diese besondere Fähigkeit der Makrophagen erlaubt diesen Zellen, chronische Entzündungsprozesse wie die Atherogenese zu modulieren.

Der Zelltod von Kardiomyozyten tritt während eines akuten Myokard-Infarktes infolge von kardialem Ischämie/Reperfusion (I/R)-Schaden auf. Dies hat einen erheblichen Einfluss auf die Lebensqualität und das Überleben von Patienten, die an einer koronaren Arterienerkrankung leiden. Trotz optimaler Therapie ist die Morbidität und Mortalität der Patienten mit einem akuten Myokardinfarkt (MI) noch sehr hoch. Kürzlich wurde von unserer Gruppe nachgewiesen, dass körpereigene extrazelluläre RNA (eRNA) an den Stellen der Gewebe- oder Gefäßverletzungen angereichert ist und als pro-inflammatorischer Mediator wirken kann.

In dieser Arbeit wird (a) die Rolle von eRNA in einer fettreichen Diät (HFD)-induzierten Atherosklerose im Tiermodell beschrieben. Aufgrund der Assoziation von eRNA mit Makrophagen in atherosklerotischen Läsionen wurde untersucht, ob von Makrophagen gebildete eRNA selbst Entzündungsantworten in diesen Zellen, unabhängig von Toll-like-Rezeptoren, induzieren kann. In einem weiteren Teil wurde (b) die Rolle von eRNA als neues therapeutisches Zielmolekül beim Schutz des Herzes gegenüber pathologischen Einflüssen beim akuten I/R-Schaden *in vivo* (Tiermodell), *ex vivo* (isoliertes Herz) und in Zellkultur untersucht.

(a) Die Assoziierung von eRNA mit atherosklerotischen Läsionen konnte in HFD-gefütterten LDL-Rezeptor-defizienten ($Ldlr^{-/-}$) Mäusen in zeitabhängiger Weise gezeigt werden. Im Plasma, dieser Tiere stieg die RNase-Aktivität um mehr als 50% innerhalb der ersten zwei Wochen unter HFD an, gefolgt von einem Abfall des Enzyms unter die Messbasis nach 4 Wochen HFD. Die durch rekombinanten Maus-MCSF induzierte Differenzierung von Knochenmark-Makrophagen (BMDM) wurde durch Behandlung der Zellen mit eRNA in Richtung M1 (inflammatorischer Phänotyp) polarisiert. Die Folge war eine Überexpression von inflammatorischen Markern wie *Tnf-α, Arg2, Il-1β, Il-6* oder *Ifn-γ* sowie *Il-12* und *iNOS*, während anti-inflammatorische Gene wie *Il-10* und *Il-4* sowie *Arg1* und *Makrophagen-Mannose-Rezeptor-2* (*Cd206*) durch eRNA signifikant herunterreguliert

wurden. Demzufolge war die Freisetzung von Tumor-Nekrose Faktor-α (TNF-α) und IL-6 Proteinen durch die eRNA-Stimulation der Zellen signifikant erhöht. Darüber hinaus war die Kapazität von GMCSF-induzierter BMDM-Differenzierung (welche bereits den M1-Phänotyp zeigte) in Anwesenheit von eRNA zu noch stärkerer M1-Polarisation eher moderat, jedoch kam es zu einer signifikanten Runterregulation von M2-Markern.

(b) In Patienten mit akuter globaler I/R während einer Herz-Bypass-Operation wurde eine signifikante Erhöhung der Plasmaspiegel von eRNA und TNF-α beobachtet. Zudem waren die Konzentrationen von eRNA und kardialen Verletzungsmarkern nach *in vivo* myokardialer I/R in Mäusen oder im isolierten, perfundierten Langendorff-Rattenherz nach I/R erhöht. Ähnliches zeigte sich in hypoxischen Kardiomyozyten, in denen eRNA freigesetzt wurde und resultierte in der weiteren Sezernierung von TNF-α durch die Aktivierung des TNF-α konvertierenden Enzyms (TNF-α converting enzyme, TACE). Umgekehrt begünstigte TNF-α die weitere eRNA-Freisetzung vor allem unter Hypoxie, was einen destruktiven Teufelskreis während der I/R mit einer massiven Produktion von Sauerstoffradikalen zur Folge hatte. Die Gabe von RNase1 oder TAPI (TACE-Inhibitor) unter I/R-Bedingungen wirkte protektiv auf Kardiomyozyten und reduzierte den Myokardinfarkt signifikant. Ebenso führte die Gabe von RNase1 zu einer signifikanten Erhöhung der Energieausbeute unter I/R, der verzögerten Öffnung der mitochondrialen Permeabilitäts-Transitionspore sowie der deutlichen Verringerung des oxidativen Schadens in Kardiomyozyten.

Mechanistisch beruht der Haupteffekt von eRNA auf der Freisetzung von TNF-α aus seiner membranverankerten Vorform in das hochaktive diffusionsfähige Zytokin, welches dann selbst diesen Prozess reziprok durch die Induktion von weiterer eRNA-Freisetzung verstärken kann und schließlich zu einer massiven Produktion von Sauerstoffradikalen führt. Dieser für die Situation des kardialen I/R-Schadens aufgedeckte zellzerstörende Teufelskreis konnte durch die Gabe von RNase1 oder den TACE-Inhibitor unterbrochen bzw. unterdrückt werden. Diese neuen Behandlungen lassen einen Zellschutz erkennen und unterdrücken die Energie-Erschöpfung in gleichem Maße wie den oxidativen Schaden in Kardiomyozyten durch die Aufrechterhaltung der Expression von antioxidativen Enzymen.

Damit stellen RNase1 und die TACE-Inhibition neue therapeutische Strategien für die Inhibierung des nachteiligen eRNA-TNF-α Zusammenspiels dar, welches während der I/R-Phase auftritt. Dieser Therapieansatz kann den Zelltod von Kardiomoyzyten unterdrücken, die Myokardinfarktgröße limitieren und die Herzfunktion bewahren. Der beschriebene fundamental neue pathogene Mechanismus zur Auslösung eines I/R-Schadens kann möglicherweise ebenso in anderen Organen und Geweben ablaufen.

1 Introduction

1.1. Atherosclerosis development

Atherosclerosis and its sequelae are the most frequent cause of death in Western societies (Writing Group et al., 2010). The continuing age-related narrowing of (coronary) arteries can necessitate the need for percutaneous transluminal angioplasty. The long-term effects of such therapy, however, are still limited by an excessive arterial remodeling and restenosis (Inoue et al., 2011; Weber and Noels, 2011).

Atherosclerosis as a cardiovascular disease, and it has predominantly been appreciated as a chronic inflammatory reaction in the vascular wall in response to dyslipidemia and endothelial distress involving the inflammatory recruitment of leukocytes and the activation of resident vascular cells (Weber et al., 2010). This collection of inflammatory cells, made up almost entirely of monocyte-derived macrophages, promotes smooth muscle cell proliferation and extracellular matrix elaboration, thereby increasing the lesion size (Hartman and Frishman, 2014).

Atherosclerosis involves a long-term expansion of the arterial intima, a normally small area between the endothelium and the underlying smooth muscle cells of the media, with lipids, proinflammatory cells and extracellular matrix, which contributes to the plaque instability, and to acute cardiac events including thrombus formation, myocardial infarction and sudden cell death produced by coronary plaque disruption **(Figure 1.1)**.

1.2. Myocardial ischemia/reperfusion Injury

Cardiomyocyte death occurring during acute myocardial infarction has a significant impact on the quality of life and survival of patients suffering from coronary artery disease (Yellon and Hausenloy, 2007). Severe myocardial ischemia secondary to a thrombotic coronary occlusion at the site of a ruptured atheromatous plaque results in an extensive cardiomyocyte death involving most of the area at risk unless coronary blood flow is rapidly restored by pharmacological or mechanical interventions (Hausenloy and Yellon, 2013).

Here, affected coronary vessels are usually occluded by arteriosclerotic plaque material, resulting in stenotic blood flow, a largely decreased oxygen supply of the myocardium, termed ischemia, as well as oedema formation.

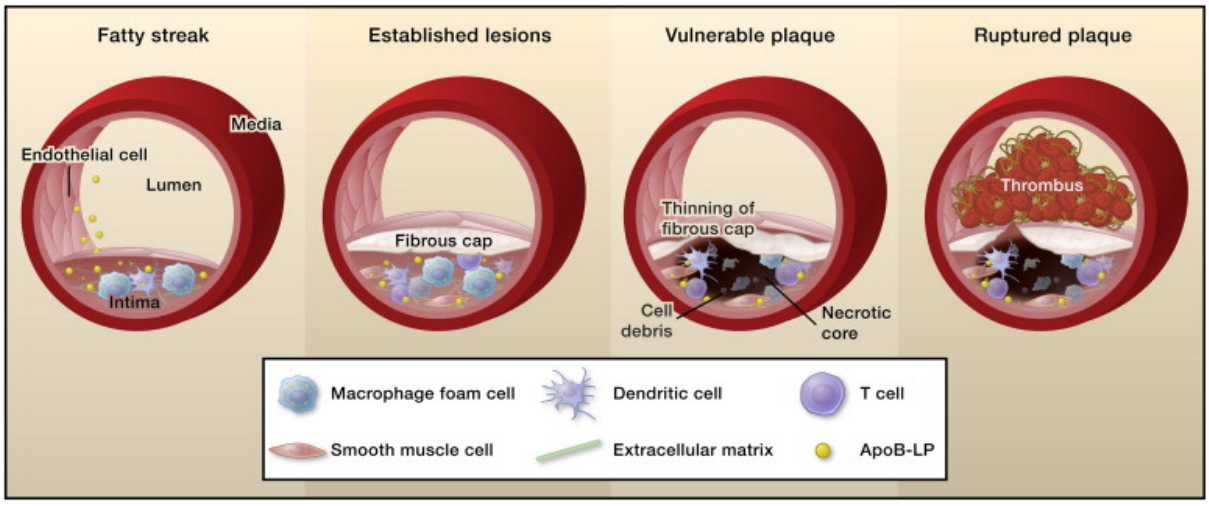

Figure 1.1. Progression of an atherosclerotic lesion. Early fatty streak lesions are characterized by the accumulation of apolipoprotein B-containing lipoproteins (ApoB-LPs) in the subendothelial space, which incites the recruitment of dendritic cells and macrophages. As the atherosclerotic lesion progresses, smooth muscle and T cells also infiltrate the intima, and apoB-LP retention is amplified. Vulnerable plaques are characterized by the accumulation of apoptotic cells and defective phagocytic clearance (efferocytosis), resulting in the lipid-filled necrotic core. A thinning fibrous cap decreases lesion stability, making these atherosclerotic plaques susceptible to rupture and the formation of a thrombus. (Moore and Tabas, 2011).

Although emergency coronary recanalization serves to open occluded arteries, it may not prevent subsequent major cell death that takes place during the first minutes of reperfusion. However, although early reperfusion salvages viable myocardium, limits infarct size and markedly improves the prognosis of patients with acute myocardial infarction, its beneficial effect is limited by the occurrence of additional cardiomyocyte death during the initial minutes of reflow, a phenomenon described as lethal ischemia/reperfusion (I/R) injury (Piper et al., 1998; **Figure 1.2)**. Since cell death can also propagate to adjacent cardiomyocytes via gap junctions, I/R injury may limit the benefit achieved by the restoration of coronary artery patency in patients with acute myocardial infarction (Garcia-Dorado et al., 2012). However, none of these approaches have been introduced into clinical practice. Nevertheless, application of non-invasive intermittent limb I/R (designated as remote ischemic preconditioning), applied either prior to heart operations (Thielmann et al., 2013) or by a paramedic to patients with ST-segment elevation myocardial infarction (STEMI) upon primary percutaneous coronary intervention (PPCI; Botker et al., 2010), have recently been found to be beneficial for the outcome of cardiac ischemic damage (Heusch, 2013; Ovize et al., 2013).

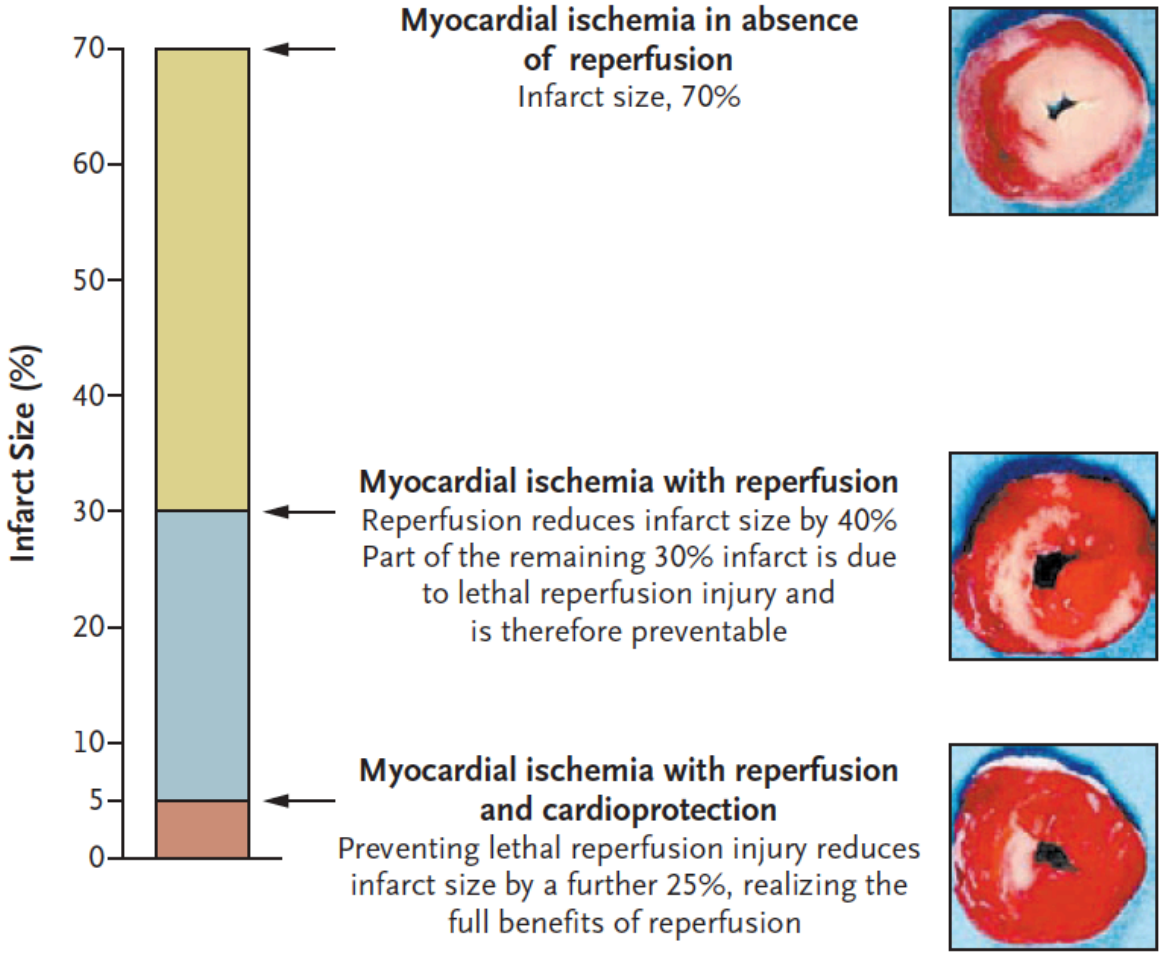

Figure 1.2. Contribution of lethal reperfusion injury to final myocardial infarct size.
This hypothetical scheme shows the large reduction in myocardial infarct size obtained by early and successful myocardial reperfusion after a sustained episode of acute myocardial ischemia. The full benefits of myocardial reperfusion are not realized because of the presence of lethal reperfusion injury, which diminishes the magnitude of the reduction in infarct size elicited by myocardial reperfusion. This concept is revealed by the further reduction in myocardial infarct size obtained by preventing lethal reperfusion injury with the administration of a cardioprotective intervention at the beginning of myocardial reperfusion. Infarcted myocardium is depicted in pink, and the viable, at-risk myocardium is stained red. Infarct size is expressed as a percentage of the volume of myocardium at risk for infarction (Yellon and Hausenloy, 2007).

1.2.1. Pathophysiologic mechanisms of myocardial ischemia/reperfusion injury

This paradoxical phenomenon, known as "myocardial ischemia/reperfusion (I/R) injury" **(Figure 1.3)**, has largely been studied in experimental animal models and is known to be caused by a network of mechanisms causing Ca^{2+}-overload (Ruiz-Meana et al., 2007), mitochondrial permeabilization (Di Lisa et al., 2011; Di Lisa et al., 2009) or ATP-dependent hypercontracture (Abdallah et al., 2010; Ladilov et al., 2003) that may limit myocardial salvage achieved by reperfusion (Garcia-Dorado et al., 2012).

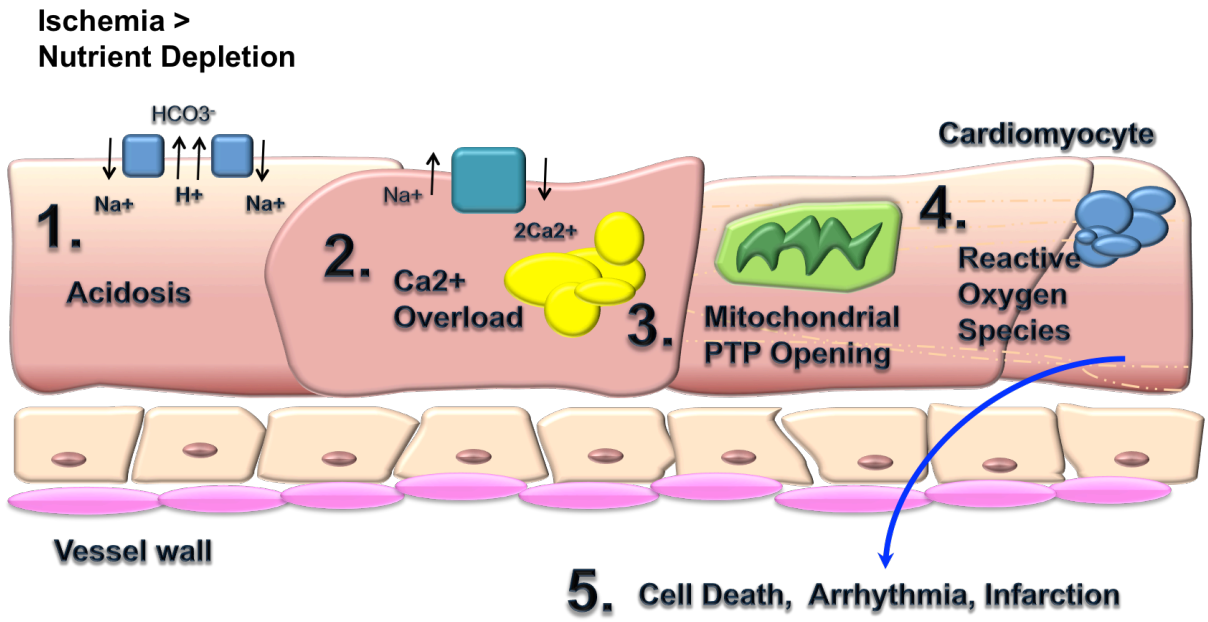

Figure 1.3. Mediators in myocardial reperfusion injury. During myocardial reperfusion the rapid restoration of physiological pH **(1)**, Ca2+ overload **(2)** and further ATP-depletion through opening of the mitochondrial permeability transition pore, mPTP **(3)** leads to the generation of reactive oxygen species (ROS, **4**). As a result, the existence of lethal reperfusion injury is confirmed by cardiomyocyte death and the size of a myocardial infarct (5). (Frank et al., 2012 with modifications).

Although experimental studies have convincingly demonstrated that infarct size can be markedly reduced by therapeutic interventions applied at the time of reperfusion, such as ischemic postconditioning (Zhao et al., 2013), and diverse pharmacological interventions, including contractile blockers, inhibitors of Na^+/Ca^{2+} (Schafer et al., 2001) and Na^+/H^+ exchange (Ruiz-Meana et al., 2000), or particulate guanylyl cyclase agonists (Agullo et al., 2005), none of them have been introduced into clinical practice. Moreover, the cardio-protective mechanisms of existing drugs are not well established or understood to allow the translation of experimental findings (Rodriguez-Sinovas et al., 2007).

Experimental studies thus far have not taken into account that factors from the irreversibly damaged cardiac tissue itself may contribute to reperfusion injury. Although it is well known that disrupted cells may release cytosolic proteins during reperfusion, such as creatine kinase or cardiac troponins, these and other factors have only been used for diagnostic evaluation (McErlean et al., 2000; Santos et al., 2011). Another component that is detectable in the extracellular space during tissue hypoxia or cell damage are ribonucleic acids (RNA), which are released by dying cells and may be detected as extracellular RNA (eRNA) (Kannemeier et al., 2007).

The majority of eRNA consists of ribosomal RNA, which may bind to different basic proteins in blood plasma or on cell surfaces, and thereby promotes a variety of extracellular functions, particularly related to vascular diseases (Fischer et al., 2014).

1.3. Role of extracellular RNA in the pathogenesis of inflammation

The presence and activity of extracellular nucleic acids in any natural or experimental situation has to be critically evaluated as to the nature, quantity, quality, size and structure of these poly-anionic compounds and whether they are derived from the host (self) or from external sources (non-self, such as from bacteria or viruses) (Fischer et al., 2014).

The multiple functions of nucleic acids are classically considered to be operative inside eukaryotic cells: Nuclear and mitochondrial DNA are required for genome replication and gene transcription, while different types of RNA are available as primary and post-transcriptionally modified mRNA transcripts, as tRNA, rRNA, microRNA or other RNA-species to participate in and control post-transcriptional and translational events. Yet, more than 50 years ago (Mandel and Metais, 1947), self-nucleic acids were identified in extracellular fluids and cell supernatants and eventually, their appearance in the blood circulation was associated with some disease states. As an early example, extracellular DNA (eDNA) was detected in the serum of patients with systemic lupus erythematosus (Tan et al., 1966), and due to its neoantigenic nature it may provoke the formation of autoantibodies, relevant for the development of this autoimmune disease. Furthermore, RNA-proteolipid complexes and also free eRNA were initially identified in cancer patients and were proposed to represent a specific secretory product of cancer cells that could mediate host-tumor interactions (Kopreski et al., 2001; Wieczorek et al., 1985). Moreover, amplification of circulating mRNA in these patients proved to be useful as potential biomarker in tumor diagnosis (Kopreski et al., 2001; Kopreski et al., 1999).

During the last decade it has been demonstrated that self eRNA becomes released from cells under tissue-damaging or pathological conditions, whereas under quiescent conditions, the level of eRNA in body fluids is rather low (Kopreski et al., 2001; Kopreski et al., 1999; Wieczorek et al., 1985). Moreover, eRNA provides unexpected functional properties, including prothrombotic, proinflammatory and vessel permeability-inducing functions (Fischer et al., 2007; Kannemeier et al., 2007),

rendering it a new alarm signal in the context of body defense but also a damaging factor in relation to cardiovascular diseases (Fischer and Preissner, 2013; Simsekyilmaz et al., 2014). The multiple functional activities of eRNA were prevented or inhibited by vascular ribonuclease1 (RNase1), which is predominantly expressed in endothelial cells (Fischer et al., 2011). Although largely unrecognized so far, the eRNA/RNase1 system represents a new regulatory entity of our body that contributes to the balance of vascular homeostasis, however, considerable effort is needed to further characterize its contribution in the pathomechanism of cardiovascular diseases.

1.3.1. Mechanism of self-eRNA-induced cytokine release and vascular permeability changes

Self-eRNA (predominantly rRNA) not only induces vascular permeability by activation of VEGF-dependent signalling, but also promotes the shedding or release of cytokines like TNF-α or IL-6 from monocytes/macrophages (Fischer et al., 2013; Fischer et al., 2012); in a yet undefined mechanism. In particular, the liberation of bioactive trimeric TNF-α from its membrane-associated proform requires the activation of TNF-α-converting enzyme (TACE) (Blobel, 2005). TACE, also designated as ADAM17 ("A Disintegrin And Metalloprotease"), belongs to the family of (membrane-linked) proteases and serves as sheddase to cleave the membrane-anchored precursor of the cytokine as well as several other biological mediators, including IL-6 receptor or VEGF receptor-2 (Rose-John, 2013). In which way eRNA as an ubiquitous alarm signal may directly or indirectly trigger TACE-activation (either by extracellular de-encryption of inactive TACE or by mobilization of the vesicle-stored sheddase) to amplify cytokine release in the endogenous inflammatory cascade remains to be investigated **(Figure 1.4)**.

Among these, TNF-α and IL-6 are both known to effectively induce the permeability across epithelial and endothelial cell monolayers (Beynon et al., 1993; Marcus et al., 1996; Sedgwick et al., 2002), whereby the underlying cellular mechanisms are only incompletely understood. Also, TNF-α-mediated disruption of the blood-brain-barrier induces activation of cyclooxygenases with an amplification of the inflammatory response (de Vries et al., 1996). It remains to be characterized, whether non-self eRNA (such as viral dsRNA) may also promote TNF-α shedding, since West Nile virus dsRNA can promote the breakdown of the blood-brain-barrier by activating TNF-α receptor-1 signalling (Wang et al., 2004).

1.4. RNase1: The natural counterpart of eRNA

The lifespan as well as the reactivity of eRNA-species in the blood circulation or in other extracellular fluids depends to a large degree on the type of complexation with e.g. proteins, microparticles or cell surfaces. Despite these constraints, eRNA is degraded in the vascular system by circulating RNases, of which thermostable RNase1 is the most powerful antagonist of eRNA **(Figure 1.4)**. Besides the production of RNase1 in the pancreas as the major ribonuclease of the gastrointestinal tract, vascular RNase1 is predominantly expressed and released by endothelial cells from medium and large vessels (Fischer et al., 2011; Landre´ et al., 2002; Moenner et al., 1997). Interestingly, the counteracting functions of RNase1 that were reported in various cardiovascular models are safe, since RNase1 does not operate in a cytotoxic way, due to an ubiquitously expressed extremely high affinity RNase-inhibitor in all body cells (Gaur et al., 2001).

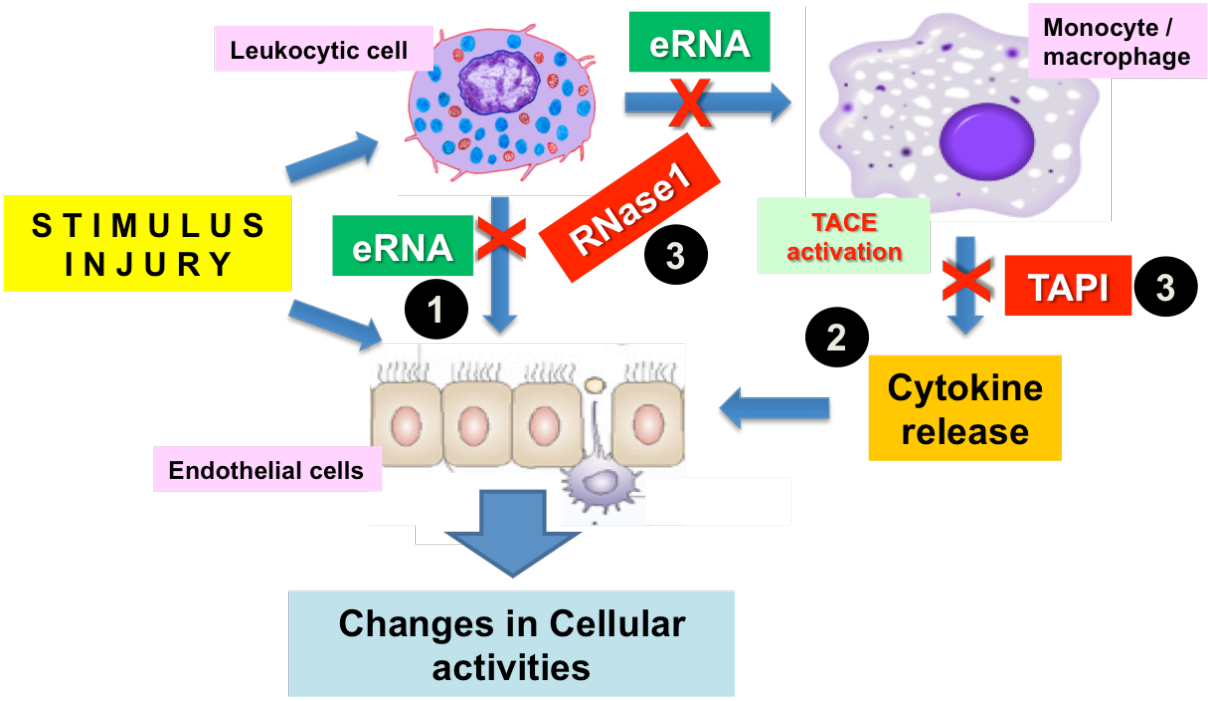

Figure 1.4. Proposed mechanisms for the generation and functions of eRNA in cytokine-mediated disturbance of the vascular endothelial barrier. Upon release of eRNA, initiated by exogenous or endogenous stimuli or by injury and trauma, self eRNA may directly or indirectly (through vascular endothelial growth factor or other factors liberated by leukocytic cells) stimulate the vascular endothelium to induce hyper-permeability and thereby affect the endothelial barrier function and cellular activities **(1).** Alternatively, eRNA provokes liberation of TNF-α and other cytokines (particularly by inducing TACE activation on monocytes/macrophages), resulting in changes of vascular barrier function as well **(2).** The activities of eRNA are counteracted by RNase1, whereas TACE activation is blocked by the inhibitor TACE **(3)**. (Fischer et al., 2014 with modifications).

Proinflammatory or prothrombotic agents as well as eRNA itself or vasopressin may induce the short term release of RNase1 from its endothelial storage sites, the Weibel-Palade bodies, such that the eRNA/RNase1 system can be considered as an important regulator of vascular homeostasis and vessel wall integrity (Fischer et al., 2011c). Moreover, systemic treatment with RNase1 was shown to rescue mice from arterial thrombotic occlusion, to limit cerebral edema and infarct size after acute stroke, and to serve as a potent anti-inflammatory regimen *in vitro* and *in vivo* (Fischer et al., 2007; Fischer et al., 2011; Fischer et al., 2012; Kannemeier et al., 2007; Walberer et al., 2009).

In vitro experiments demonstrated that, upon RNase1-mediated degradation, split products of eRNA were unable to induce vascular permeabililty changes. This confirms that the protective effects of RNase1 are most likely due to the elimination of cell-damaging eRNA and are not mediated by creating hydrolysis products of eRNA (Fischer et al., 2007). In essence, RNase1 inhibits or prevents the various endothelial cell-inducing, barrier-disturbing activities of eRNA and it is thereby considered to be a potent vessel-protective and barrier-stabilizing factor (Fischer and Preissner, 2013). Ongoing clinical studies aim to prove its availability as potential drug for the intervention in cardiovascular diseases.

2. Aim of the study

Different types of high and low molecular weight self extracellular RNA (eRNA) are liberated from cells upon conditions of tissue damage or vascular disease and have been demonstrated *in vivo* and *in vitro* to influence the integrity and barrier function of the vascular endothelium. eRNA has been characterized as an early alarm signal for tissue stress or damage, and to induce respective responses by activating blood coagulation/thrombosis, releasing tumor necrosis factor-α (TNF-α) and other cytokines as well as promoting inflammatory processes, including leukocyte trafficking. This data may shed light of the association of eRNA and macrophages in a chronic inflammatory environment as during atherosclerosis. Among the types of self eRNA studied in this respect, ribosomal eRNA appears to engage cytokines to induce hyper-permeability, while RNase1 serves as potent counteracting and vessel-protective factor.

Thus, the aims of this study with regard to the mechanisms of atherogenesis and ischemic heart disease were:

1) To investigate the role of eRNA in high-fat-diet induced atherosclerosis in low density lipoprotein receptor-deficient (*Ldlr*$^{-/-}$).
2) To analyze whether eRNA is generated by macrophages and may induce inflammatory responses within macrophages.
3) To identify and quantify circulating eRNA in mice and humans following cardiac ischemia/reperfusion (I/R) injury, and to characterize its functional role.
4) To study whether the existence of eRNA can be related to the cell destructive outcome during cardiac I/R, particularly in relation to the action of TNF-α.
5) To investigate the effect of eRNA in the cardiomyocyte inflammatory response.
6) To describe the molecular mechanism underlying the role of the eRNA/RNase1 system within cardiovascular diseases.
7) To evaluate whether the administration of RNase1 or TAPI (inhibitor of TNF-α converting enzyme) may successfully prevent and/or reduce the pathological parameters that are characteristic for I/R injury and substantially improve the early post-ischemic functional myocardial recovery.

3 Material and methods

3.1 Materials

3.1.1 Reagents

Product Name	Company	Country
2-mercapto-ethanol	Sigma-Aldrich	Germany
2-propanol	Fluka	Germany
Acetic acid	Sigma-Aldrich	Germany
Acetone	Roth	Germany
Alexa Fluor 488 donkey anti-rabbit IgG	Invitrogen	Germany
Alexa Fluor 546 Monoclonal Antibody Labeling Kit	Invitrogen	Germany
Alexa Fluor 555 donkey anti-mouse IgG	Invitrogen	Germany
Anti-smooth muscle α-actin	Sigma-Aldrich	Germany
Anti-GAPDH	Santa Cruz	USA
Anti-IκBα	Santa Cruz	USA
Anti-MOMA-2	Abcam	UK
BAY 11-7082	Enzo Life Sciences	Germany
BBL™ GasPak™	BD Biosciences	Germany
BSA	Sigma-Aldrich	Germany
Chow diet Prolab Isopro Mouse 3000	Agway Inc.	USA
Cy3	Abcam	UK
Cytotoxicity detection kit	Roche	Germany
Cytokine Profiler	R&D Systems	USA
DAPI - Vectashield	Vector laboratories	USA
Dihydroethidium	Invitrogen	Germany
ECL plus western blotting detection system	GE healthcare	Germany
Ethanol	Roth	Germany
Ethidium bromide	Sigma-Aldrich	Germany
EDTA	Roth	Germany
Evans-Blue	Sigma-Aldrich	Germany
GenElute Mammalian Genomica RNA Miniprep Kit	Sigma-Aldrich	Germany

GenElute Mammalian Genomica DNA Miniprep Kit	Sigma-Aldrich	Germany
GM-CSF	PeproTech	USA
GoScript™ Reverse Transcription System	Promega	USA
HFD	Harlan Teklad Inc.	USA
IL-6 ELISA kit	eBioscience	Germany
Ketamine hydrochloride	Sigma-Aldrich	Germany
Langendorff heart perfusion system	Physiology Institute, JLU-Giessen	Germany
Master Pure™ RNA Purification kit	Epicentre Biotechnologies	USA
M-CSF	PeproTech	USA
Methanol	Roth	Germany
Milk powder	Roth	Germany
Millar Mikro-Tip®	Millar Instruments	USA
Osmotic pump (model 1004)	Alzet	USA
Paraformaldehyde	Roth	Germany
PBS	Fischer Scientific	USA
Penicillin/streptomycin	Invitrogen	Germany
Primer	Fisher Scientific	USA
RNase1	Fermentas	Germany
RNase-inhibitor	Fermentas	Germany
RNeasy minikit	Qiagen	USA
SDS	Sigma-Aldrich	Germany
SYBR Green assays	Applied Biosystems	USA
SYTO® RNASelect™ dye	Invitrogen	Germany
TEMED	Sigma-Aldrich	Germany
TMRE	Invitrogen	Germany
TNF-α ELISA kit	eBioscience	Germany
TNF-α Recombinant	R&D Systems	USA
TriPure isolation reagent	Roche	Germany
Tris	Roth	Germany
Trisodium citrate dehydrate	Roth	Germany
Triton X-100	Sigma-Aldrich	Germany

TRIzol® Reagent	Invitrogen	USA
Trypan blue	Sigma-Aldrich	Germany
TrypLE Express	GIBCO-Invitrogen	Germany
TTC	Roth	Germany
Tween 20	Sigma-Aldrich	Germany
Xylazine hydrochloride	Sigma-Aldrich	Germany
Zymo RNA MicroPrep kit	Zymo Research	USA

3.1.2 Equipment

Name	**Company**	**Country**
6-Well Chamber Slides (LabTek)	Thermo Fisher Scientific	USA
96-Well Plates for ELISA and Binding assays (MaxiSorp)	Thermo Fisher Scientific	USA
96 Well PCR Detection Plate	Thermo Fisher Scientific	USA
96-Well plates for cell culture (steril)	Thermo Fisher Scientific	USA
AutoQuant X2 software	Bitplane	Switzerland
CASY Cell Counter Systems	Schärfe Systems	Germany
Cell culture incubator (IR Sensor)	Sanyo	USA
Centricon tubes	Millipore	Germany
Centrifuge - Fresco 17	Thermo Fisher Scientific	USA
Confocal NIKON-microscope ECLIPSE TE200-E	Nikon	Germany
Coverslips (24x60 mm)	Roth	Germany
Cryo Tube Vials	Thermo Fisher Scientific	USA
Disposable pipettes (2 ml, 5 ml, 10ml, 25 ml, 50 ml)	Greiner Bio-One	Germany
Electrophoresis chambers	BioRad	Germany
ELx 808 absorbance ultra microplate reader	BIO-TEK Instruments	Germany
Falcon tubes (15 and 50 ml)	Greiner Bio-One	Germany
Film cassette	Kodak	USA
Filter tips: 10; 100; 1000 µl	Eppendorf	Germany
Liquid Nitrogen	Linde	Germany
Liquid Nitrogen tank	Messer	Germany

FLx800™ Multi-Detection Microplate Reader	BioTek Instruments	Germany
Freezer (-80°C)	Thermo Fisher Scientific	USA
Gel blotting paper	Amersham Biosciences	UK
Hybond-P PVDF Membran	GE Healthcare	Germany
Ice machine	Scotsman	USA
Incubator (TS1)	Biometra	Germany
KC4 Version 3.0 Power Reporter Software	BioTek Instruments	Germany
LaminAir Sterilbank	Thermo Fisher Scientific	USA
Leica DMR fluorescence microscope	Leica	Germany
Leica TCS SP2 confocal microscope	Leica	Germany
Metamorph Imaging Version7.0	Molecular Devices	USA
Parafilm	Pechiney Plastic Packaging	USA
PCR-tubes	Eppendorf	Germany
PCR-Thermocycler (T3000)	Biometra	Germany
pH-Meter (Hi208)	Hanna	Germany
Pipetboy	Eppendorf	Germany
Power supply	Biometria	Germany
Pure Lab Plus	USF Eliga	Germany
Scale (SI-2002)	Denver Instruments	USA
S-Monovette® EDTA	Sarstedt	Germany
StepOnePlus Real-time PCR System	Applied Biosystems	USA
Sterile pippettes for cell culture	Greiner Bio-One	Germany
Tissue culture dishes	Greiner Bio-One	Germany
UV-transparent plastic cuvettes	Sarstedt	Germany
Vacum suction pump (Vario18)	Medela	Germany
Vortexer (Charley2)	Süd-Laborbedarf GmbH	Germany
Water bath for cell culture	Medingen	Germany

3.2. Methods

3.2.1. High-fat-diet driven atherosclerosis in LDL-receptor-deficient mice

Wild-type and *Ldlr*$^{-/-}$ mice (both on the C57BL/6J background, n=6 per group) were obtained from Jackson Laboratory. Animals were manteined on regular chow containing 4.5% fat and 0.022% cholesterol (Prolab Isopro Mouse 3000; Agway Inc., Syracuse, NY), or were fed an atherogenic diet containing 15.8% (wt/wt) fat and 1.25% cholesterol (no cholate, diet 94059; Harlan Teklad, Madison, WI, USA) for 8, 12 or 36 weeks (Han et al., 2010). All animal procedures were approved by the University of Hawaii Institutional Animal Care Committee. The animals were handled in accordance with good animal practice as defined by the relevant animal welfare bodies.

3.2.2. Immunohistochemistry, confocal microscopy and quantification of RNA

Cryosections (5 μm thick) of aortic sinus from *Ldlr*$^{-/-}$ mice were air dried and fixed with 4% paraformaldehyde and then incubated with 1% bovine serum albumin for 30 min to block non-specific binding sites. After rinsing in phosphate buffered saline (PBS), the samples were incubated 2 h at room temperature with primary antibodies against smooth muscle α-actin TRITC-labeled (Sigma-Aldrich). After repeated washes with PBS, the tissue sections were incubated with SYTO® RNASelect™ dye (Invitrogen) used for RNA localization. Nuclei were visualized with DAPI (Vector laboratories). Tissue sections were examined by laser scanning confocal microscopy (Leica TCS SP2), and confocal optical sections were taken using a Leica x63/1.32 objective lens. Each recorded image was taken using multi-channel scanning and consisted of 1024 x 1024 pixels. To improve image quality and to obtain a high signal to noise ratio, each image from the series was signal-averaged and was deconvoluted using AutoQuant X2 software (Bitplane, Zürich, Switzerland). For three-dimensional image reconstructions, an Imaris 6.3.1 multichannel image processing software (Bitplane) was used.

For quantification of eRNA, all tissue samples were simultaneously immunolabeled under identical conditions of fixation and dilutions of primary and secondary antibodies. Ten randomly chosen fields of vision were quantified using three-dimensional “Quantification“ and “VoxelShop“ options of Imaris 6.3.1 (Bitplane). The area of specific labelling for eRNA was calculated as arbitrary fluorescent units of positive labelling, each for the media area or neointima area, as previously described (Cai et al., 2000).

To determine the distribution of eRNA in atherosclerotic lesions, mice were sacrificed at indicated time points and perfused via the left ventricle with 10 ml PBS containing 1 mM EDTA and 30 ml fixative (PBS, 4% paraformaldehyde and 5% sucrose), and the atherosclerotic lesions were analyzed in the heart aortic valve as described previously (Han et al., 2010). Immunohistochemistry was performed on 5 µm cryostat tissue sections, fixed for 15 min in acetone at -20°C. SYTO® RNASelect™ dye (Invitrogen, USA) and the primary antibody recognizing rat anti-mouse MOMA-2 monoclonal antibody (Abcam, Cambridge, UK) against monocytes/macrophages were incubated for 1 h at room temperature followed by a secondary antibody conjugated with Cy3 (Abcam). Tissue sections were counterstained with DAPI (1µg/ml, Sigma Aldrich) for nuclei detection. Specimens were visualized using the confocal NIKON-microscope ECLIPSE TE200-E (Nikon, Düsseldorf, Germany), sections were taken through the tissue at 0.25 µm intervals, and analyzed by image acquisition software EZ-C1 Goldversion 3.8. (Abassi et al., 2011).

3.2.3. RNase1 assay

At indicated time points, human or mice plasma was taken for analysis of RNase1 activity by an enzymatic assay as described (Fischer et al., 2011). All activity values were normalized to the same protein concentration in different samples.

3.2.4. Cell culture

Bone marrow-derived macrophages (BMDM) were generated from WT bone marrow cells in M-CSF-containing L929-conditioned medium as described (Han et al., 2009; Han et al., 2010), or by incubation with mouse recombinant M-CSF or GM-CSF (50 ng/ml each;(Neu et al., 2013). Experiments were carried out for 24 h in 6-well trays (1.5 x 10^6 cells/ml) in the absence or presence of eRNA (1, 10 or 25 µg/ml), as indicated. Control cells were treated with growth medium alone (vehicle). For quantitation of TNF-α and Interleukin (IL)-6 protein production, BMDM were treated with eRNA (1, 10 or 25 µg/ml) for 24 h, followed by centrifugation and concentration of cell supernatants using centricon tubes (Millipore, Frankfurt, Germany) with a cutoff at 10 kDa. TNF-α and IL-6 ELISA were performed using commercially available kits from eBioscience (Frankfurt, Germany).

3.2.5. Patients´ samples and ethics statement

Patients undergoing cardiac surgery participated in this study **(Table 1)**. All patient gave a written informed consent, approved by the Ethics Committee, Medical Faculty, Justus-Liebig-University, Giessen (file number 166/11). Data were analysed anonymously. Upon blood withdrawal into S-Monovette® EDTA anticoagulated tubes (separate 5 ml blood specimens from each patient at different time points during heart surgery), RNase-inhibitor (RiboLock, Fermentas®, 40 U/ml) was added. Plasma was separated by centrifugation at 1600 g for 10 min at +4°C and aliquoted into 150 µl fractions which were kept at −80°C until analysis. Samples from each patient were analysed at the same time.

Table 1. Perioperative characteristics of patients.

Age	F/M	Diagnosis	Surgery
78	F	AS, CAD	CABG + AVR
84	F	AS, CAD	CABG + AVR
58	M	MR, CAD, AF	MVR + Maze
60	M	MR, CAD	CABG + MVR
78	M	CAD, AF	CABG + Maze
81	M	CAD	CABG
81	M	AS, CAD	CABG + AVR
81	M	MR, CAD, AF	CABG + MVR + Maze
51	M	CAD	CABG
52	M	ME, MR	CABG + MVR
80	M	CAD	CABG
74	M	CAD, MR	CABG, MVR
68	M	CAD	CABG
70	M	AS, CAD	AVR, CABG

Abbreviations: F (Female), M (Male), AS (Aortic stenosis), CAD (Coronary artery disease), MR (Mitral regurgitation), AF (Atrial fibrillation), AVR (Aortic valve replacement), CABG (Coronary artery bypass grafting), MVR (Mitral valve reconstruction), Maze (Atrial ablation)

3.2.6. I/R in mice: Treatment with RNase1 or RNase-Inhibitor (RI)

The established *in vivo* experimentation was exactly carried out as previously described (Liehn et al., 2010). Animals (6 to 8 weeks old male C57/b6 mice) were intubated under general anesthesia (100 mg/kg ketamine, 10 mg/kg xylazine, intraperitoneal application) and positive pressure ventilated with oxygen and 0.2% isofluran using a rodent

respirator. Hearts were exposed by left thoracotomy, and myocardial infarction was induced by suture occlusion of the left anterior descending artery over a silicon tube.

After 60 min of ischemia, the tube and suture were removed to permit reperfusion. Animals were treated with a continuously treatment (started three days before surgery) with RNase1 (Fermentas®, 100 µg/mouse) or RNase Inhibitor (RiboLock, Fermentas®, 80 U/mouse) via a subcutaneously implanted miniature infusion Alzet® osmotic pump (model 1004). The muscle layer and skin incisions were closed with a silk suture. All animal experiments and study protocols were approved by local authorities of the University Hospital of RWTH Aachen, complying with Romanian and German animal protection laws.

Experiments involving TNF-deficient mice (TNF-KO from C57BL/6 genetic background; Frias et al., 2013) were approved by the Health Science Faculty Animal Ethics Committee, University of Cape Town. Animals were housed and treated in accordance with the Guide for Care and Use of Laboratory Animals (Eighth Edition), published by the US National Institute of Health Publications.

3.2.7. Quantitative immunohistochemistry and immunofluorescence

Following 2h reperfusion, mice hearts were excised, washed with PBS, and the ligature over the left anterior descending artery (LAD) was renewed and 200 µl Evans-Blue were perfused through the aorta. The hearts were stored at -20°C for 1h and cut into four slices, which were incubated in tetrazolium solution (TTC) at 37°C for 10 min and thereafter in 10% formaldehyde for 10 min (Liehn et al., 2010). The slices were fixed between microscopic slides for photography and measurements. The total ventricle area, the blue-stained normally perfused area, red-stained injured but still viable area and white non-viable area were measured using Image J-software (Schneider et al., 2012). Area at risk was calculated as the difference between the total and blue-stained areas and expressed as percent of total ventricle area. Infarction size was calculated as white unstained area and expressed as percent of total ventricle area. For the evaluation of cardiac infarct size after 14 days reperfusion, serial sections (10-12 sections/mouse, 400 µm apart, up to the mitral valve) were stained with Gomori's 1-step trichrome stain (Liehn et al., 2010). The infarcted area was determined in all sections using Diskus software (Hilgers) and expressed as percentage of total left ventricular volume (Liehn et al., 2010).

3.2.8. In vivo assessment of cardiac function

Two weeks after ischemia/reperfusion (I/R), mice were anesthetized with ketamine/ xylazine, and a Millar Mikro-Tip® Pressure Transducer Catheter (Millar Instruments) was introduced into the right common carotid artery. After ligation, the catheter was slowly advanced into the left ventricle, and blood pressure in the left ventricle as well as increase (dP/dtmax) and decrease (dP/dtmin) of left ventricle pressure was measured.

3.2.9. Langendorff heart perfusion system

Specific pathogen-free Wistar rats were kept at the animal care facility at the Justus-Liebig-University (Giessen) with free access to food and water, in accordance with the Guide for the Care and Use of Laboratory Animals published by the US National Institute of Health (NIH publication no. 85-23, revised 1996).

Experiments were performed on isolated hearts from Wistar rats (10-12 weeks old; weighing 225–300 g) as previously described (Grohe et al., 2004). Hearts were rapidly excised, and the aorta was equipped with a cannula for retrograde perfusion containing a 16-gauge needle connected to a Langendorff perfusion system. Isolated rat hearts were submitted to I/R (45 min ischemia, followed by 120 min reperfusion). A modified Krebs-Henseleit buffer was used (140 mM NaCl; 2.7 mM KCl; 0.4 mM NaH_2PO_4; 1 mM $MgCl_2$; 1.8 mM $CaCl_2$; 24 mM $NaHCO_3$; 5 mM glucose, pH 7.4) at 37°C, saturated with 95% O_2 and 5% CO_2. A polyvinyl chloride balloon was inserted into the left ventricle through the mitral valve and held in place by a suture tied around the left atrium. The intra-ventricular balloon was inflated to give a diastolic pressure of 10 mmHg and balloon volume was held constant thereafter. The other end of the tubing was connected to a pressure transducer for continuous measurement of left ventricular (LV) pressure.

Left ventricular developed pressure (LVdevP) was calculated as the difference between peak LV systolic pressure and end-diastolic pressure (LVEDP). The flow was adjusted to a perfusion pressure of 50 mmHg and held constant with the exception of the time during no-flow ischemia. Temperature was constantly measured via a thermo-probe inserted in the perfusion chamber and maintained at 37±0.2°C. Experiments on isolated rat hearts were performed under different conditions as indicated in the corresponding legends to Figures.

3.2.10. eRNA quantification

eRNA was quantified in plasma obtained from 14 patients undergoing cardiac surgery, in mice plasma, in the perfusate obtained from the isolated Langendorff heart as well as in conditioned medium from rat cardiomyocytes using the Master Pure^{TM} RNA Purification kit (Epicentre Biotechnologies); values were normalized to the effluent protein concentration. Likewise, eRNA was quantified in 1 ml cardiomyocytes conditioned medium and normalized to the cardiomyocyte-lysate protein concentration. Total RNA concentration was quantified with NanoDrop ND-2000 (peqLab Biotechnologie GmbH).

3.2.11. Microparticles isolation

Langendorff heart-perfusate (1 ml fractions) was collected at each time point and combined to perform ultracentrifugation isolation for microparticles, as described (Wakui et al., 1990). Microparticles were resolved in phosphate-buffered saline (PBS) (without calcium and magnesium, Fischer Scientific). Microparticle-associated total RNA was isolated with GenElute Mammalian Genomica RNA Miniprep Kit (Sigma-Aldrich) and normalized to the effluent protein concentration.

3.2.12. Quantification of cell death

Lactate dehydrogenase (LDH) activity in the Langendorff heart-perfusate was spectrophotometrically measured in the coronary effluent throughout the reperfusion period. After 120 min of reperfusion, hearts were cut into four slices that were incubated at 37°C for 10 min in 1% triphenyltetrazolium chloride (TTC; pH 7.4) and imaged under white light to outline the area of infarct as described previously (Inserte et al., 2009).

3.2.13. Isolation of adult rat cardiomyocytes

Ventricular heart muscle cells were isolated from 4-months old Wistar rats as described previously (Schluter and Schreiber, 2005). Briefly, hearts were excised under deep anesthesia by isoflurane (2-chloro-2-(difluoromethoxy)-1,1,1-trifluoro-ethane), transferred rapidly to ice-cold saline and mounted on the cannula of a Langendorff perfusion system. Heart perfusion and subsequent steps were performed at 37°C. First, hearts were perfused in the non-circulating mode for 5 min at 10 ml/min with 110 mM NaCl, 1.2 mM KH_2PO_4, 1.2 KCl, 1.2 $MgSO_4$, 25 mM $NaHCO_3$, 11 mM glucose, gassed with 5% CO_2–95% O_2. Thereafter, perfusion was continued with recirculation of 50 ml

of the above-mentioned perfusate supplemented with 0.06% (v/v) crude collagenase and 25 μM $CaCl_2$ at 5 ml/min. After 30 min, ventricular tissue was minced and incubated for 20 min in recirculating medium with 1% (v/v) bovine serum albumin under 5% CO_2– 95% O_2. Gentle trituration through a pipette released cells from tissue chunks. The resulting cell suspension was filtered through a 200-μm nylon mesh. The filtered material was washed twice by centrifugation (3 min, 25 x g) and resuspended in the above perfusate, in which the concentration of $CaCl_2$ was increased stepwise to 0.2 and 0.5 mM. After further centrifugation (3 min, 25 x g), the cell pellet was resuspended into serum-free culture medium (medium 199 with Earle's salts supplemented with 5 mM creatine, 2 mM L-carnitine, 5 mM taurine, 100 IU/ml penicillin, and 100 μg/ml streptomycin), and cells were plated at a density of 10 x 10^4 per 35 mm culture dish (Falcon, type 3001). One h after plating, cultures were washed with serum-free medium 199 to remove round and non-attached cells, and cells were used for the experiments as described in the result section.

3.2.13. Hypoxia treatment of cardiomyocytes

Cardiomyocytes were cultured in a hypoxia chamber (BBL™ GasPak™, BD Biosciences) at 37 °C for 1h, according to the manufacturer's instructions.

3.2.14. Isolation of adult mouse cardiomyocytes

Mice were heparinised (250 IU) and anesthetized via an intraperitoneal injection of sodium pentobarbital (60 mg/kg). The heart was quickly excised and the aorta was cannulated for retrograde perfusion in a Langendorff apparatus at a constant flow rate of 3 ml/min at 37°C. The heart was perfused for 1 min with oxygenated perfusion buffer (PB) (NaCl 113 mM, KCl 4.7 mM, KH_2PO_4 0.6 mM, Na_2HPO_4 0.6 mM, $MgSO_4.7H_2O$ 1.2 mM, $NaHCO_3$ 12 mM, $KHCO_3$ 10 mM, taurine 30 mM, HEPES 10 mM, glucose 11 mM, 2,3-butanedione monoxime 10 mM), followed by digestion for 13 min with collagenase II (0.9 mg/ml, Worthington) in PB (collagenase buffer - CB). After digestion, the heart was removed and cardiomyocytes were suspended in CB. This suspension was oxygenated and shaken for 20 min at 37°C. Cardiomyocytes were centrifugated at 600 rpm for 3 min and the pellet was resuspended in PB2 ($CaCl_2$ 12.5 mM and bovine serum albumin (BSA) 1% in PB). Calcium was reintroduced via a stepwise manner over a period of 20 min and cardiomyocytes were left to settle via gravity sedimentation for 10 min. The pellet was resuspended in culture media (BSA

0.2%, creatine 5.8 mM, taurine 5 mM, carnitine 2 mM and penicillin/streptomycin 1% in medium 199). Cardiomyocytes were plated onto 6 well plates precoated with laminin and incubated for 1 h at 37°C.

3.2.15. Measurement of cell viability

Normoxic controls were cardiomyocytes without treatment and kept under normoxic conditions. Hypoxic controls were cardiomyocytes without treatment and submitted to 1 h of hypoxia in simulated ischemia (SI) buffer ($MgCl_2.6H_2O$ 1.2 mM, KCl 16 mM, KH_2PO_4 1 mM, NaCl 74 mM, $CaCl_2$ 1.2 mM, $NaHCO_3$ 10 mM, sodium lactate 20 mM, HEPES 25 mM, pH 6.7) using a Gentronics CO_2 and O_2 Gas Controller. O_2 levels were maintained at 1% and CO_2 levels at 5%. Treated cardiomyocytes were submitted to 1 h of hypoxia in SI buffer while being exposed to eRNA (10 µg/ml). Following hypoxia, cells were loaded with 0.04% trypan blue and cell viability was immediately analyzed using a light microscope at 40× magnification. The number of viable (unstained) and nonviable (blue stained) cells was recorded as previously described (Frias et al., 2013).

3.2.16. Isolation of RNA and DNA for treatment of cardiomyocytes

Total RNA was isolated from freshly obtained hearts (mice, rats) with GenElute Mammalian Genomica RNA Miniprep Kit (Sigma-Aldrich). Cells were washed once with PBS and extraction was performed according to the manufacturer's instructions. RNA was hydrolysed by incubation with RNase1 (Fermentas®) for 1 h at 37°C. Hydrolysed RNA was always used at the same concentration as cellular eRNA.

Total RNA concentration was quantified with NanoDrop ND-2000 (peqLab Biotechnologie GmbH). Quality of total RNA and hydrolysed RNA was determined with the 2100 Bioanalyzer using "Eukaryote total RNA Nano Assay" (Agilent Technologies). All chips were analysed as duplicates.

DNA was isolated with GenElute Mammalian Genomica DNA Miniprep Kit (Sigma-Aldrich) from confluent cultures of smooth muscle cells. Quality of total DNA was confirmed by electrophoresis on 1% agarose gel followed by ethidium bromide staining.

3.2.17. Quantitation of LDH-release

Cardiomyocytes were treated with 1% Triton X-100 (maximum LDH release or "high control"), with different treatments as indicated (indicated as "experimental values") or

kept untreated (spontaneous LDH release or "low control"). Cardiomyocyte conditioned medium was collected and filtered through 0.2-µm filter to remove any residual debris. LDH release in the supernatant was assessed by LDH-release detection kit (Roche Diagnostics) according to the manufacturer's instructions. Degree of cytotoxicity was calculated as described (Cabrera-Fuentes et al., 2013; Saffarzadeh et al., 2012).

3.2.18. Induction of mitochondrial membrane permeabilization

Rat cardiomyocytes were loaded with 100 nM tetramethyl-rhodamine-ethylester for 10 min, washed and maintained at 37°C in a control solution containing 140 mM NaCl, 3.6 mM KCl, 1.2 mM $MgSO_4$, 1 mM $CaCl_2$, 20 mM HEPES, 5 mM glucose, at pH 7.4. To induce oxidative damage resulting in mitochondrial membrane permeabilization, tetramethyl-rhodamine-ethylester-loaded cells were intermittently illuminated in an Olympus IX70 system with an Ar/Kr laser system (Yokogawa CSU10, Nipkow spinning disk, Visitech, UK) at 560 nm (2s every 3s, 30% intensity power). Mitochondrial permeabilization was detected as a decrease in 590 nm fluorescence emission that progressed as a wave throughout the cell and eventually induced rigor contracture secondary to ATP depletion, as previously described (Ruiz-Meana et al., 2007). Changes in fluorescent intensity were quantified with a commercial software (Voxcell Scan, Visitech, UK) and expressed as percentage of change throughout time with respect to the value obtained at baseline conditions.

3.2.19. NMR Spectroscopy

NMR spectroscopy was performed on a 9.4 T vertical bore magnet interfaced to a Bruker Avance spectrometer operating at 161.9 MHz as previously described (Inserte et al., 2011). Briefly, an additional series of hearts were subjected to the same study protocol but perfused with phosphate-free Krebs-Henseleit buffer. Phosphocreatine levels were normalized to pre-ischemic values.

3.2.20. ROS immunolabeling and fluorescent microscopy

Hearts from the different experimental groups were removed from the Langendorff system, weighed and rapidly frozen in liquid nitrogen. *In situ* reactive oxygen species (ROS) were determined using labeling with dihydroethidium as described (Abassi et al., 2011). Tissue sections were examined by laser scanning confocal microscopy (Leica TCS SP2, Mannheim, Germany). A series of confocal optical sections were obtained

using a Leica Planapo ×40/1.00 or ×63/1.32 objective lens. Each recorded image was obtained using dual-channel scanning and consisted of 1024 x 1024 pixels. To improve image quality and to obtain a high signal to noise ratio, each image from the series was signal-averaged. After data acquisition, the images were transferred to a workstation (Silicon Graphics, Fremont, CA) for restoration and three-dimensional reconstruction using Imaris 4.5 multichannel image processing software (Bitplane, Zurich, Switzerland).

For each heart at least 10 random fields of vision were analysed with a fluorescent microscope (Leica-Microsystems) using a x40 Planapo objective. Immunolabeled cryosections were studied using image analysis (Leica) and Image J software. Cardiomyocyte area and diameter were determined by delineating the β-actin-labeled myocytes. The fluorescence intensity was measured as AU/μm^2. For each quantification procedure a specific setting was established and kept constant in all measurements. Quantification of ROS was performed by measuring the fluorescence intensity using a range of 0 to 255 gray values. Arbitrary units of the fluorescence intensity were calculated per unit myocardial area (AU/μm^2).

3.2.21. Quantitation of TNF-α

Langendorff-heart perfusate and cardiomyocyte conditioned medium were collected and filtered through 0.2 μm filter to remove any residual debris. TNF-α production by heart tissue submitted to I/R or released from cardiomyocytes was assessed by enzyme-linked immune-sorbent assay (ELISA) (Quantikine®, R&D Systems) according to manufacturer's protocol. Absorbance values for individual reactions were determined using VersaMax™ Microplate Reader with SoftmaxPro 3.0 data processing software. TNF-α release was quantified (together with other cytokines) using the Cytokine Profiler (R&D Systems) according to manufacturer's protocol.

3.2.22. Tissue homogenization

Frozen ventricular tissue (25 mg) was pulverized using a mortar and a pestle in liquid nitrogen. Samples were then homogenized in TriPure isolation reagent (Roche Molecular Biochemicals) for extraction of total RNA and protein according to manufacturer's instructions.

3.2.23. RNA isolation and quantitative real time PCR analysis (qRT-PCR)

After incubation with or without eRNA (1 - 25 μg/ml), total cellular RNA was extracted from BMDM using T*RIzol*® Reagent (Invitrogen, USA). RNA samples were then subjected to RNA purification using the RNeasy minikit (Qiagen, USA). One μg of DNase-treated total RNA was reverse-transcribed using GoScript™ Reverse Transcription System (Promega, USA). Real-time quantitative RT-PCR (q-PCR) was performed at Genomics Core Facility, John A. Burns School of Medicine, Hawaii. The gene products were quantified using SYBR Green assays (Applied Biosystems).

DNA-free total RNA was extracted from plasma of mice using Zymo RNA MicroPrep kit (Zymo Research) omitting a lysis step and with an additional DNase digestion step, from the previously homogenised heart tissue, or from cardiomyocytes treated under different conditions and lysed using T*RIzol*® Reagent (Invitrogen). RNA samples were then subjected to RNA purification using the RNeasy minikit (Qiagen). One μg of DNase-treated total RNA was reverse-transcribed using GoScript™ Reverse Transcription System (Promega). cDNA fragments were amplified by 45 cycles of PCR (denaturing at 95°C for 15s, annealing at 58°C for 30s, and extension at 72°C for 30s); the last extension was performed at 50°C for 2 min. The gene products were quantified using SYBR Green assays (Applied Biosystems). Melting curve analysis and gel electrophoresis were performed to confirm the exclusive amplification of the expected PCR product. To determine the differences in expression, the CT values were normalized to reference gene using the ΔΔCt method, normalized for the expression of the reference gene and related to the control treatment. mRNA signal from *Hprt* or *GAPDH* was used for normalization, respectively. The 50 pmol of each primer was used; primer sequences are listed in **Table 2**.

Table 2. Real-Time rat and mice primer-probe sets used for RT-PCR Analysis.

Primer	Forward	Reverse
r-Hprt	5'- CCAGCGTCGTGATTAGTGAT-3'	5'- CAAGTCTTTCAGTCCTGT CC-3'
r-Prdx3	5'- TTAGCACCAGTTCCTCTTTCCA-3'	5'- CCCTTAAAGTCGTCGAGACTCA-3'
r-SOD1	5'- AAGGCCGTGTGCGTGCTGAA-3'	5'- ACATGGAACCCATGCTCGCCT-3'
r-SOD2	5'- ATGTTGTGTCGGGCGGCGTG-3'	5'- TCGCGTGGTGCTTGCTGTGG-3'
r-SOD3	5'- TGCTGCCTCCCGATCAGCCA-3'	5'- CCCTGGCTCAGGTCCCCGAA-3'
r-iNOS	5'- AAGAGACGCACAGGCAGAG-3'	5'- CAGCAGGCACACGCAATG -3'
r-MCP1	5'- TCACGCTTCTGGGCCTGTTGT-3'	5'- TCCAGCCGACTCATTGGGATCA-3'
r-TNF-α	5'- TCATGCACCACCATCAAGGA-3'	5'- GACATTCGAGGCTCCAGTGAA-3'
m-GAPDH	5'- GGCAAATTCAACGGCACAG-3'	5'- CGCTCCTGGAAGATGGTGA-3'
m-Serca 2a	5'- CCGATGACAATGGCACTTTCT-3'	5'-CTCCAGTATTGCAGGCTCCAG-3'
m-α-Sma	5'-CTGACAGAGGCACCATGAA-3'	5'-AGAGGCATAGAGGGACAGCA-3'
m-Tcf21	5'- CATTCACCCAGTCAACCTGA-3'	5'- CCACTTCCTTCAGGTCATTCTC-3'
m-Cd31	5'-CTCCAACAGAGCCAGCAGTA-3'	5'-GACCACTCCAATGACAACCA-3'
m-Cd115	5'-GACCTGCTCCACTTCTCCAG-3'	5'-CCAGTCCAAAGTCCCCAATC -3'
m-Elane	5'-GCACTGGCCTCAGAGATTGT-3'	5'-CCATGGCCAGACATGGAGTT-3'
m-Mcpt6	5'-GCAGCTAAGATGCTGAAGCG-3'	5'-GCAGCTAAGATGCTGAAGCG-3'
m-Inf-γ	5'-TGGCTCTGCAGGATTTTCAT-3'	5'-TCAAGTGGCATAGATGTGGA-3'
m-Tnf-α	5'-CATCTTCTCAAAATTCGAGTGACAA-3'	5'-TGGGAGTAGACAAGGTACAACCC-3'
m-Il-1β	5'-GGGCCTCAAGGAAAAGAATC-3'	5'-TTCTCCTTGAGAGGTGCTCA-3''
m-Il-6	5'-GAGGATACCACTCCCAACAGACC-3'	5'-AAGTGCATCATCGTTGTTCATACA-3'
m- Il-10	5'-TGCACTACCAAAGCCACAAGG-3'	5'-TGGGAAGTGGGTGCAGTTATTG-3'
m-Il-4	5'-CAACGAAGAACACCACAGAGAG-3'	5'-ATGAATCCAGGCATCGAAAAGC-3'
m-Il-12	5'-CCCTGTGCCTTGGTAGCATC-3'	3'-CTGAAGTGCTGCGTTGATGG-3'
m-Arg2	5'-CCTCCCTGCCAATCATGTTC-3'	5'-CCTCCCTGCCAATCATGTTC-3'
m-iNOS	5'-CTCTGGTCTTGCAAGCTGATGGTCA-3'	5'- TCCTGGAACCACTCGTACTTGGGAT-3'

Abbrevations: r (rat), m (mouse), *Hprt* (Hypoxanthine-phophoribosyl-transferase), *Prdx3* (peroxiredoxin 3), *SOD* (superoxide dismutase): *SOD1*-cytoplasmic, *SOD2*-mitochondrial, *SOD3*-extracellular, *iNOS* (inducible nitric oxide synthase), *MCP1* (monocyte chemoattractant protein-1), *TNF-α* (tumor necrosis factor-α), *GAPDH* (glyceraldehyde-3-phosphate dehydrogenase), *Serca2a* (Rohman et al., 2003) (Cardiac sarcoplasmic reticulum Ca^{2+} -ATPase2a), *α-Sma* (α-smooth muscle actin), *Tcf21* (Acharya et al., 2012) (bHLH transcription factor), *Cd31/PECAM-1* (Platelet endothelial cell adhesion molecule-1), *Cd115/Csf1r* (colony stimulating factor 1 receptor), *Elane* (neutrophil elastase), *Mcpt6* (tryptase beta-2), *Inf-γ* (Interferon-**γ**), *Il-* (Interleukin-), *Arg2* (arginase-2).

3.2.24. Western Blot analysis

Homogenised heart tissue or cardiomyocytes treated under different conditions were lysed using RIPA buffer as described previously (Fischer et al., 2012b). Thirty µg per lane of total protein was submitted to 12% SDS–polyacrylamide gel electrophoresis and subsequently blotted onto polyvinylidene difluoride membranes. Membranes were blocked with TBS containing 5% skim milk or 5% BSA, 50 mM Tris HCl, 150 mM NaCl, 0.1% Tween 20, pH 7.6 for 1 h at room temperature. Primary antibodies against IκBα and glycerinaldehyd-3-phosphat-dehydrogenase were purchased from Santa-Cruz and were used at 1:1,000 dilution. Secondary antibodies coupled to alkaline phosphatase were used at a dilution of 1:30,000. The Immun-Star™ alkaline phosphatase substrate (Bio-Rad) was used for detection according to the manufacturers' instructions. The protein bands were visualized by exposing the blots to Kodak Biomax MR Films and quantified with the help of the Bio-Rad Gel Doc 2000 system.

3.2.25. Statistics

Data were analyzed by ANOVA analysis of variance followed by Tukey's, Dunnett's or Bonferroni's multiple comparisons test was performed, when appropriate and paired and unpaired Student's *t*-test when analysing two groups to determine statistical significance of the differences using GraphPad Prism version 6.00 for Mac OS X, GraphPad Software, La Jolla California U.S.A. (www.graphpad.com). Significance values are *P<0.05, **P<0.01, ***P<0.001 and ns for non-significant (p>0.05).

4. Results

4.1. eRNA accumulates within lesions, whereas plasma RNase activity decreases with the progression of atherosclerosis

The presence of eRNA was evaluated by immuno-histochemical staining in aortic root tissue from 8 week old *Ldlr*$^{-/-}$ mice fed a chow diet and *Ldlr*$^{-/-}$ mice fed a HFD for 8, 12 or 36 weeks in comparison to chow-fed Bl6 wild type mice. While no eRNA was detected in chow-fed BL16 or *Ldlr*$^{-/-}$ mice (RNA staining detectable in DAPI^{+} cell nuclei only), eRNA accumulated in atherosclerotic lesions of HFD-fed *Ldlr*$^{-/-}$ mice in a time-progressive fashion (**Figure 4.1**).

Quantification of eRNA showed a continuous increase in both the media and intima of *Ldlr*$^{-/-}$ mice with increasing durations of HFD feeding; while relative staining for eRNA increased in the media exceeding that in the intima at early time points, eRNA was abundantly present predominantly in the intima at later time points, as reflected by an intense staining in this area **(Figure 4.1F)**.

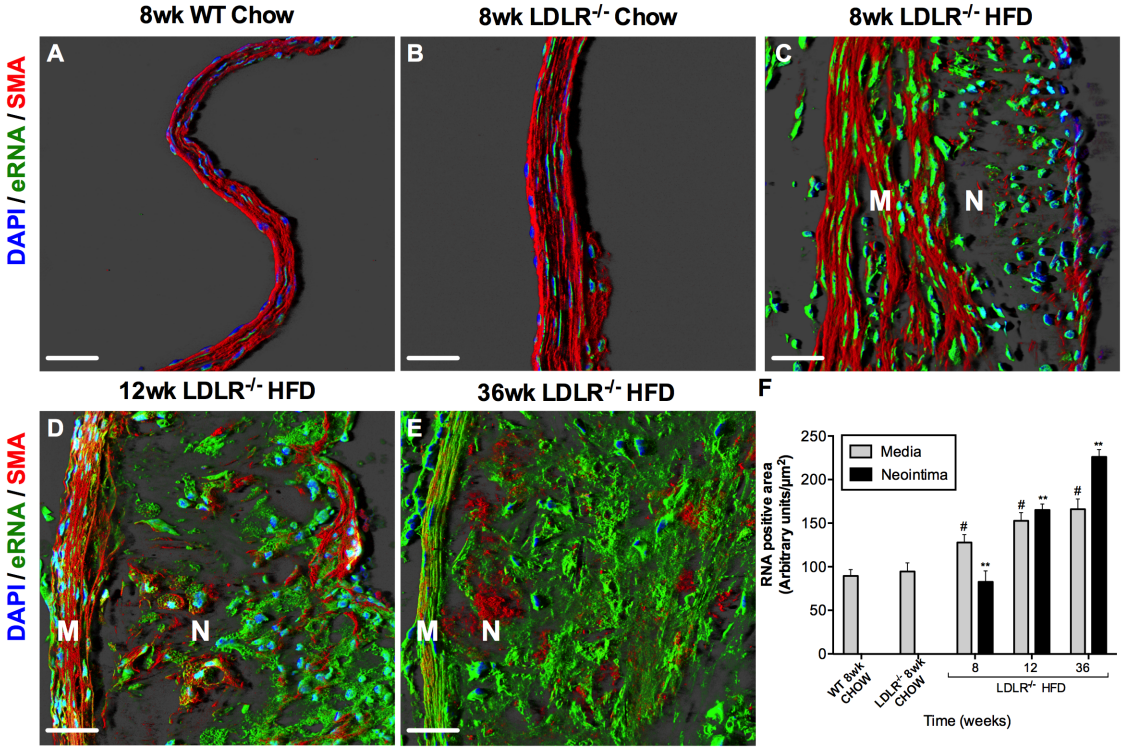

Figure 4.1. Time-progressive distribution of extracellular RNA (eRNA) in atherosclerotic lesions. The presence of eRNA in aortic root tissue from WT or *Ldlr*$^{-/-}$ mice fed a chow diet for 8 weeks **(A-B)** or from *Ldlr*$^{-/-}$ mice fed a high-fat-diet (HFD) for 8 **(C)**, 12 **(D)** or 36 weeks **(E)**, as indicated, confocal images with merged immunostaining for RNA-binding fluorescence dye (RNA-Select, green) together with cell nuclei staining (DAPI, blue) and smooth muscle cell actin (SMA, red); M: media; N: neointima. (n=6 per group). **(F)** Quantitative analysis of eRNA-associated fluorescence intensity in aortic root tissue in the media and neointima in wild-type (WT) and *Lldr*$^{-/-}$ mice fed a normal chow or high fat diet for indicated time periods. Values are expressed as mean ± SD from six independent experiments per group; #p<0.05 *vs*. media, and **p<0.001 *vs*. neointima in chow-fed *Lldr*$^{-/-}$ mice; One-way ANOVA, Dunnett's test.

After 36 weeks of HFD, eRNA was detectable not only along the luminal lining (**Figure 4.1E)** and in the vicinity of lesional MOMA-2^{+} macrophages (**Figure 4.2A-D**), but also within acellular necrotic core areas (**Figure 4.1E, Figure 4.2E-J**).

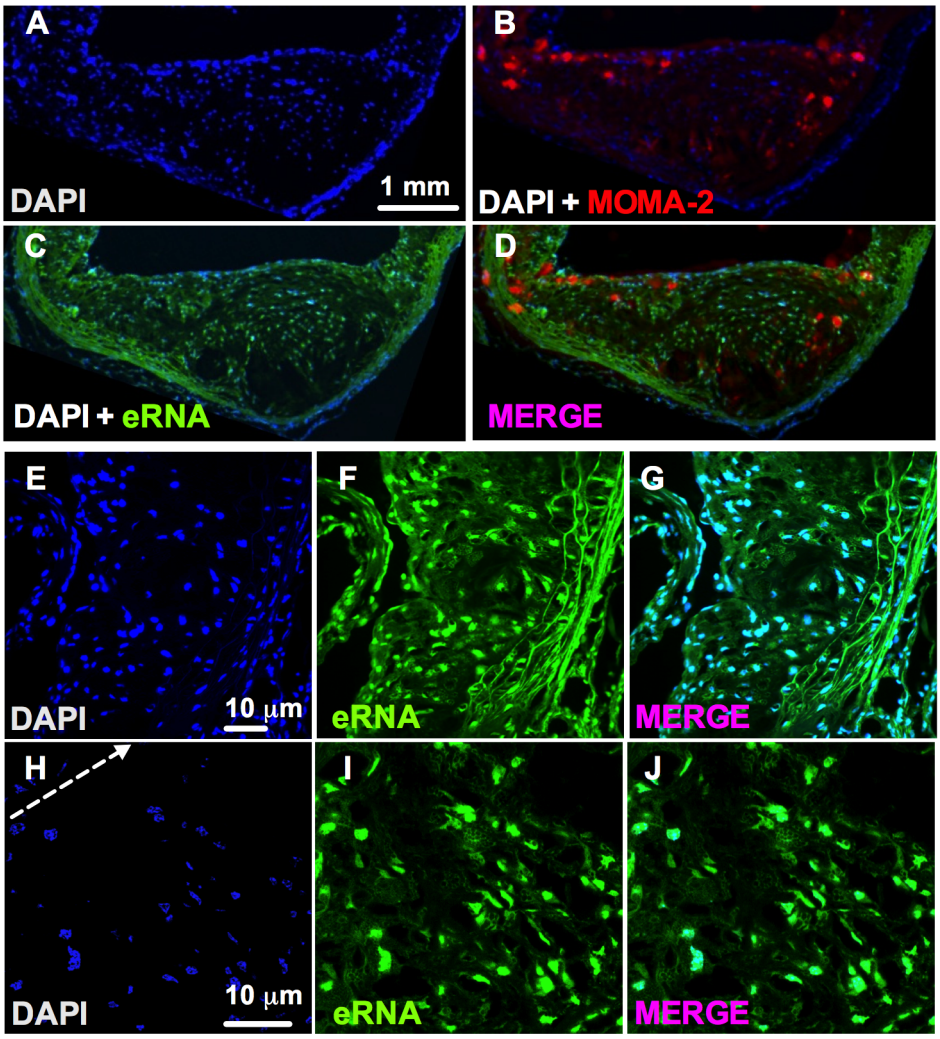

Figure 4.2. Co-localization of eRNA and macrophages in atherosclerotic lesions of *Ldr*$^{-/-}$ mice after 36 weeks on HFD. (A-D) Imunofluorescence staining in cryosections of atherosclerotic lesions from *Ldlr*$^{-/-}$ mice after 36 weeks on HFD. Staining for eRNA **(C)** was performed by an RNA-binding fluorescence dye (RNA-Select, green), macrophages **(B)** were identified by the anti-MOMA-2 monoclonal antibody (red), and cell nuclei **(A)** were marked by DAPI staining (blue). **(E-J)** Higher magnifications of atherosclerotic lesions are shown stained with DAPI (blue, E, H; arrow indicates cellular towards acellular necrotic core regions) and RNA-binding fluorescence dye (green, F,I); merged images are indicated in **(G, J)**. All images were obtained under identical conditions of confocal laser beam intensity and exposure time; representative images are displayed (n=4).

We further assessed RNA-degrading RNase activity in plasma samples from these mice during the course of HFD-feeding, and observed a biphasic characteristic with a temporary increase during the first 2 weeks (44 ± 9 *vs.* 70 ± 7 mU/mg protein; p=0.0012), followed by a significant and sustained decrease to about 20-40% of the

activity in baseline controls, starting at 4 weeks of HFD-feeding (44 ± 9 *vs*. 12 ± 2 mU/mg protein; p<0.0001) (**Figure 4.3**).

These data indicate that plasma RNase activity is enhanced in early atherosclerosis, but decreases during further plaque growth, when eRNA accumulates within atherosclerotic lesions in a time-progressive manner.

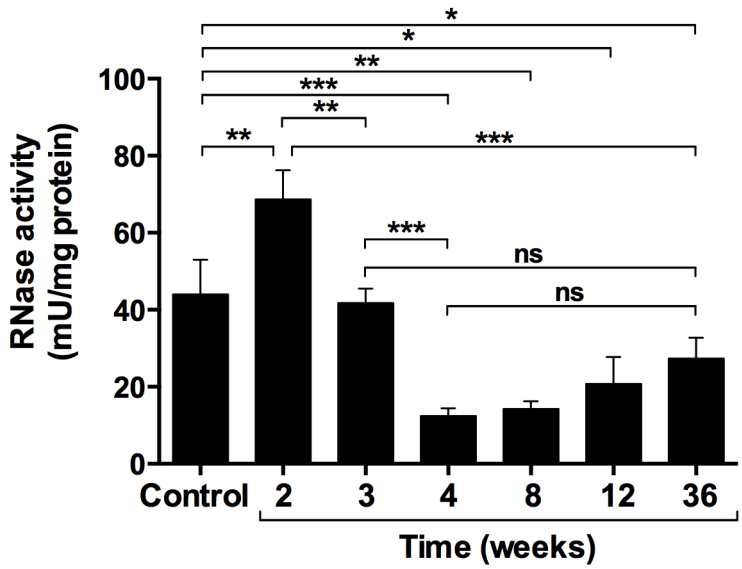

Figure 4.3. RNase activity in mouse plasma. RNase activity in *Ldlr*$^{-/-}$ mouse plasma was quantified for each time point and normalized to plasma protein concentration. Values are expressed as mean ± SD (n=6-12 per group); ns=non-significant, *p<0.05, **p<0.01, ***p<0.001; One-way ANOVA, Tukey's post test.

4.2. eRNA enhances cytokine secretion from macrophages

Given the association of eRNA with macrophages within atherosclerotic lesions, it was assessed whether eRNA induces inflammatory responses in macrophages. Upon 24 h of stimulation of bone marrow-derived macrophages (BMDM) with eRNA *in vitro*, mRNA expression of pro-inflammatory cytokines *Tnf-α*, *Arg2*, *Il-1β*, *Il-6*, *Ifn-γ* was significantly upregulated in a concentration-dependent manner, while a reciprocal down-regulation of the anti-inflammatory cytokines *Il-10* and *Il-4* was observed (**Figure 4.4A**). Similarly, recombinant mouse M-CSF-driven BMDM-differentiation was skewed towards the M1-phenotype by exposure to eRNA, resulting in overexpression of inflammatory markers such as *Tnf-α*, *Arg2*, *Il-1β*, *Il-6*, *Ifn-γ* together with *Il-12* and inducible nitric oxide synthase (*iNOS*), whereas anti-inflammatory genes together with *Arg1* and macrophage mannose receptor-2 (*Cd206*) were significantly downregulated by eRNA **(Figure 4.4B)**.

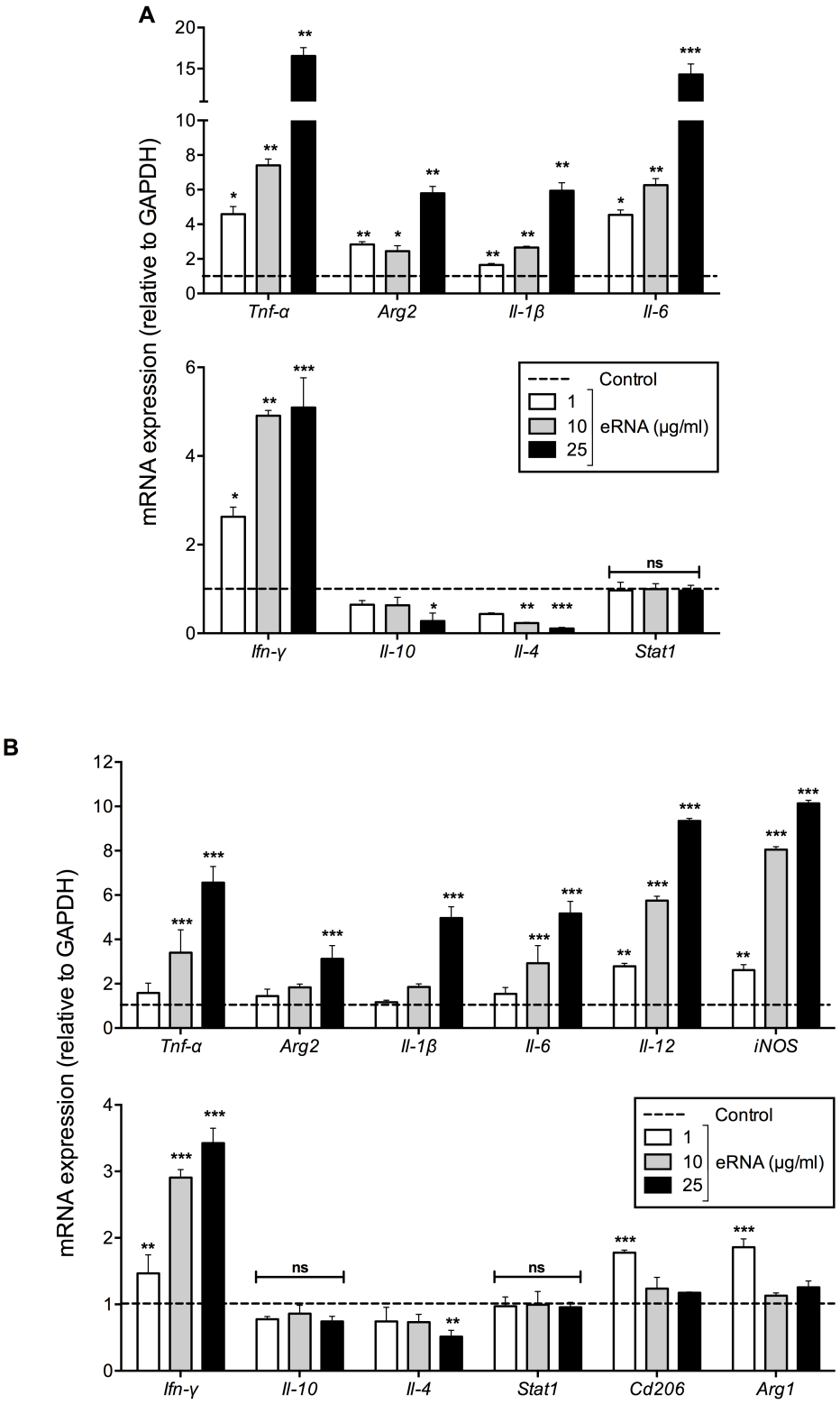

Figure 4.4. Influence of extracellular RNA on pro- and anti-inflammatory mediators in BMDM. mRNA expression of *Tnf-α, Arg2, Il-1β, Il-6*, *Ifn-γ, Il-10*, *Il-4* and *Stat1* in wild-type BMDM, differentiated in the presence of M-CSF-containing L929-conditioned medium **(A)** or in the presence of mouse recombinant M-CSF **(B)** was analyzed by real-time PCR in the absence (control, dotted line) or presence of eRNA (1, 10, or 25 μg/ml) for 24 h. Data are expressed as changes in the ratio between target gene expression and *GAPDH* mRNA. Values represent mean ± SD (n=6 per group); *p<0.05, **p<0.01, ***p<0.001 vs. control, ns = non-significant; One-way ANOVA, Dunnett's test.

The capacity of GM-CSF-driven BMDM-differentiation (already representing a M1-phenotype) (Neu et al., 2013; Tugal et al., 2013) towards further M1 polarization in response to eRNA was moderate; nevertheless, a significant down-regulation of M2 markers was confirmed (**Figure 4.4**). In accordance with our proposal, these data clearly corroborate that self-eRNA serves as a pro-inflammatory alarming signal.

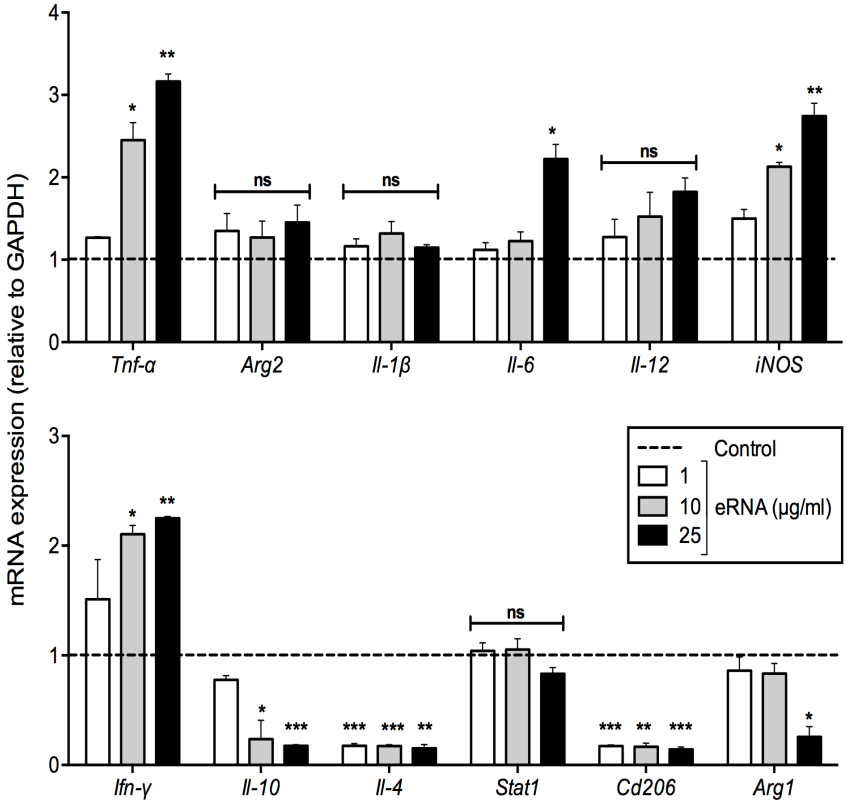

Figure 4.5. Influence of extracellular RNA on pro- and anti-inflammatory mediators in GM-CSF-driven BMDM. mRNA expression of *Tnf-α, Arg2, Il-1β, Il-6*, *Il-12, iNOS, Ifn-γ, Il-10*, *Il-4*, *Stat1, Cd206* and *Arg1* in wild-type BMDM, differentiated in the presence of mouse recombinant GM-CSF was analyzed by real-time PCR in the absence (control, dotted line) or presence of eRNA (1, 10, or 25 µg/ml) for 24 h. Data are expressed as changes in the ratio between target gene expression and *GAPDH* mRNA. The results were obtained from three independent experiments carried out in duplicates. Values represent mean ± SD; *p<0.05, **p<0.01, ***p<0.001 *vs*. control, ns = non-significant; One-way ANOVA, Dunnett's test.

Accordingly, the release of TNF-α and IL-6 proteins into the cell supernatants was significantly increased by eRNA stimulation in a concentration-dependent manner (**Figure 4.6**).

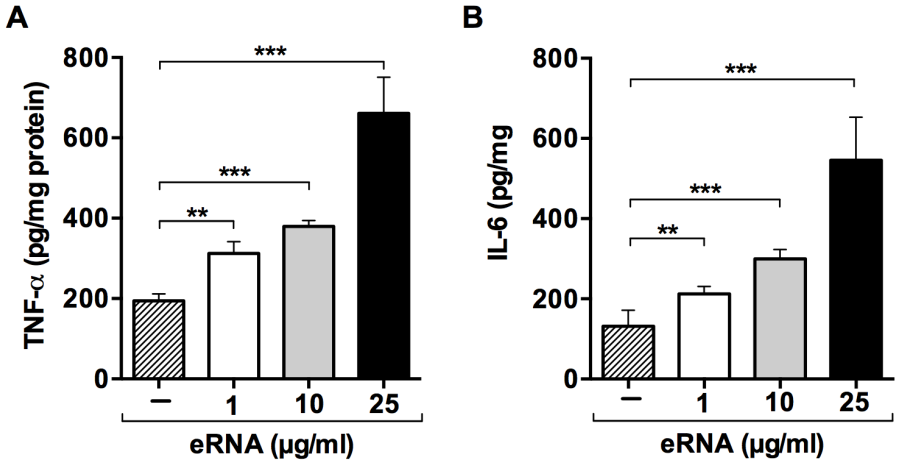

Figure 4.6. Influence of extracellular RNA on the release of pro-inflammatory cytokines. (A) TNF-α or **(B)** IL-6 protein concentration was measured in the supernatants of BMDM following treatment in the absence (control) or presence of eRNA (1, 10, or 25 µg/ml) as indicated. Values correspond to mean ± SD (n=9 per group). *p<0.05, **p<0.01, ***p<0.001, ns=non-significant; One-way ANOVA, Dunnett's test.

We furthermore assessed whether these effects were mediated by eRNA-induced Toll-like receptor (TLR)-mediated signaling. Based on findings that no changes in *Stat1* expression were found in macrophages upon stimulation with eRNA (**Figure 4.4A**,**B** and **Figure 4.5**), we can conclude that eRNA does not engage in TLR-2 and TLR-4 signalling (Rhee et al., 2003). Likewise, no alterations in the mRNA expression of the cytokines studied were observed after poly-IC treatment **(Figure 4.7)**, indicating that also TLR-3 did not contribute to eRNA-mediated cytokine induction. Thus, eRNA functions as a powerful inducer of inflammatory cytokine responses in macrophages, independent of TLR-2, TLR-3 and TLR-4 signaling.

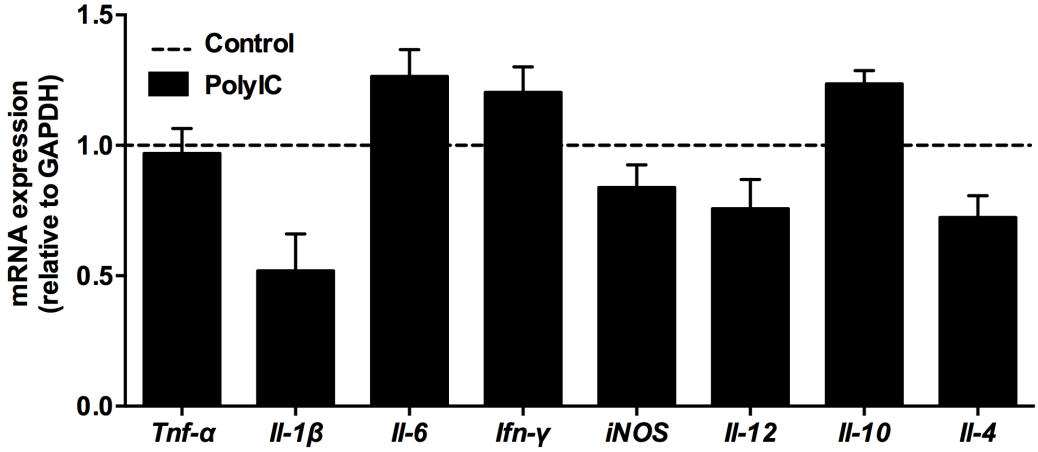

Figure 4.7. Influence of PolyIC on pro- and anti-inflammatory mediators in BMDM. mRNA expression of *Tnf-α, Il-1β, Il-6*, *Ifn-γ, iNOS, Il-12*, *Il-10* and *Il-4* in wild-type BMDM, differentiated in the presence of M-CSF-containing L929-conditioned medium was analyzed by real-time PCR in the absence (control, dotted line) or presence of 10 µg/ml PolyIC for 24 h. Data are expressed as changes in the ratio between target gene expression and *GAPDH* mRNA. Values represent mean ± SD (n=6 per group); *p<0.05, **p<0.01, ***p<0.001 vs. control, ns = non-significant; One-way ANOVA, Dunnett's test.

4.3. Association between eRNA and TNF-α in myocardial I/R injury during cardiac surgery

Upon tissue damage or vascular injury, significant amounts of extracellular RNA (eRNA) (composed predominantly of 18S and 28S ribosomal RNA) are released that promote procoagulant and proinflammatory processes, as was observed in our earlier studies (Fischer et al., 2011; Kannemeier et al., 2007; Walberer et al., 2009). To characterize the pathogenic situation of cardiac ischemia/reperfusion (I/R) injury in this respect, 14 cardiac patients **(Table 1)** were analysed for eRNA and tumor necrosis factor-α at different time points during surgery: Blood samples were taken from the radial artery, directly before and after aortic clamping as well as from the coronary sinus.

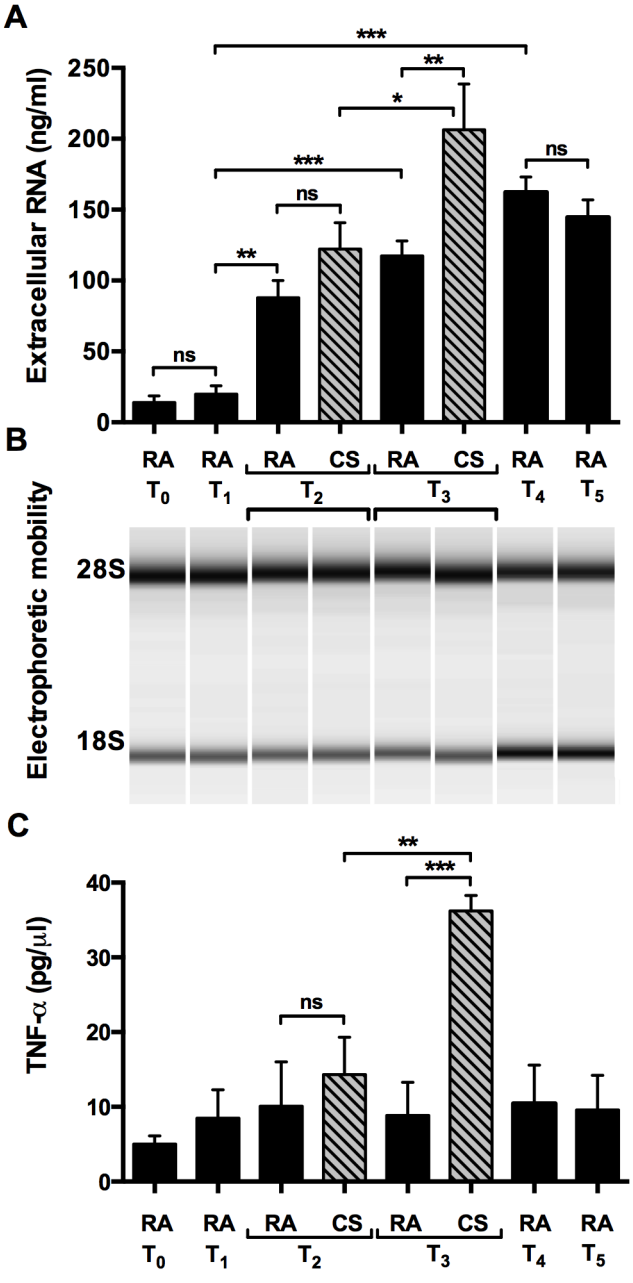

Figure 4.8. Association between eRNA and TNF-α in myocardial I/R injury during cardiac surgery. (A) Extracellular RNA and **(C)** TNF-α were quantified in plasma from cardiac patients undergoing surgery that was withdrawn from radial artery (RA) or coronary sinus (CS) at the indicated time points: T_0 (anesthesia induction – basal level), T_1 (thoracotomy), T_2 (2 min before aortic clamping), T_3 (2 min before aortic unclamping), T_4 (15 min after aortic unclamping), T_5 (30 min after aortic unclamping). Data represent mean ± SEM (n=14); *p<0.05, **P<0.01, ***P<0.001, ns=non-significant; Two-way ANOVA, Bonferroni's test.
(B) Representative analysis of patient´s extracellular RNA, isolated from plasma and subjected to capillary gel electrophoresis, reveals high RNA stability, indicated by the 28S and 18S rRNA bands at each time point.

Figure 4.8A demonstrates a massive increase by 10 to 20 fold of eRNA (predominantly intact 18S/28S rRNA) **(Figure 4.8B)** and a significant elevation of TNF-α (>7-fold) **(Figure 4.8C)** particularly in coronary sinus blood after aortic clamping. This indicates that ischemic, albeit cardioplegia-protected, human myocardium is a major source of eRNA during cardiac surgery which may, in concert with TNF-α, contribute to the pathogensis of I/R injury and myocardial infarction.

4.4. eRNA promotes I/R injury and myocardial infarction

In order to prove the release of eRNA upon ischemic heart disease, a myocardial infarction model in mice and the isolated rat Langendorff heart model, exposed to I/R injury, were investigated. Following coronary artery ligation in mice for 60 min, eRNA levels were significantly elevated during the subsequent 120 min reperfusion phase **(Figure 4.9A)**. In order to delineate the cellular origin of eRNA, RT-PCR analysis was carried out to amplify cell-specific mRNA that was found associated with the released 18S/28S rRNA **(Figure 4.9B, insert)**. Results indicate that eRNA is derived mainly from cardiomyocytes (expressing SERCA; Rohman et al., 2003) and to a much lesser degree from smooth muscle cells (expressing α-smooth muscle actin; Simsekyilmaz et al., 2014) and myofibroblasts (expressing bHLH transcription factor - *Tcf21*; Acharya et al., 2012) **(Figure 4.9B)**.

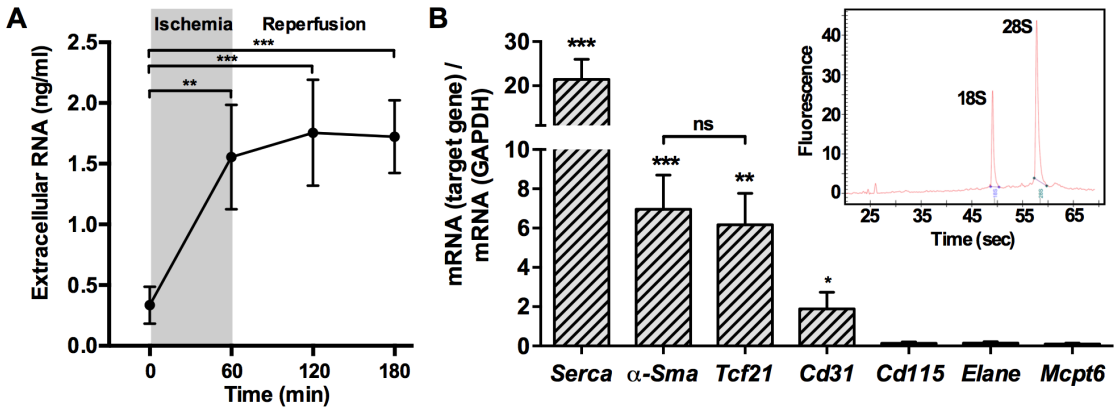

Figure 4.9. Release of extracellular RNA during myocardial infarction following I/R. (A) Following induction of the *in vivo* cardiac I/R mice model with 60 min ischemia and 180 min reperfusion, plasma extracellular RNA was quantified at the indicated time points. Data represent mean ± SEM (n=6 mice per group); **P<0.01, ***P<0.001; Two-way ANOVA, Post-hocs test. **(B)** After coronary ligation for 60 min without reperfusion, the mRNAs of the following genes were quantified by real-time PCR to deduce their cellular origin: *Serca* – cardiomyocytes, α-*Sma* – smooth muscle cells, *Tcf21* – cardiac fibroblast, *Cd31* – endothelial cells, *Cd115* – macrophages, *Elane* – neutrophils and *Mcpt6* – mast cells. Values are expressed as mean ±SEM (n=6); *P<0.05, **P<0.01, ***P<0.001 *vs GAPDH* expression; One-way ANOVA, Tukey's post test. The insert indicates the electropherogram of 28S and 18S rRNA in a representative sample.

After excision and perfusion equilibration of isolated rat hearts on the Langendorff apparatus, blood-free perfusion was arrested for 45 min to achieve global ischemia and thereafter, reperfusion was resumed for 120 min. At the start of the reperfusion phase, a significant increase in eluted eRNA was observed **(Figure 4.10A)**, together with other markers of myocardial injury such as lactate dehydrogenase (LDH), cardiac troponins and creatine kinase (Vorderwinkler et al., 1996) (data not shown). In contrast to the latter parameters, a second washout peak of eRNA during reperfusion between 15 and 60 min was noted that related to more than 60% of the totally recovered eRNA. Analysis of eRNA collected from the entire 120 min reperfusion phase revealed a significant portion of microparticle-associated eRNA **(Figure 4.10A, insert)**.

To further delineate these findings in a cell culture model, a significant increase in the accumulation of eRNA in the supernatants of isolated cardiomyocytes, exposed to hypoxia for 1h, as compared to 3h of normoxia, was observed **(Figure 4.10B)**. Moreover, exposure of cells towards TNF-α significantly enhanced the eRNA release, both under normoxic and hypoxic conditions.

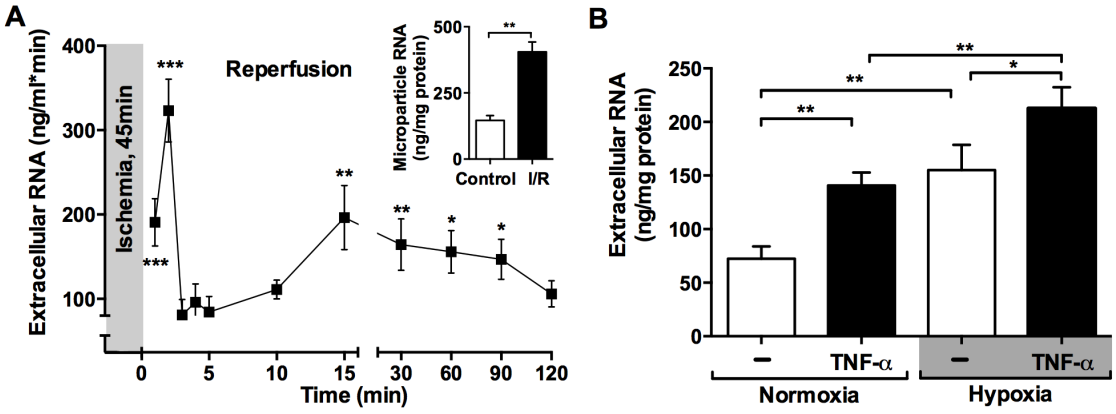

Figure 4.10. eRNA increases after cardiac injury. (A) Isolated rat hearts (Langendorff-model) were submitted to I/R (45 min ischemia, followed by 120 min reperfusion), and extracellular RNA was quantified in the effluent fractions for each time point. Values are normalized to the effluent protein concentration and represent mean ± SD (n=9 hearts) as compared to the minimal values at 3-5 min; *P<0.05, **P<0.01, ***P<0.001; One-way ANOVA, Tukey's post test. The insert indicates the microparticle-associated total RNA that was quantified from collected perfusate over 120 min and normalized to the effluent protein concentration. Values represent mean ± SD (n=9 hearts); **P<0.01; unpaired t test. (**B**) Extracellular RNA was quantified under normoxia (3h) or hypoxia (1h) in supernatants of untreated (-) or TNF-α-treated cardiomyocytes. Values represent mean ± SD (n=6); *P<0.05, **P<0.01; One-way ANOVA, Bonferroni's test.

4.5. Hypoxia and eRNA promote cardiac I/R-induced TNF-α release

To define the conditions of I/R injury under which TNF-α release occurs, *in vivo*, *ex vivo* and *in vitro* experiments were performed. While in the murine heart ligation model under constant perfusion no significant TNF-α liberation was observed in the animal circulation **(Figure 4.11A)** as well as in heart tissue **(Figure 4.11B)**, exposure to ischemia for 60 min, followed by various time intervals of reperfusion (0, 2 and 120 min) all resulted in massive increase in TNF-α release with I/R of 60 min/2 min showing the highest value (>20 fold) **(Figure 4.11A)**. These conditions were also associated with a dramatic appearance of TNF-α in heart tissue of these animals **(Figure 4.11B)**. While the administration of RNase1 resulted in a drastic reduction of TNF-α release and tissue deposition, the application of an RNase inhibitor (RI) had no significant influence on the eRNA/hypoxia-induced liberation of TNF-α.

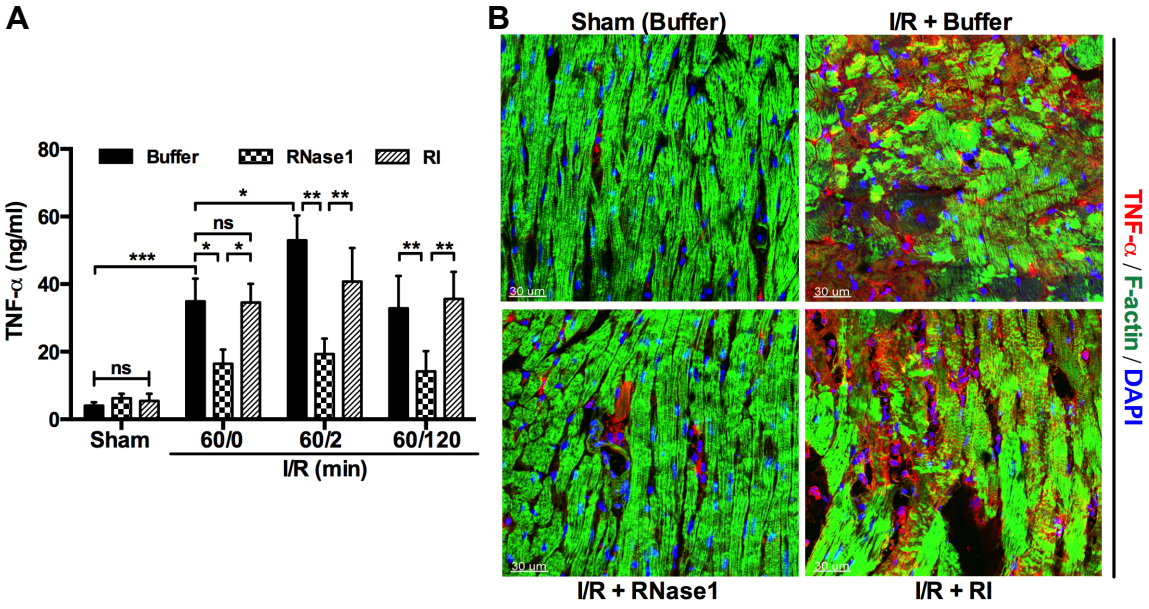

Figure 4.11. Extracellular RNA potentiates the release of TNF-α under hypoxia. (**A**) After induction of the *in vivo* cardiac ischemia/reperfusion (I/R) mice model, sham-operated or coronary occluded animals with the following time intervals of I/R (in min): 60/0, 60/2 and 60/120, respectively, were left untreated (Buffer) or were treated with RNase1 (100 µg/mice) or RNase-inhibitor (RI, 80 U/mice) as indicated, and plasma TNF-α was quantified at the end of the respective experiment. Data represent mean ± SD (n=6-8 mice per group); *P<0.05, **P<0.01, ns=non-significant; One-way ANOVA, Dunnett's test. (**B**) Following induction of the *in vivo* cardiac I/R (60 min/120 min) mice model, the presence of TNF-α in cryosections from heart tissue was demonstrated by confocal microscopy. Representative merged images from immunofluorescence staining for TNF-α (red), F-actin (green) and nuclear DNA (DAPI, blue) are displayed. All images were obtained under identical conditions of confocal laser beam intensity and exposure time (n=6).

Upon I/R exposure in isolated rat hearts, significantly increased levels of TNF-α were detectable in the perfusate during the initial 15 min reperfusion phase in accordance with a report in which the gene for this cytokine was found to be transcribed during this I/R phase (Gilles et al., 2003). Treatment with RNase1 reduced the level of TNF-α almost to background values **(Figure 4.12A)**, while after 120 min reperfusion, TNF-α mRNA was significantly decreased in the RNase1 treatment group **(Figure 4.12B)**. In contrast, administration of RI had neither an influence on liberation of TNF-α nor on its mRNA expression when compared to the I/R group.

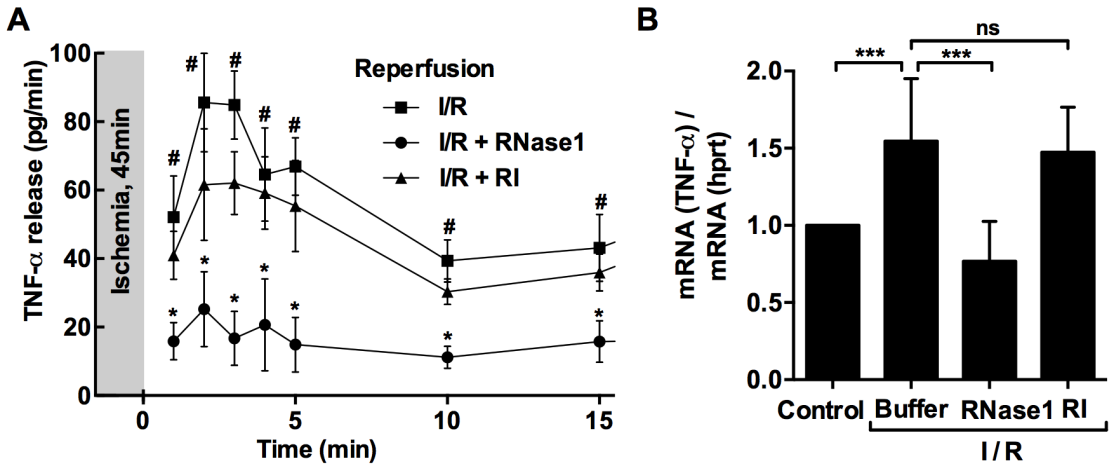

Figure 4.12. Ischemia potentiates the release and production of TNF-α. (**A**) TNF-α-release was quantified in fractions throughout the first 15 min reperfusion period in the Langendorff heart, submitted to the I/R protocol in the absence (squares) or presence of 10 µg/ml RNase1 (circles) or 2 U/ml RI (triangles). TNF-α values are corrected for the respective flow rate and normalized to the effluent protein concentration and represent mean ± SD (n=3-6 hearts); $^{\#}$P<0.001 (I/R *vs.* pre-ischemic values); *P<0.001 (I/R+RNase1 *vs.* I/R); One-way ANOVA, Dunnett's test. (**B**) TNF-α mRNA was quantified by RT-PCR at the end of the I/R protocol in isolated rat hearts, perfused for 3h under normoxia (control) or submitted to the Langendorff I/R protocol alone or in the presence of RNase1 (10 µg/ml) or RI (2 U/ml). Data represent mean ± SD (n=3-6 mice per group); ***P<0.001, ns=non-significant; One-way ANOVA, Dunnett's test.

In previous studies, we have demonstrated that exposure of monocytes to eRNA resulted in the induction of TNF-α release, which largely relied on the sheddase TNF-α-converting enzyme (TACE/ADAM17) (Fischer et al., 2012). Likewise, upon stimulation of cardiomyocytes by eRNA under normoxic conditions, a significantly enhanced release of TNF-α was noted, while in the presence of RNase1, TNF-α shedding was minimal. eRNA-induced TNF-α liberation was confirmed by data from a cytokine profile array, showing a significant increase of TNF-α under conditions of normoxia and hypoxia **(Figure 4.13A)**. Moreover, upon incubation of cardiomyocytes

with eRNA for 1h under hypoxia, a significantly elevated TNF-α release was noted that was totally prevented by RNase1 treatment **(Figure 4.13B)**. RNase1 alone was also effective under hypoxia as significantly reduced the level of released TNF-α **(Figure 4.13B)**.

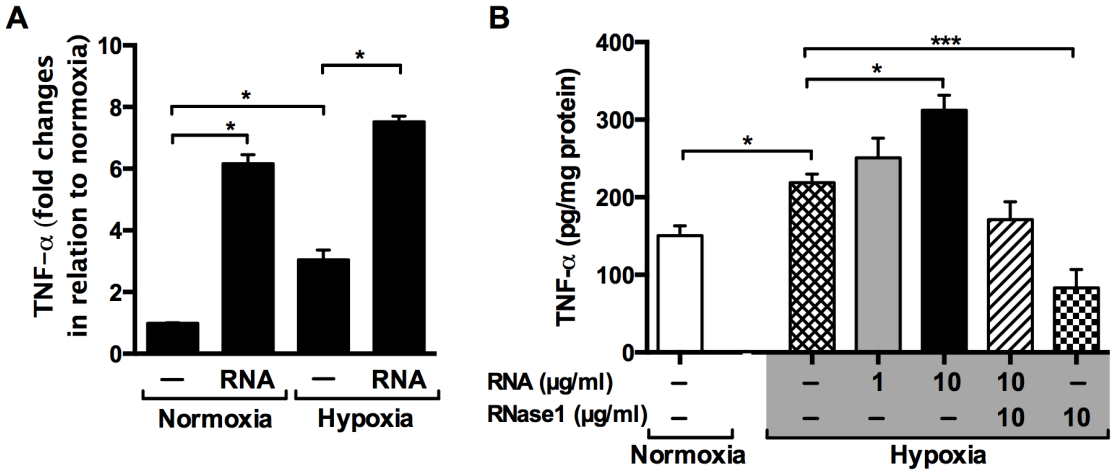

Figure 4.13. Induction of TNF-α expression and release by extracellular RNA, reinforced under hypoxia. (A) eRNA-induced TNF-α liberation was confirmed by data from a proteome/cytokine profiler array, showing a significant increase of TNF-α under normoxia and hypoxia. Values represent mean ± SD (n=3); *p<0.05; One-way ANOVA, Dunnett's test. **(B)** Cardiomyocytes were treated under normoxia (3h) or hypoxia (1h) with RNA, hydrolyzed RNA or RNase1 (10 µg/ml), followed by analysis of TNF-α in corresponding cell supernatants. Values represent mean ± SD (n=3); *P<0.05, **P<0.01, ***P<0.001; One-way ANOVA, Dunnett's test.

4.6. Production of reactive oxygen species (ROS) during I/R injury and prevention by RNase1

The production of ROS during ischemic heart disease is a causally-related hall-mark in the pathogenesis of myocardial infarction, playing a significant role in damaging the heart during I/R (Carpi et al., 2009; Rodrigo et al., 2013).

Upon exposure of mice to 60 min regional ischemia (by coronary artery ligation), followed by different time intervals of reperfusion, inspection of heart tissue by confocal microscopy revealed a markedly disturbed cardiomyocyte structure, accompanied by a significant elevation of ROS, which were found at intra-nuclear sites overlapping with the DAPI stain for condensed DNA, both in **Figure 4.14**.

The same was true when tissue samples from the isolated Langendorff heart model, under conditions of 45 min ischemia and various reperfusion intervals, were inspected **(Figure 4.15)**.

In contrast, in RNase1-treated mice or isolated rat hearts, not only was the tissue architecture greatly preserved, but the fluorescence intensity of ROS was low, similar to control sections, not exposed to I/R. ROS content in cardiac tissue (mice: 199 ± 15 AU/μm^2, isolated rat hearts: 209 ± 11 AU/μm^2) following I/R was reduced upon RNase1 treatment to 88 ± 20 AU/μm^2 in mice and 70 ± 12 AU/μm^2 in isolated rat hearts ($P<0.001$ for each case) **(Figure 4.16)**. As expected, RI treatment did not prevent tissue destruction, and ROS accumulation was as extensive as in the non-treated I/R injury groups.

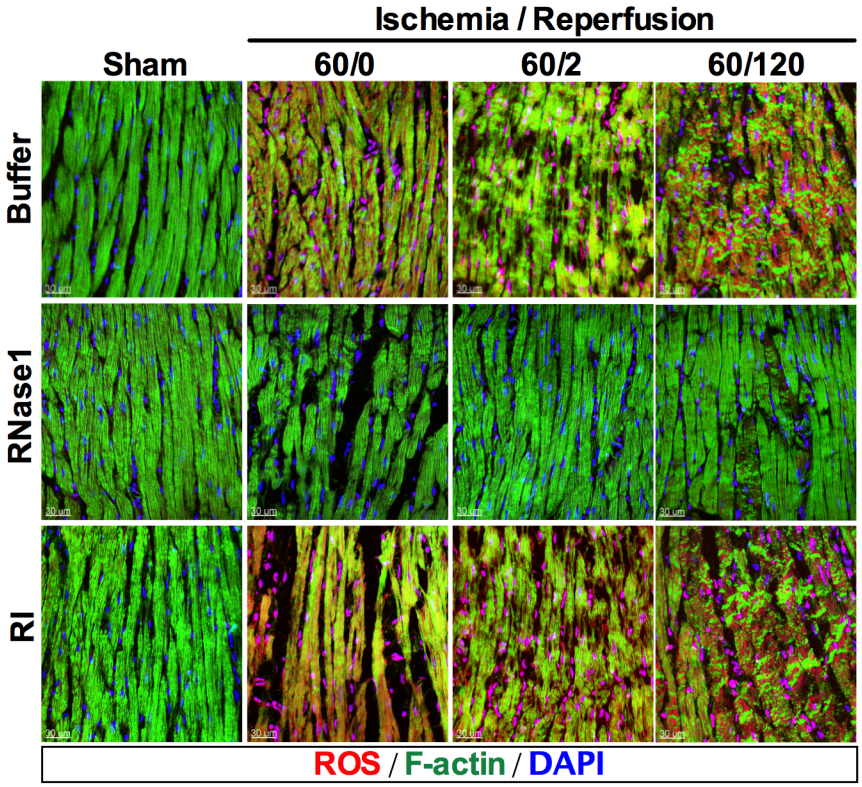

Figure 4.14. *In vivo* prevention of ROS production by RNase1. After induction of the *in vivo* cardiac I/R mice model, sham-operated or coronary occluded animals with the following time intervals of I/R (in min): 60/0, 60/2 and 60/120, respectively, were left untreated (Buffer) or were treated with RNase1 (100 μg/mice) or RNase-inhibitor (RI, 80 U/mice) as indicated. Representative merged images from immunofluorescence staining for ROS (dihydroethidium, red) production together with detection of F-actin (green) and nuclear DNA (DAPI, blue) are displayed. All images were obtained under identical conditions of confocal laser beam intensity and exposure time (n=6-8 per group).

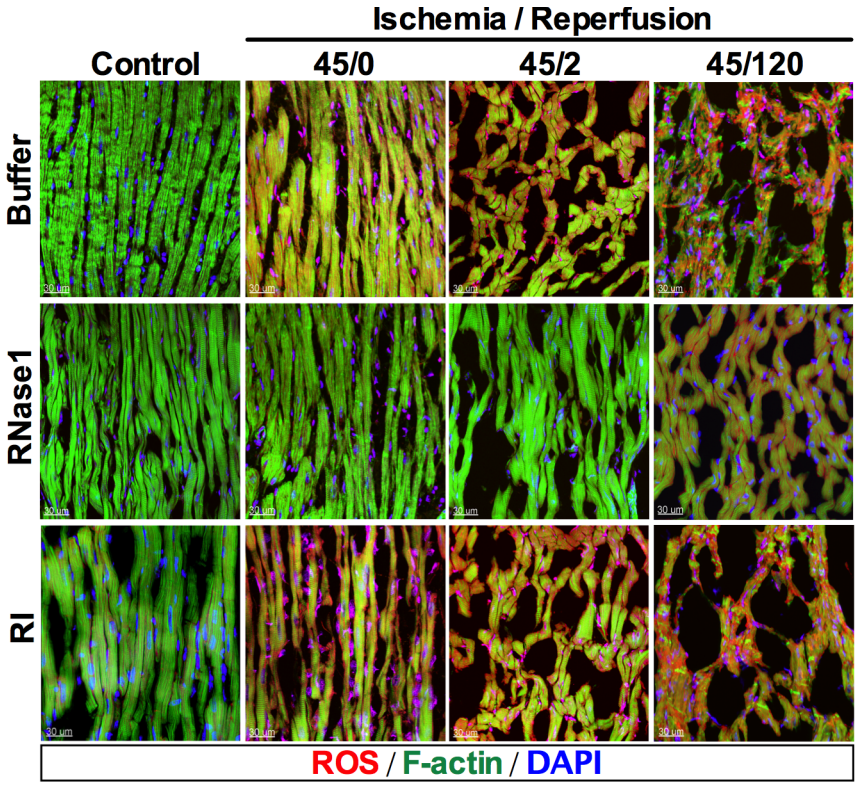

Figure 4.15. *Ex vivo* prevention of ROS production by RNase1. Isolated Langendorff-perfused hearts were either submitted to 3h perfusion under normoxia (control) or exposed to the I/R protocol with the following time intervals of I/R (in min): 45/0, 45/2, 45/120, in the absence (Buffer) or in the presence of RNase1 (10 µg/ml) or RI (2 U/ml) as indicated. Representative merged images from immunofluorescence staining for ROS (dihydroethidium, red) production together with detection of F-actin (green) and nuclear DNA (DAPI, blue) are displayed. All images were obtained under identical conditions of confocal laser beam intensity and exposure time (n=6-8 per group).

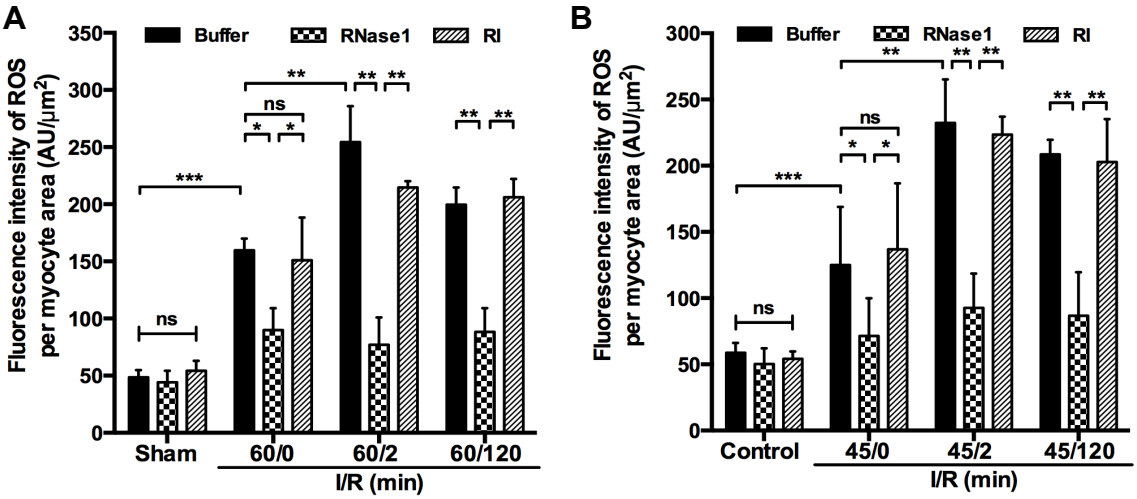

Figure 4.16. RNase1 significantly prevents ischemic ROS production. The distribution of ROS (dihydroethidium, red) production together with detection of F-actin (green) and nuclear DNA (DAPI, blue) was quantified by immunofluorescent staining in microslices of mice (*in vivo*, **A**) or rat (*ex vivo*, **B**) cardiac tissue in each case. All samples received the same manipulation and all images were obtained under identical conditions of laser beam intensity and exposure time using confocal microscopy. Values represent mean ± SD (n=6-8 per group); *P<0.05, **P<0.01, ***P<0.001; One-way ANOVA, Dunnett's test.

To further substantiate the influence of anti-oxidant enzymes in cardiomyocytes on ROS production, RT-PCR analysis of peroxiredoxin 3 and isoforms of superoxide dismutase (SOD), representing cytoplasmic SOD1, mitochondrial SOD2 and extracellular SOD3, was performed in the Langendorff heart model as well as in isolated cardiomyocytes, exposed to the ischemia-related protocols. While low mRNA levels of these antioxidant enzymes were found in the isolated heart after 120 min reperfusion only, administration of RNase1 in isolated hearts submitted to I/R resulted in significantly elevated mRNA levels of these enzymes, particularly peroxiredoxin 3 and SOD2 **(Figure 4.17A)**. Likewise, upon 3h exposure of isolated cardiomyocytes towards eRNA or TNF-α under normoxia, significantly reduced mRNA levels of the indicated antioxidant enzymes were found **(Figure 4.17B)**, whereas RNase1 application fully restored their expression at normal values. The administration of the TACE-inhibitor TAPI in isolated cardiomyocytes led to a superimposable beneficial restoration of mRNA expression of the antioxidant enzymes as well **(Figure 4.17B)**.

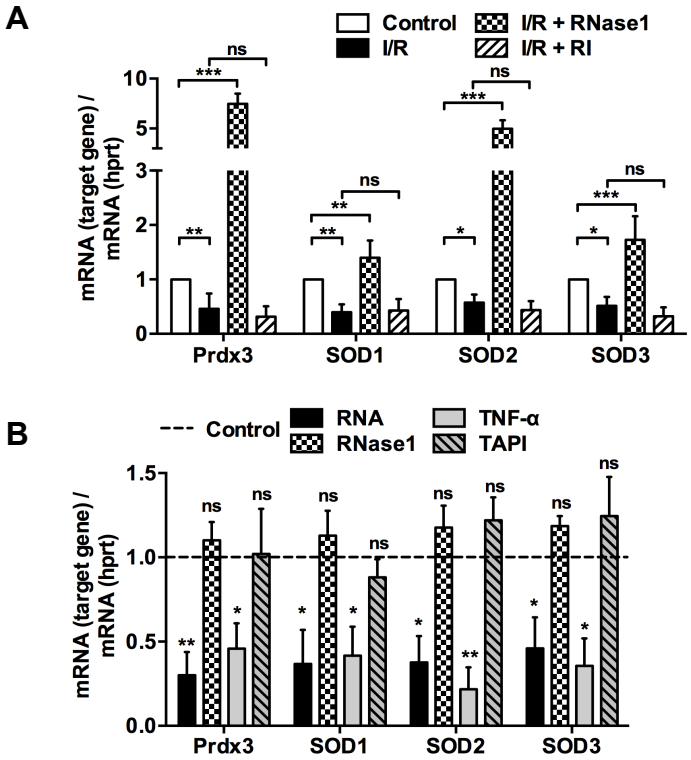

Figure 4.17. Extracellular RNA and TNF-α mediate down-regulation of antioxidant enzymes in cardiomyocytes. (A) The mRNA level of peroxiredoxin 3 (Prdx3) and superoxide-dismutases (SOD) 1-3 in cardiac tissue obtained from Langendorff hearts submitted to 3h normoxic perfusion (control) or submitted to the I/R protocol alone or in the presence of RNase1 (10 μg/ml) or RI (2 U/ml) are indicated. Data indicate changes in the ratio between target and hprt mRNA and represent mean ± SD (n=3 hearts); *P<0.05, **P<0.01, ***P<0.001, ns=non-significant; One-way ANOVA, Dunnett's test. **(B)** mRNA levels of Prdx3, SOD1, SOD2 and SOD3 in cardiomyocytes, untreated (control) or treated with 10 μg/ml extracellular RNA, 10 μg/ml RNase1, 20 ng/ml TNF-α or 10 μM TAPI, respectively, for 3h under normoxia were quantified by RT-PCR. Data represent changes in the ratio between target and hprt mRNA (n=3, each in duplicate) with mean ± SD; *P<0.05, **P<0.01; One-way ANOVA, Dunnett's test.

4.7. RNase1 protects against cardiac I/R injury and reduces infarct size

Following induction of acute cardiac I/R injury in the mouse model, infarct size expressed as a percentage of the area of risk was smaller in hearts administered with RNase1 when compared to those administrated with buffer alone or RI, respectively **(Figure 4.18)**, indicative of the causal contribution of eRNA to cardiac tissue damage.

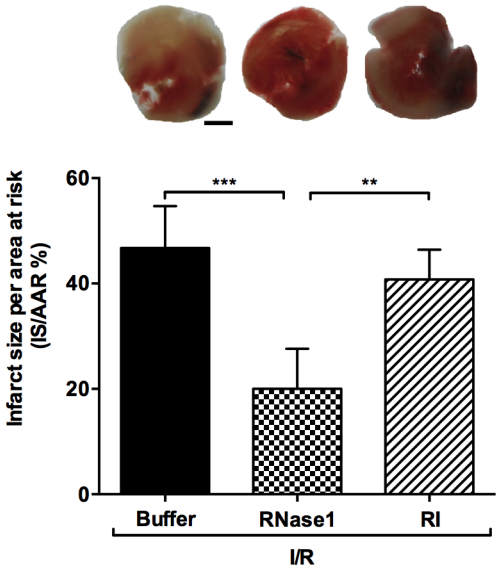

Figure 4.18. Prevention of acute myocardial infarction by RNase1. Following the induction of the *in vivo* acute cardiac I/R mice model, infarct size in mice hearts was quantified after coronary occlusion followed by 2h reperfusion in the absence (Buffer) or presence of RNase1 (100 µg/mice) or RNase-inhibitor (RI, 80 U/mice), respectively. Representative pictures show myocardial infarct size in heart sections indicated by dual staining with 2,3,5-triphenyltetrazolium (TTC) and Evans blue. Data represent mean ± SEM (n=6-8 mice per group); *P<0.05, ***P<0.001, ns=non-significant; One-way ANOVA, Dunnett's test.

Likewise, vehicle-treated mice after 14 days of reperfusion developed myocardial infarcts comparable to the RI-treated group (16 ± 3% vs. 15 ± 2%), whereas the RNase1 treatment group (3 ± 1%) was protected against infarct development **(Figure 4.19)**. Intra-ventricular measurements revealed a significant decrease in left ventricular developed pressure, contraction and relaxation in the control and RI-treated groups, whereas the RNase1-treated group exhibited preserved heart function comparable with sham or uninjured mice **(Figure 4.20)**.

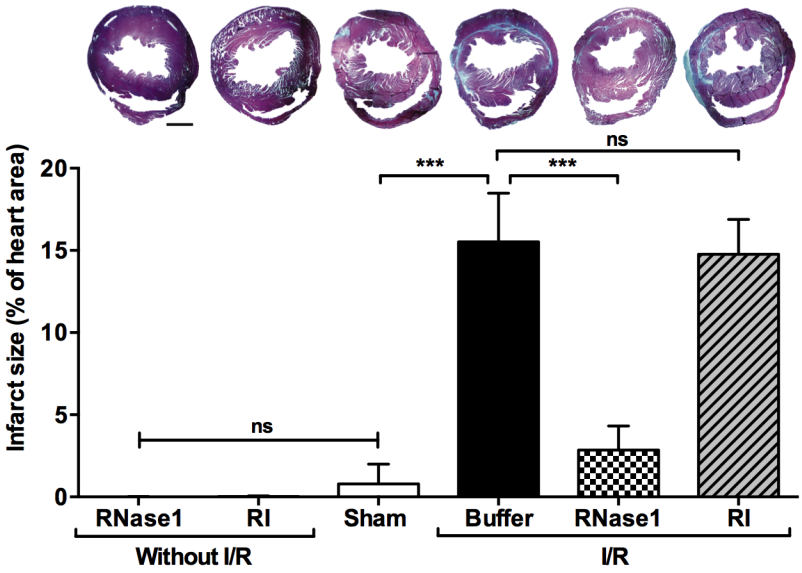

Figure 4.19. Prevention of infarct size by RNase1. Following the induction of the *in vivo* long-term cardiac I/R mice model, histo-morphological analysis was used to evaluate infarct size in mice hearts in the absence (without I/R) or presence (I/R) of coronary occlusion followed by 14 days of reperfusion. In comparison to sham-operated animals, the other groups were continuously treated with buffer only or with RNase1 (100 µg/mice) or RNase-inhibitor (RI, 80 U/mice), respectively, by infusion via subcutaneously implanted osmotic pump. Representative pictures show myocardial infarct size in heart sections indicated by Gomori 1-step stain. Data represent mean ± SEM (n=6-8 mice per group); *P<0.05, ***P<0.001, ns=non-significant; One-way ANOVA, Dunnett's test.

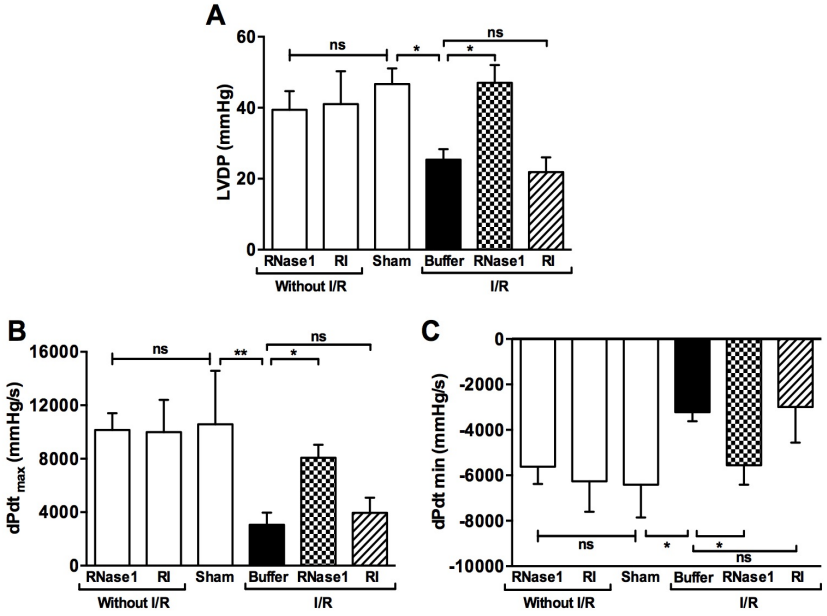

Figure 4.20. *In vivo* cardiac ischemia/reperfusion (I/R) in mice: Physiological parameters and consequences of RNase1 treatment. After the induction of the *in vivo* long-term cardiac I/R mice model, the following physiological parameters were analyzed in mice hearts in the absence (without I/R) or presence (I/R) of coronary occlusion followed by 14 days of reperfusion: **(A)** Left ventricular developed pressure (LVDP); **(B)** maximal time-derived pressure (dPdtmax); **(C)** relaxation described by minimal time-derived pressure (dPdtmin) were measured and quantitated in hearts. In comparison to sham-operated animals, the other groups were continuously treated with buffer only or with RNase1 (100 µg/mice) or RNase-inhibitor (RI, 80 U/mice), respectively, by infusion via subcutaneously implanted osmotic pump. Data represent mean ± SEM (n=6-8 mice per group); *P<0.05, ***P<0.001, ns=non-significant; One-way ANOVA, Tukey's post test.

To characterize the beneficial effects of RNase1 upon physiological parameters in the Langendorff heart model under I/R conditions, three groups receiving increasing concentrations of RNase1 as well as one RI-group were studied. The drugs were administered together with the perfusion buffer prior to the induction of 45 min ischemia **(Figure 4.21A)**. Measurements of left ventricular end-diastolic pressure (LVEDP, a measure of the magnitude of ischemic rigor contracture) in the RI-group (34 ± 5 mmHg) revealed a similar or even higher value when compared to non-treated I/R hearts (26 ± 4 mmHg), whereas RNase1 in a concentration-dependent manner significantly reduced the adverse outcome of I/R (11 ± 3 mmHg at 10 µg/ml) and was effective over the entire reperfusion phase **(Figure 4.21B)**. Similarly, cardiomyocyte hypercontracture (a measure of I/R-mediated injury) was significantly reduced in the RNase1-treated groups (30 ± 4 mmHg at 10 µg/ml), while RI-administration (104 ± 8 mmHg) resulted in an even worse (although not significant) effect when compared to the untreated I/R group (66 ± 9 mmHg) **(Figure 4.21C)**.

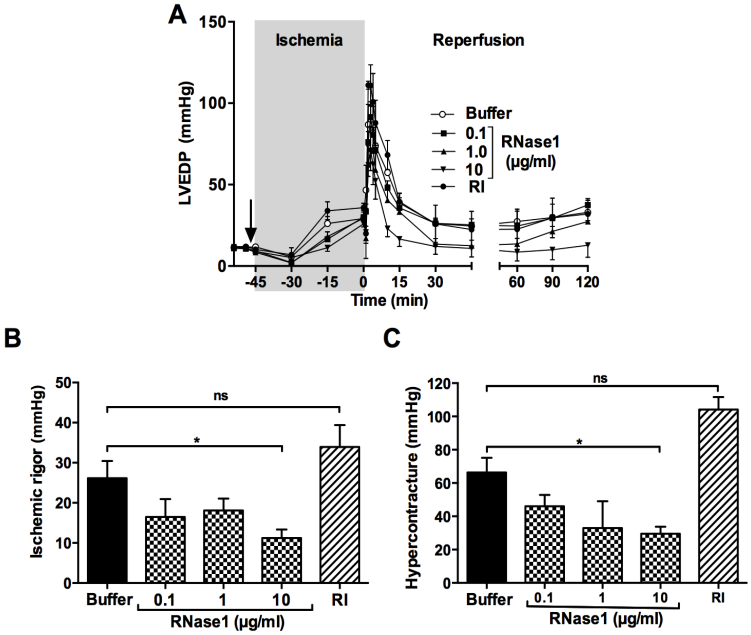

Figure 4.21. Cardiac ischemia/reperfusion (I/R) in the isolated rat heart (Langendorff model): Physiological parameters and consequences of RNase1 treatment. Isolated rat hearts (Langendorff-model) were submitted to perfusion only under normoxia (Control) or submitted to I/R (45 min/120 min) in the absence (Buffer) or presence of 10 µg/ml RNase1 or 2 U/ml RI, respectively, and the following physiological parameters were quantified: **(A)** Changes in left ventricular end-diastolic pressure (LVEDP) were analyzed during the whole ischemia/reperfusion protocol in the absence (Buffer) or presence of different doses of RNase1 or 2 U/ml RI as indicated. Values represent mean ± SD (n=6-9 hearts). **(B)** Following the I/R protocol in isolated rat hearts, the magnitude of ischemic rigor contracture was assessed by peak left ventricular end developed pressure (LVEDP) during ischemia (45 min) in the absence (Buffer) or presence of different doses of RNase1 or 2 U/ml RI as indicated. Values represent mean ± SD (n=6-9 hearts); *P<0.05, ns=non-significant; One-way ANOVA, Tukey's post test. **(C)** Maximal reperfusion-induced hypercontracture was determined as the maximal increase in LVEDP with respect to the value obtained at the end of 45 min ischemia in the absence (Buffer) or presence of different doses of RNase1 or 2U/ml RI. Values represent mean ± SD (n=6-9 hearts); *P<0.05, ns=non-significant; One-way ANOVA, Tukey's post test.

Furthermore, only minor quantities of LDH were detectable in all perfusate fractions in the RNase1 treatment groups, indicating markedly reduced necrotic cell death, whereas the typical early release of LDH following reperfusion was documented in the control and the RI-treated groups **(Figure 4.22A)**. The cumulative LDH release was markedly reduced in the RNase1 group (44 ± 7 UI/g tissue, *vs.* 127 ± 32 UI/g tissue in I/R group) (**Figure 4.22B)**.

Most importantly, RNase1-administration substantially decreased infarct size in the isolated heart (23% *vs.* 66 ± 5%, P<0.001) **(Figure 4.23A)**, while the application of RI did had no effect on these parameters when compared to I/R injury alone. Likewise, in the RNase1 treatment group, contractile recovery (expressed as left ventricular developed pressure, LVdevP) was significantly improved (73 ± 13% of basal values, *vs.* 38 ± 12% of basal values in I/R group) after 120 min reperfusion **(Figure 4.23B)**.

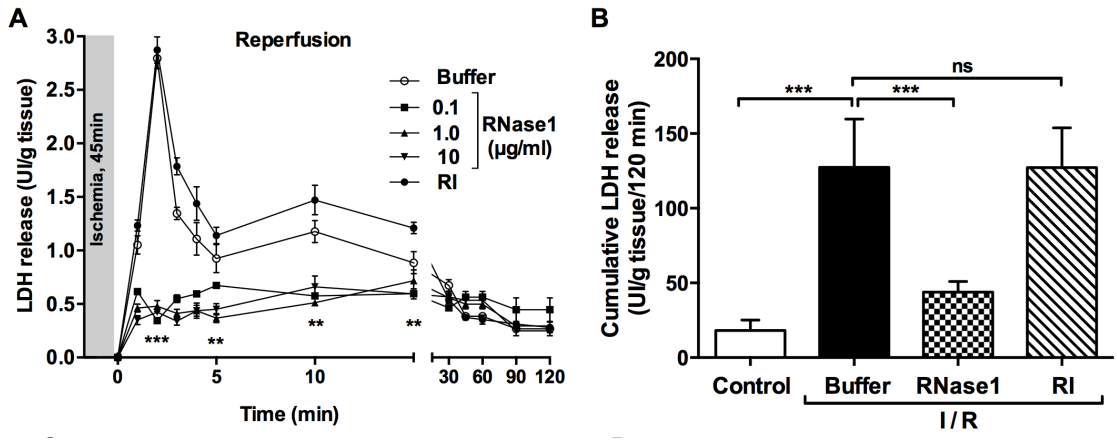

Figure 4.22. RNase1 markedly reduces LDH reléase during I/R injury. (A) Isolated rat hearts (Langendorff-model) were submitted to perfusion only under normoxia (Control) or submitted to I/R (45 min/120 min) in the absence (Buffer) or presence of 10 µg/ml RNase1 or 2 U/ml RI, respectively. Release of lactate dehydrogenase (LDH) during 120 min reperfusion was measured in the absence (Buffer) or presence of different doses of RNase1 or RI (2 U/ml) as indicated. LDH activity was quantified for each time point and normalized to the tissue weight. Values represent mean ± SEM (n=6-9 hearts); **P<0.01, ***P<0.001; One-way ANOVA, Tukey's post test. **(B)** Cumulative LDH release was analyzed during 120 min reperfusion, calculated as the area under the curve from all measured time points for the indicated conditions. Values represent mean ± SD (n=6-9 hearts); **P<0.01, ***P<0.001, ns=non-significant; One-way ANOVA, Dunnett's test.

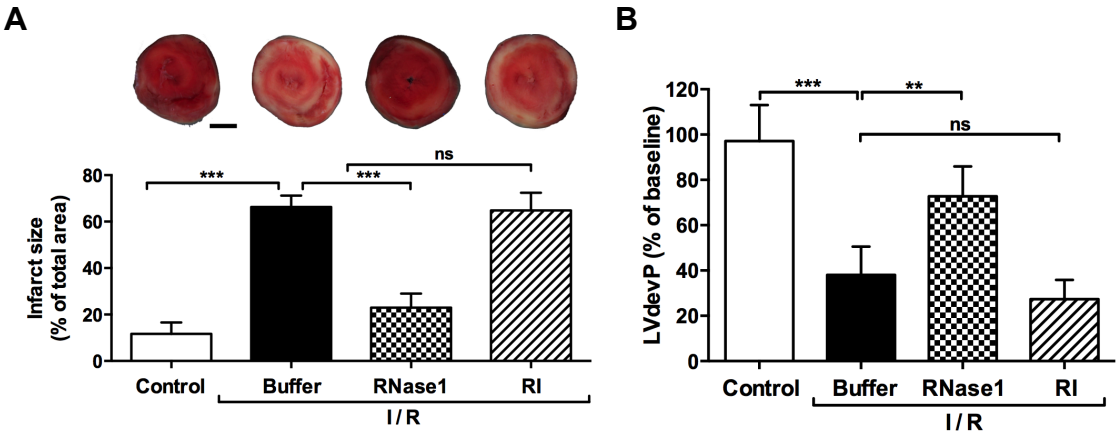

Figure 4.23. RNase1 improves ventricular recovery by reducing infarct size. (A) Infarct size was quantified by the TTC reaction in heart sections and expressed as the percentage of necrotic tissue with respect to total ventricular mass in the different treatment groups indicated. Values represent mean ± SD (n=6-9 hearts); **P<0.01, ***P<0.001, ns=non-significant; One-way ANOVA, Dunnett's test. **(E)** Release of LDH from cardiomyocytes was quantified as an index of sarcolemmal rupture after treatment with RNA (10 µg/ml), hydrolyzed RNA (10 µg/ml), with RNase1 (10 µg/ml), RNase-Inhibitor (RI, 40 mU/ml) or DNA (10 µg/ml), respectively, under normoxia (3h) or hypoxia (1h, grey zone) as indicated. Values represent mean ± SD (n=4); **P<0.01, ***P<0.001, ns=non-significant. **(B)** Recovery of left ventricular developed pressure (LVdevP, measured as the difference between systolic and diastolic pressure) was determined after 120 min of reperfusion and expressed as percent of basal values in Langendorff-perfused rat hearts. Values represent mean ± SD (n=6-9 hearts); **P<0.01, ***P<0.001, ns=non-significant; One-way ANOVA, Dunnett's test.

4.8. Cytoprotective functions of RNase1

While under normoxia, eRNA, RNase1, RI or DNA did not influence basal LDH release in cardiomyocytes, a substantial increase of LDH release was observed upon exposure of cells towards 1h hypoxia **(Figure 4.24A)**. Further addition of eRNA, but not hydrolyzed RNA, DNA or RI, respectively, resulted in significantly increased LDH release that was almost completely abolished by treatment with RNase1, independent of the presence of exogenous eRNA. Moreover, TNF-α markedly promoted LDH release, particularly under conditions of hypoxia **(Figure 4.24B)**, similar to the activity of eRNA **(see Figure 4.24A)**. Simultaneous addition of TNF-α and eRNA did not further enhance LDH release. Conversely, TAPI significantly suppressed eRNA-induced LDH release **(Figure 4.24B)**, but not to the same extent as it was demonstrated for RNase1-treatment in the hypoxia-induced LDH release **(see Figure 4.24A)**.

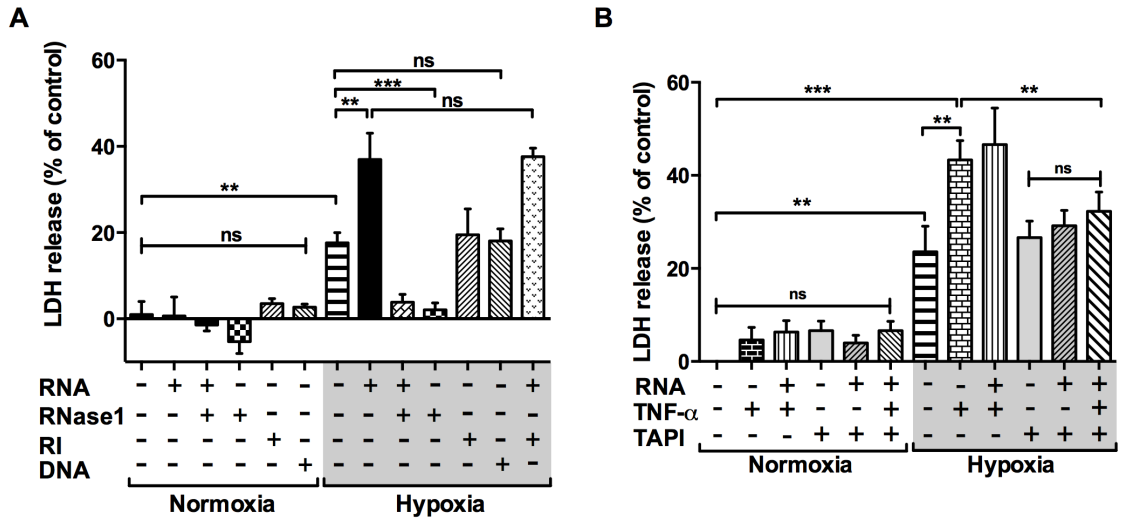

Figure 4.24. Extracellular RNA-induced cell death during hypoxia: Promotion via TNF-α and prevention by RNase1 treatment. (A) Release of LDH from cardiomyocytes was quantified as an index of sarcolemmal rupture after treatment with RNA (10 μg/ml), hydrolyzed RNA (10 μg/ml), with RNase1 (10 μg/ml), RNase-Inhibitor (RI, 40 mU/ml) or DNA (10 μg/ml), respectively, under normoxia (3h) or hypoxia (1h, grey zone) as indicated. Values represent mean ± SD (n=4); **P<0.01, ***P<0.001, ns=non-significant; One-way ANOVA, Dunnett's test. (**B**) LDH release was measured in the supernatants of cardiomyocytes after treatment with RNA (10 μg/ml) or TNF-α (20 ng/ml) in the absence (-) or presence of TAPI (10 μM) under normoxia (3h) or hypoxia (1h, grey zone), respectively. Values represent mean ± SD (n=3, each in triplicate); *P<0.05, **P<0.01, ***P<0.001, ns=non-significant; One-way ANOVA, Dunnett's test.

Ischemia in the isolated rat heart induced a rapid exhaustion of phosphocreatine as an indicator of energy depletion with only partial recovery in the control I/R group (45 ± 5%) after 15 min of reperfusion, whereas in the RNase1 treatment group intracellular phosphocreatine remained elevated at a significantly higher level (73 ± 5%, P=0.032) and promoted substantial heart recovery **(Figure 4.25A)**.

Since dysregulated opening of the mitochondrial permeability transition pore (mPTP) provokes mitochondrial dysfunction, which is associated with uncoupled oxidative phosphorylation and ATP hydrolysis, cardiomyocyte hypercontracture may ultimately lead to cell death (Halestrap, 2006; Hausenloy et al., 2003; Javadov et al., 2009; Ruiz-Meana et al., 2007). Exposure of cardiomyocytes towards eRNA significantly reduced the time of contracture related to mPTP opening **(Figure 4.25B)** as assessed by the fluorescent dye tetramethyl-rhodamine-ethylester, which is readily sequestered by healthy mitochondria.

In contrast, RNase1 abolished this effect as reflected by a value that was indistinguishable from the control. Furthermore, TNF-α promoted mPTP opening and induced cardiomyocyte hypercontracture, which became significant at a concentration of TNF-α at 50 ng/ml; anti-TNF-α reversed this effect **(Figure 4.25C)**. As an established protective agent, cyclosporin-A markedly prolonged the time to cardiomyocyte contracture, as expected.

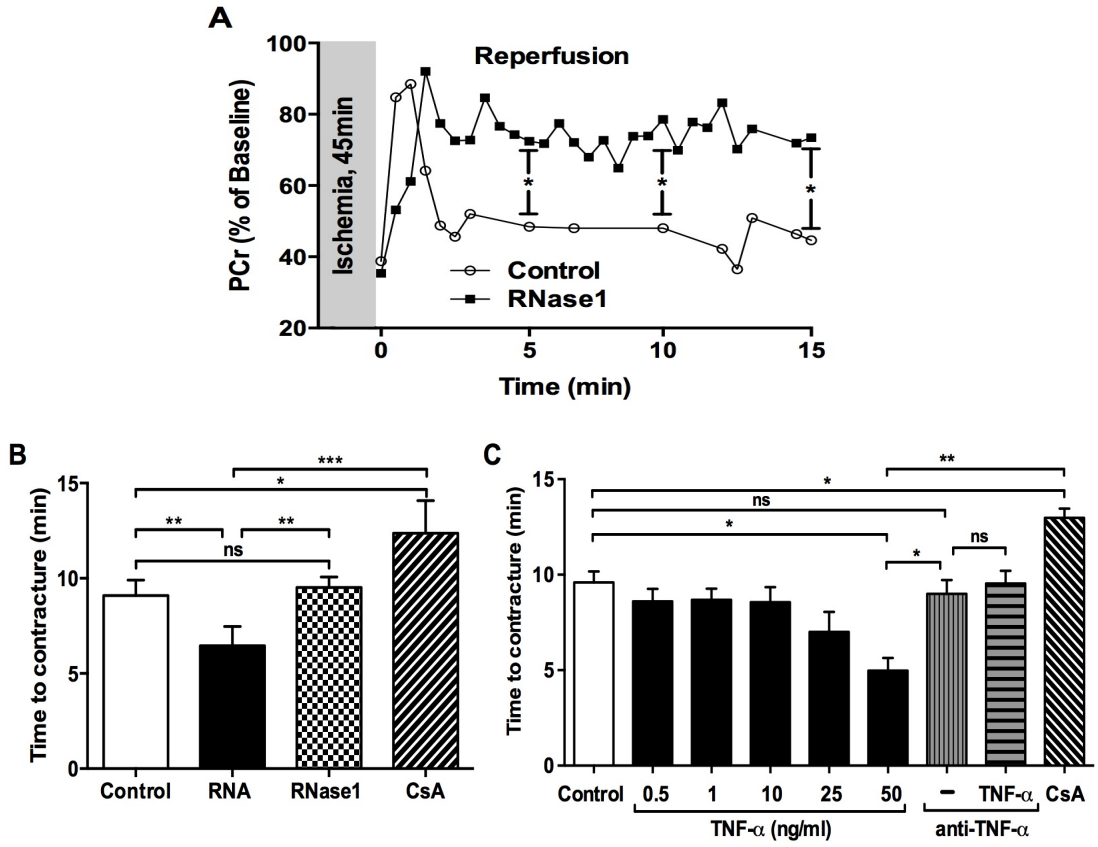

Figure 4.25. Protective functions of RNase1 on cardiomyocytes upon ischemia/reperfusion injury. (A) Recovery of cell energy (% of phosphocreatine, PCr) was quantified by NMR spectroscopy during the initial minutes of reperfusion in rat hearts submitted to 45 min of ischemia in the absence (control) or presence of RNase1 (10 μg/ml); values represent mean ± SD (n=3 hearts); *P<0.05; One-way ANOVA, Dunnett's test. **(B)** Changes in the intensity of fluorescence induced by intermittent laser illumination in tetramethyl-rhodamine-ethylester-loaded cardiomyocytes were registered under control conditions or in the presence of RNA (10 μg/ml) or RNase1 (10 μg/ml). Data represent mean ± SEM of n>13 cells per group; *P<0.05, **P<0.01, ns=non-significant; One-way ANOVA, Dunnett's test. **(C)** The time span at maximal cell shortening secondary to mPTP opening (under intermittent laser illumination) was analyzed in the absence (control) or presence of increasing concentrations of TNF-α in isolated tetramethyl-rhodamine-ethylester-loaded cardiomyocytes. In a subset of experiments, anti-TNF-α (25 μg/ml; in the absence (-) or presence of TNF-α, 50 ng/ml) as well as cyclosporin A (CsA, 1 μM), were included. Data represent mean ± SEM of n>13 cells per group; *P<0.05, **P<0.01, ns=non-significant; One-way ANOVA, Dunnett's test.

4.9 Prevention of cardiomyocyte death by inhibition of TACE/ADAM17

To specify the mechanism underlying eRNA-induced liberation of TNF-α and the subsequent adverse interplay of both components, the role of the metalloproteinase TACE/ADAM17 was explored in the established *ex vivo* and *in vitro* models. In the isolated rat heart, TNF-α release (maximal peak, 85 ± 10 pg/min *vs.* pre-ischemic values 12 ± 5 pg/min) during the initial reperfusion phase was significantly reduced upon treatment with TAPI (22 ± 8 pg/min) **(Figure 4.26A)**. Likewise, in isolated cardiomyocytes, eRNA-induced TNF-α release was significantly prevented in the presence of the metalloproteinase inhibitors GM6001 or TACE-specific TAPI **(Figure 4.26B)**. Furthermore, since activation of the NF-κB pathway was considered to be related to eRNA activity as well, TNF-α liberation was also blocked by the IκB phosphorylation inhibitor Bay11-708210 (Bay11). Neutralising antibodies against TNF-α completely blocked the TNF-α release mediated in the absence or presence of eRNA **(Figure 4.26B)**.

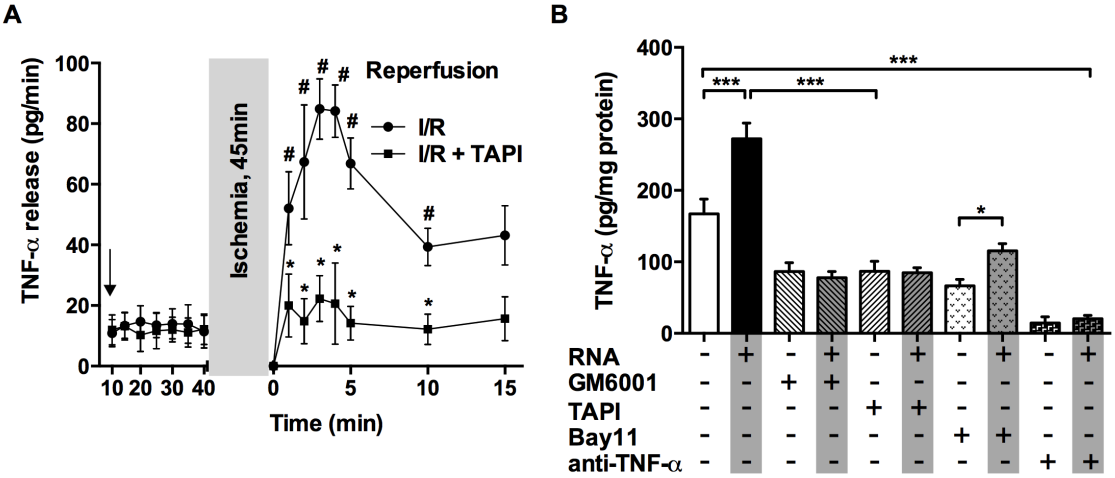

Figure 4.26. Inhibition of metalloproteinases prevents TNF-α release. (**A**) Release of TNF-α was quantified in the perfusate fractions throughout the 40 min stabilization and first 15 min reperfusion period in Langendorff hearts submitted to I/R protocol alone or after administration (arrow) of TAPI (1 μM). TNF-α values are corrected for respective flow rate and normalized to the effluent protein concentration and represent mean ± SD (n=3 hearts); $^{\#}$P<0.001 (I/R *vs.* pre-ischemic values); *P<0.001 (I/R+RNase1 *vs.* I/R); One-way ANOVA, Tukey's post test. (**B**) Cardiomyocytes were treated for 3h under normoxia or in the absence (-) or presence of RNA (10 μg/ml, grey zones) with GM6001 (10 μg/ml), TAPI (10 μM), Bay11 (100 μM) or anti-TNF-α (25 μg/ml), respectively, followed by quantification of TNF-α protein in the corresponding cell supernatants. Values represent mean ± SD (n=6); *P<0.05, ***P<0.001; One-way ANOVA, Dunnett's test.

These findings were corroborated by the observation that TAPI-treatment of the isolated rat heart during an interval of 30 min prior to the ischemic phase significantly decreased LDH release in comparison to the untreated I/R group **(Figure 4.27A)**. Furthermore, as compared to isolated wild-type cardiomyocytes, in TNF-α knockout cells, cell viability upon exposure to hypoxia decreased in a similar manner, but was not further reduced in the presence of eRNA **(Figure 4.27B)**, indicating that the lack of TNF-α prevented eRNA-induced cell death.

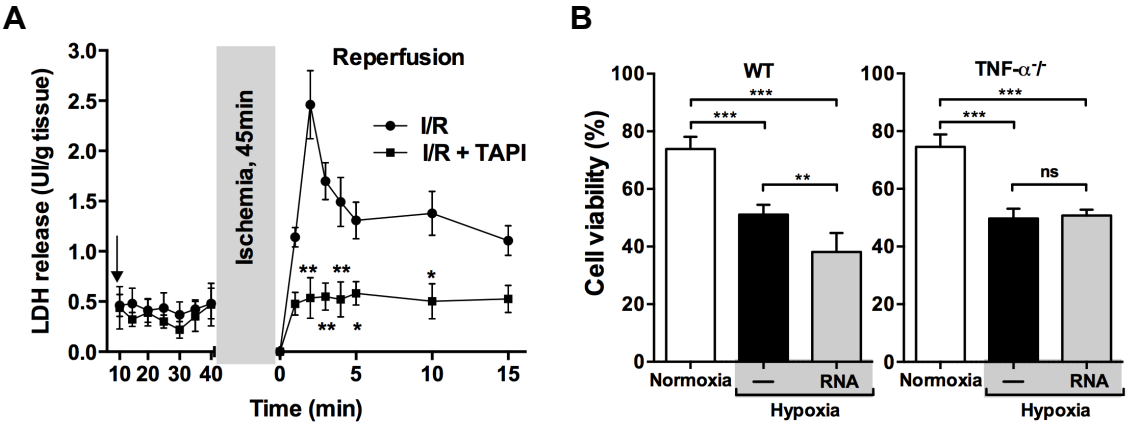

Figure 4.27. Inhibition of metalloproteinases prevents cell death. (A) LDH release was quantified in the perfusate fractions throughout the 40 min stabilization and first 15 min reperfusion period in Langendorff hearts submitted to I/R protocol alone or after administration (arrow) of TAPI (1 μM). LDH values are normalized to the tissue weight and represent mean ± SD (n=3 hearts); *P<0.05, **P<0.01 vs I/R; One-way ANOVA, Tukey's post test. **(B)** Cell viability was measured in freshly isolated cardiomyocytes from wildtype (WT) and TNF-$\alpha^{-/-}$ mice under normoxia or subjected to hypoxia (grey zone) for 2h in the absence (-) or presence of extracellular RNA. Data represent mean ± SEM (n=6); **P<0.01, ***P<0.001, ns=non-significant; One-way ANOVA, Dunnett's test. (The working group of Prof. S. Lecour at the University of Cape Town, South Africa, performed experiments with TNF-$\alpha^{-/-}$ mice)

Using confocal microscopy to inspect I/R-exposed heart tissue as demonstrated before (**see Fig. 4.15**), administration of TAPI lead to the preservation of the cardiac tissue architecture, and fluorescence intensity of ROS was low as in the non-I/R group **(Figure 4.28A)**. ROS content (211 ± 17 AU/μm^2) in I/R hearts was reduced upon TAPI-treatment to 91 ± 10 AU/μm^2 **(Figure 4.28B)**, indicative of a similar protective role of this TACE-inhibitor as documented for RNase1.

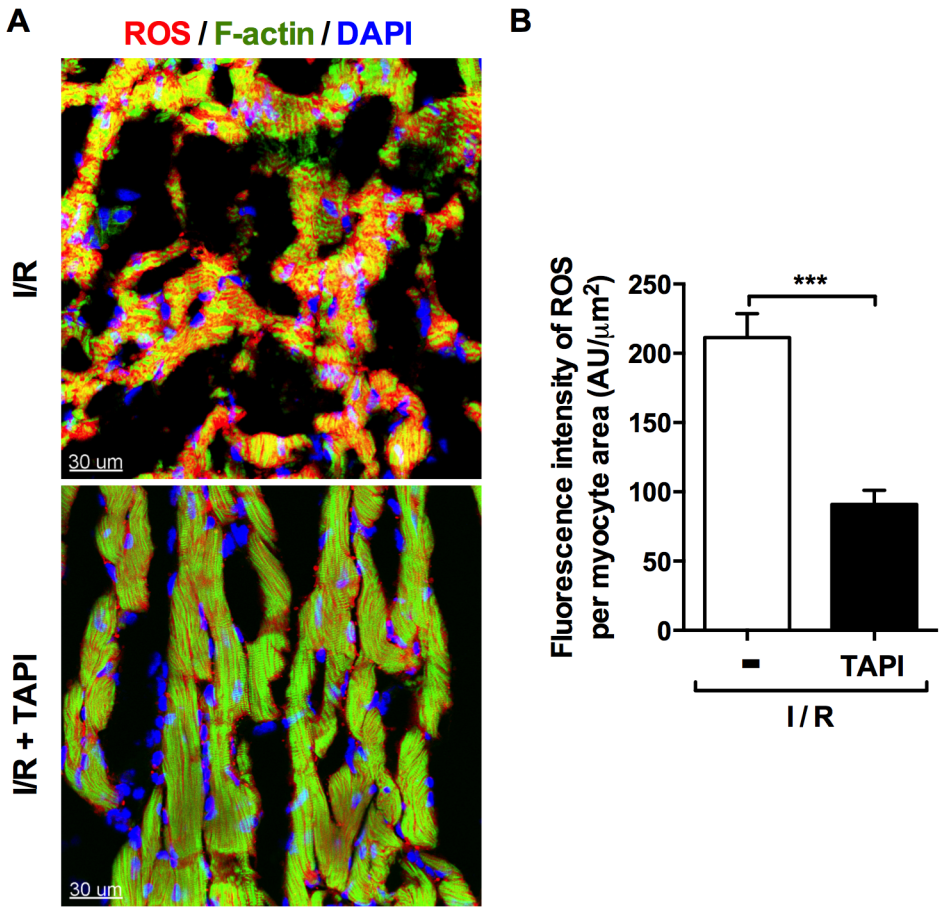

Figure 4.28. The TACE-inhibitor TAPI reduces ventricular content of ROS. (**A**) Microslices obtained from the isolated Langendorff-perfused hearts submitted to 30 min stabilization followed by 45 min ischemia and 120 min reperfusion (I/R) alone or in the presence of TAPI (10 μM) were analysed by immunofluorescent staining. ROS (dihydroethidium, red) production together with detection of F-actin (green) and nuclear DNA (DAPI, blue) was analyzed by confocal microscopy. Representative images of multiple experiments are shown. (**B**) Quantitative analysis of ROS (dihydroethidium) production described in (**A**) was performed; values represent mean ± SD (n= 3 hearts); ***P<0.001, ns = non-significant. One-way ANOVA, Dunnett's test. Representative images of multiple experiments are shown.

4.10. The eRNA-TNF-α interplay promotes cardiac I/R-induced inflammation

Upon ischemia in the isolated rat heart, the expression of the pro-inflammatory cytokine MCP-1 as well as iNOS was significantly increased, whereas treatment with RNase1 but not with RI prevented this effect **(Figure 4.29A)**. Likewise, stimulation of isolated cardiomyocytes with eRNA or TNF-α markedly increased the expression of MCP-1 and iNOS **(Figure 4.29B)**. In contrast, administration of RNase1 or TAPI, respectively, prevented the increase in mRNA levels of these inflammatory factors.

Finally, Western blot analysis revealed that I/R injury in the isolated rat heart induced a significant decrease in IκB-α protein production, whereas RNase1 treatment resulted in retaining the inactive NF-κB dimer by maintaining IκB-α in the non-phosphorylated state **(Figure 4.29C)**. Together, these data document the damaging role of eRNA and TNF-α in ischemia-related cardiac injury in different experimental models and propose a substantial protective function for RNase1 and TAPI.

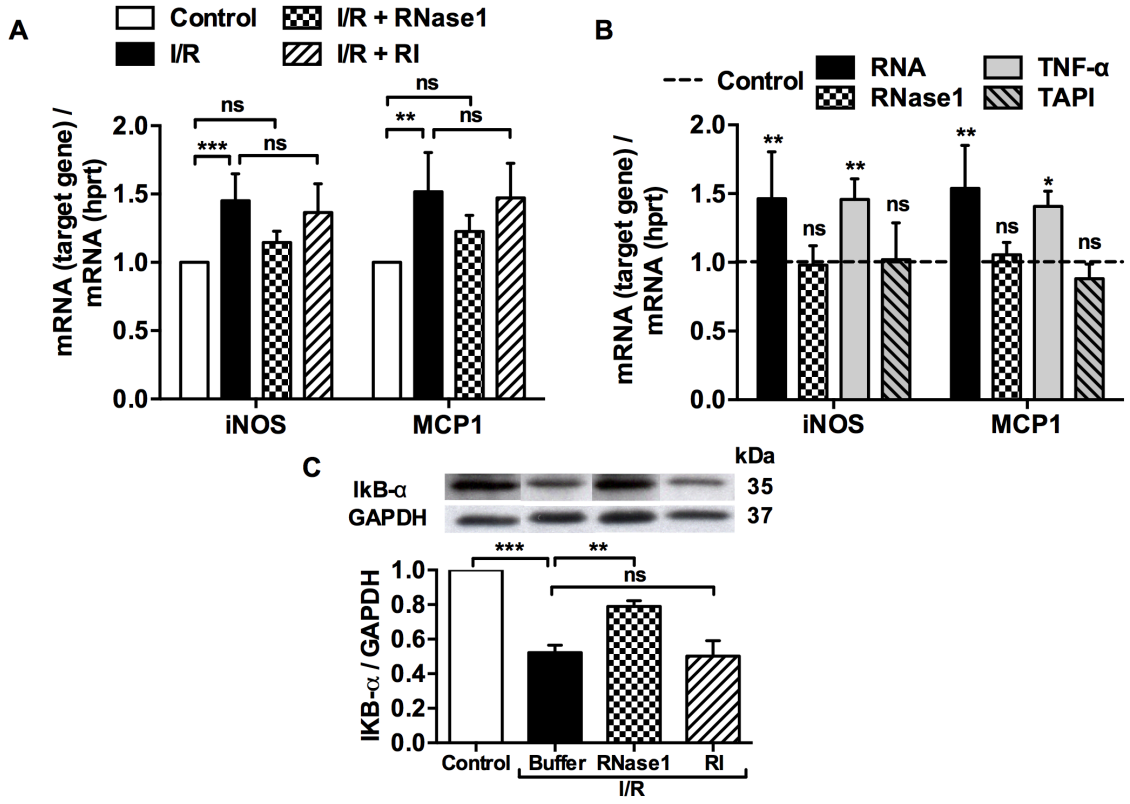

Figure 4.29. Extracellular RNA and TNF-α mediate up-regulation of proinflammatory mediators in cardiomyocytes (**A**) Changes in the cellular mRNA levels of inducible NO-synthase (iNOS) and monocyte chemotactic protein-1 (MCP1) were quantified by RT-PCR in isolated rat hearts perfused for 3h under normoxic conditions (control) or submitted to the I/R protocol alone or in the presence of 10 µg/ml RNase1 or 2 U/ml RI, respectively. (**B**) Changes in cellular mRNA levels of iNOS and MCP1 in cardiomyocytes, untreated (control) or treated with 10 µg/ml extracellular RNA, 10 µg/ml RNase1, 20 ng/ml TNF-α or 10 µM TAPI, respectively, for 3h under normoxia were quantified by RT-PCR. Data in (**A**) and (**B**) indicate changes in the ratio between target and *hprt* mRNA relative to the levels in control cells or left ventricle tissue, respectively, under non-stimulatory conditions and represent mean ± SD (n=6 in cardiomyocytes; n=6 in left ventricle tissue); *P<0.05, **P<0.01, ***P<0.001, ns=non-significant; One-way ANOVA, Dunnett's test. (**C**) Isolated rat hearts were perfused 3h under normoxic conditions (control) or submitted to the I/R protocol alone or in the presence of RNase1 (10 µg/ml) or RI (2 U/ml), respectively, and protein expression of IκB-α and GAPDH in left ventricle tissue was quantified in western blots. The bar graphs represent IκB-α levels normalized to GAPDH in the different treatment groups. Data represent mean ± SD (n=3); **P<0.01, ***P<0.001, ns=non-significant; One-way ANOVA, Tukey's post test.

5. Discussion

In the present study, novel mechanistic insights into the process of atherogenesis, macrophage-induced inflammation, cardiac I/R injury that are governed by the endogenous extracellular RNA/RNase system were obtained. The multifunctional eRNA/RNase system was characterized for its contribution to acute and chronic cardiovascular disease as it relates to the progression of atherosclerotic lesion formation. The data indicate that (a) in *Ldlr*$^{-/-}$ mice fed a HFD, eRNA accumulates in atherosclerotic plaques in a time-dependent manner; (b) conversely, a biphasic characteristic for plasma RNase activity was observed with an increase soon after the initiation of HFD, and a decline to levels below baseline during progressive plaque growth; and (c) eRNA induces an inflammatory gene expression in bone-marrow-derived macrophages, Together, these data provide strong evidence for a major role of the eRNA/RNase system in atherogenesis and establish RNase1-treatment as a potentially novel therapeutic regimen. Moreover, the interplay between eRNA-dependent and TNF-α-related pathomechanisms characterized in this study may not be limited to ischemic heart disease but may be applied generally to ischemia-mediated damage of other organs or tissues as well, such that interventions with RNase1 or TACE-inhibitors would definitely provide new regimens for cytoprotection in general.

5.1. A pro-inflammatory role of eRNA in atherosclerotic plaque formation

For the first time it is demonstrated that eRNA accumulates within arterial lesions in the media and at later stages predominantly in the neointima in a time-dependent fashion, as documented by staining of affected vascular sites with an RNA-binding dye in HFD-fed mice, but not in controls. Although eRNA may be degraded by plasma RNases, increased levels of eRNA were similarly detected in tumor patients, sepsis or lung fibrosis (Fischer et al., 2011; Fischer and Preissner, 2013).

It was propose that eRNA, released under pathological conditions, may become protected against degradation by binding to proteins and phospholipids (Wieczorek et al., 1985), or is associated with microparticles or exosomes (Ekström et al., 2012). However, the biphasic change of vascular RNases, showing an increase early after the initiation of a HFD-diet, but a decrease in the course of chronic lesion formation (observed from 4 weeks on), strongly implies a causal relationship between an

imbalance in the eRNA/RNase system and the initiation and progression of atherosclerosis.

In accordance with the damaging nature of eRNA, several pro-inflammatory cytokines (including TNF-α, IL-1ß, IL-6) were upregulated in macrophages, whereas a decrease in anti-inflammatory cytokines was demonstrated: This is in line with a shift in macrophage polarization towards the M1-phenotype, as well as a repression of typical M-2 phenotype markers such as Arg1 or CD206. No involvement of TLRs in self eRNA-cell interactions was noted. In essence, the appearance of eRNA in the diseased tissue may thus be considered as an alarm signal that amplifies tissue inflammation by the induction of cytokine production, by promotion of M1-macrophage polarization as well as by releasing bioactive TNF-α (Fischer et al., 2012), being a potent pro-atherogenic factor (Weber et al., 1993). The latter process may involve direct or indirect activation of TNF-α-converting enzyme by eRNA, as previously demonstrated by our group (Fischer et al., 2013).

eRNA was also demonstrated to mediate vascular permeability via the mobilization/stabilization and direct binding to vascular endothelial growth factor (Fischer et al., 2007). Enhanced vascular endothelial growth factor signaling induced by eRNA may in addition promote monocyte adhesion and plaque expansion (Lucerna et al., 2007). Moreover, eRNA was shown to act as a pro-thrombotic cofactor (Kannemeier et al., 2007). Accordingly, systemic treatment with RNase1 rescued mice from thrombotic occlusion of the carotid artery in a model of arterial thrombosis and reduced cerebral edema and infarction size in acute stroke (Walberer et al., 2009).

Neointimal hyperplasia after arterial injury is characterized by endothelial denudation, exposure of extracellular matrix, and adhesion of activated platelets, which all contribute to inflammatory leukocyte recruitment and neointima formation after injury (Schober et al., 2002). By contributing to platelet accumulation at the site of injury, eRNA may thus promote injury-induced leukocyte adhesion and neointimal hyperplasia, as well.

The underlying pathogenetic mechanisms of eRNA as a pro-inflammatory mediator may thus involve both direct and indirect signaling pathways. The findings thus indicate that eRNA serves as an important inflammatory mediator after vascular injury, identifying extracellular ribonucleic acids as a new target for the treatment of inflammation during vascular remodeling.

Together, the present study provides novel experimental evidence for the multifunctional properties of self-eRNA as an important trigger of different inflammatory processes that fuel atherogenesis and may culminate in atherosclerotic lesion growth.

5.2. The damaging interplay between eRNA and TNF-α triggers cardiac ischemia/reperfusion injury

The rationale for studying the role of eRNA and TNF-α in ischemic heart disease was based upon our previous findings that these poly-anionic compounds promoted arterial thrombosis (Kannemeier et al., 2007), induced the release of cytokines (including TNF-α), and served to elevate vascular permeability and edema formation *in vivo* (Fischer et al., 2009). Collectively, these functional activities of eRNA were largely inhibited by RNase1, which thereby plays a prominent role as a vessel-and tissue-protective agent (Fischer and Preissner, 2013). Moreover, in cardiac patients undergoing cardiac bypass surgery, in which the heart is subjected to ischemia/reperfusion (I/R) injury, significantly elevated levels of eRNA (>20 fold) and TNF-α (>7-fold) were found in the present study, especially in coronary sinus blood before unclamping as compared to peripheral arterial blood. These data indicate massive release of these components particularly during an ischemic phase and are in accordance with earlier findings demonstrating elevated levels of TNF-α and IL-6 in the coronary sinus blood, suggestive for these authors to conclude that the lungs may consume rather than release proinflammatory cytokines in the early phase of cardiac reperfusion (Wan et al., 1996).

In fact, the eRNA - TNF-α relation in the coronary sinus could play an important role in the inflammatory response after aortic unclamping, not only because it may directly induce symptoms, but also because it may trigger the release of other cytokines, such as IL-6, IL-8 or IL-10 (Donndorf et al., 2012; Liebold et al., 1999; Wan et al., 1996). In other reports, inflammatory responses were found to be the primary cause of microvascular incompetence in I/R injury, and global myocardial ischemia during aortic cross-clamping seems to be one of the crucial pathogenetic factors in cardiac cytokine release and the “postperfusion syndrome” upon cardiopulmonary bypass (Donndorf et al., 2012; Liebold et al., 1999). Together, these findings were prompting to further unravel the possible molecular interplay between eRNA and TNF-α under conditions of cardiac I/R injury in various experimental models.

In fact, acutely elevated levels of eRNA, both free and in association with microparticles (Fischer et al., 2014), were found upon onset of reperfusion in the isolated rat heart model as well as in hypoxia-exposed cardiomyocytes in accordance with a recent report demonstrating the release of tissue factor-bearing microparticles from cardiomoycytes under inflammatory conditions (Antoniak et al., 2009). Likewise, in acute models of vessel stenosis or chronic models of atherosclerosis in mice, increased plasma and tissue concentrations of eRNA were observed (Simsekyilmaz et al., 2013). In the Langendorff heart model, the initial reperfusion-dependent washout of eRNA together with cardiomyocyte-specific markers such as creatine kinase or troponins was followed by a second peak of eRNA, whereby the vast majority of this 18S/28S rRNA material was derived from cardiomyocytes. Thus, unlike creatine kinase, troponins or LDH, eRNA remains to be released into the perfusate over an appreciable period of time where it can directly or indirectly affect cellular functions.

Since in isolated cardiomyocytes the combined action of TNF-α and hypoxia provoked eRNA release as well, a reciprocal induction between eRNA and TNF-α is proposed that is particularly relevant under ischemic conditions. In fact, in the *in vivo* as well as in the *ex vivo* cardiac I/R injury model, substantial amounts of TNF-α were released and became deposited in cardiac tissue, whereas these TNF-α values remained almost at control level in the presence of RNase1. Collectively, these findings support the contention of an eRNA-promoted liberation of TNF-α and its reciprocal amplification in a positive feedback mechanism, particularly under conditions of I/R injury, with the result of generating appreciable amounts of this and other cytokines.

Since eRNA, in association with inflammatory processes, may provoke the release of TNF-α via a proteolytic shedding reaction, involving the metalloproteinase TACE (Fischer et al., 2012), it was tested whether this mechanism would apply to the setting of cardiac I/R injury as well. Indeed, TAPI not only prevented the generation of TNF-α in the *ex vivo* isolated heart model or in cardiomyocyte cultures, but also reduced cell death in these systems by blocking LDH-release and reducing the expression of damaging iNOS or MCP-1. In fact, the influence of TAPI on the outcome of these processes, all contributing to cardiac I/R injury and organ damage, was qualitatively superimposable with the outcome of RNase1 administration, indicative for the fact that a direct eRNA – TNF-α interplay is operative as pathological trigger.

Another group of major inducers of cellular damage under conditions of cardiac I/R injury are ROS, and their prominent contribution to organ damage is without doubt. Yet, the causal molecular relations that would lead to massive ROS generation under pathological conditions are incompletely understood. Here, we present strong evidence, both in the *in vivo* and *ex vivo* experimental models, that the elevation of ROS in plasma or perfusate as well as in association with the damaged myocardium were substantially reduced or prevented by RNase1 as well as by TAPI. Thus, it is concluded that the proven eRNA-TNF-α interplay provides a major stimulus for ROS production and deposition. Mechanistically, in combination with hypoxia/ischemia, eRNA provoked a marked reduction in the expression of antioxidant enzymes, indicative of the fact that such endogenous protective factors become down-regulated under stress conditions. Both, RNase1 or TAPI could reverse this effect by inducing the expression of such enzymes like peroxiredoxin 3 or the three isoforms of SOD in the Langendorff heart model or in isolated cardiomyocytes, respectively. In addition, RNase1 or TAPI reduced the expression of iNOS and MCP-1, factors which are known to be involved in mediating cell-damaging signals in cardiomyocytes. Together, these data strongly imply an eRNA – TNFα interplay that appears to feed a vicious circle, culminating in ROS production and cardiomyocyte death.

The adverse outcome during I/R in the isolated rat heart in hypoxic cardiomyocytes in response to eRNA / TNF-α was also reflected by their negative influence on physiological cell parameters, including left ventricular-developed pressure, cardiomyocyte hypercontracture and mPTP opening. Here, administration of RNase1 resulted in markedly reduced contractility and left ventricular end-diastolic pressure (as a measure of the magnitude of rigor contracture) of the heart, as well as in very low levels of LDH in the perfusate as a general marker for necrotic cell death. Together with the massive reduction of ROS in cardiomyocytes as well as the preservation of tissue architecture, the multitude of physiological parameters that were protected by application of RNase1 provide compelling evidence for its causative relation to tissue protection. Although it is tempting to assume that the beneficial effects of RNase1 treatment may depend on certain RNA degradation products such as adenosine (Bai et al., 2011; Bonner et al., 2013), no evidence for this relation was found. Likewise, the adenosine-receptor antagonist 8-sulfophenyltheophylline (8SPT) did not influence the infarct size-reducing effect of RNase1, and 8SPT alone did not affect the control infarct size (data not shown).

Also, it should not be ignored that low doses of TNF-α may contribute to ischemic preconditioning protection by a direct effect on mitochondria (Gedik et al., 2013; Kleinbongard et al., 2010; Skyschally et al., 2007). In contrast to intervention with antibodies against TNF-α that would capture the entire pool of the cytokine and may induce adverse effects (Kleinbongard et al., 2011), the treatments with RNase1 or TAPI in this study prevented excessive TNF-α production, but may have left sufficient quantities of the cytokine, to promote protective functions via TNF-receptor-2 signalling (Lecour et al., 2005).

Finally, the overall measure of organ damage in cardiac I/R injury is ultimately quantitated by the degree of cell death and the respective infarct size. Both, RNase1 as well as TAPI significantly prevented LDH-release, albeit to a different degree. Here, RNase1 was superior to TAPI, particularly under hypoxic conditions, indicative for the fact that eRNA indeed serves as initial upstream inducer of TNF-α liberation. Moreover, quantitation of infarct size in the acute or chronic *in vivo* disease model or the *ex vivo* Langendorff system revealed a massive protective effect in tissue recovery upon RNase1 administration. Thus, RNase1 as well as TAPI appear to be evidenced-based new protective drugs to limit cardiac infarct size, dependent on the here presented pathogenetic mechanisms. In addition, during coronary vessel canalization these drugs may be administered alone or together with a stent-operating procedure to significantly reduce or prevent the pathological outcome of ischemic heart injury.

In conclusion, release and production of eRNA upon cardiac ischemia sets in motion a reciprocal interplay with TNF-α that culminates in ROS production and cardiomyocyte death **(Figure 5)**. Interestingly enough, the proposed pathomechanism is compatible with the well-known induction of exponential cell death observed in acute myocardial ischemia, uncovering at least in part, the eRNA-TNF-α interplay as prominent trigger for this pathology.

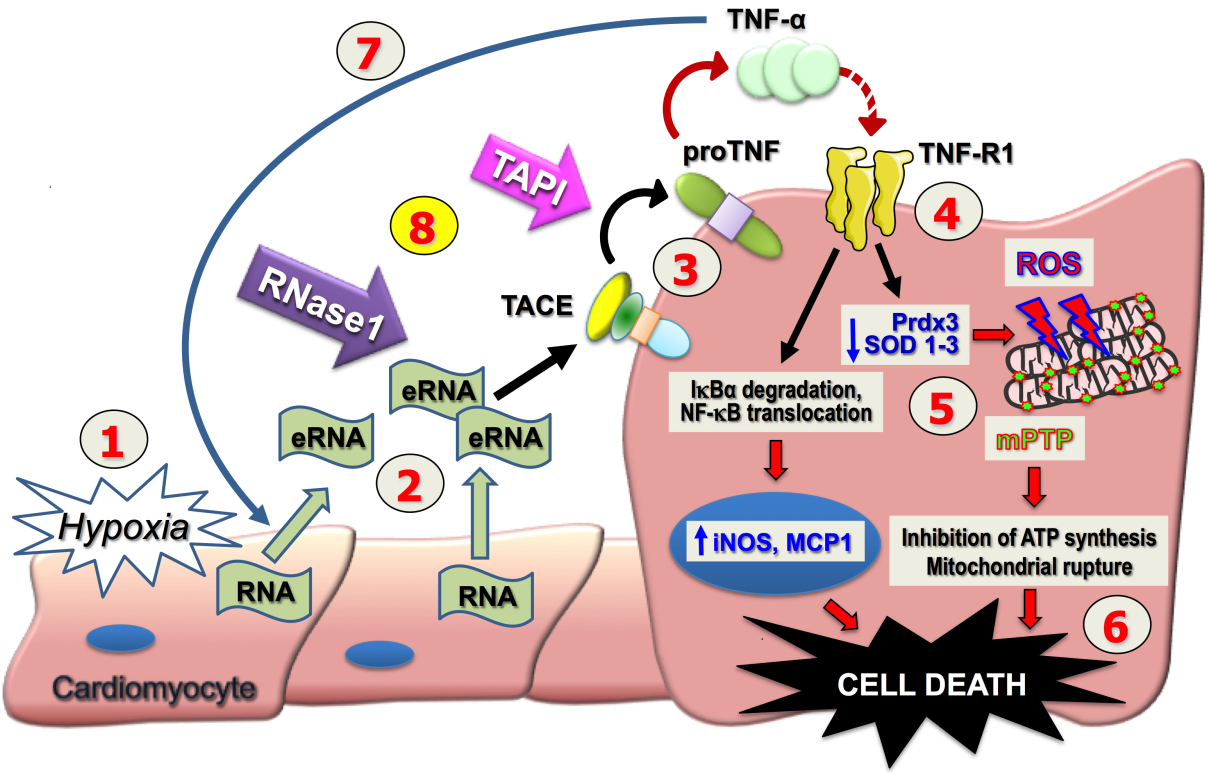

Figure 5. Mechanism of extracellular RNA-TNF-α interplay to induce cardiomyocyte damage and intervention with RNase1 or TACE-inhibitor. Upon hypoxia or cardiac ischemia (**1**), cardiomyocyte damage is accompanied by the release of extracellular RNA (eRNA) (**2**). In turn, eRNA promotes TNF-α-converting enzyme (TACE)-mediated proteolytic shedding of TNF-α from its membrane-associated proform (**3**). Active TNF-α induces intracellular signaling possibly via its receptor (TNF-R1) (**4**), involving NFκB-activation/mobilization and resulting in additional cytokine production, in the downregulation of antioxidant enzymes such as peroxiredoxin-3 (Prdx3) or superoxide-dismutases (SOD) 1-3 and the production of reactive oxygen species (ROS) (**5**). As a consequence, marked mitochondrial damage, loss of ATP-production and pathological oscillations of calcium ions (due to the opening of the mitochondrial permeability transition pore, mPTP) will lead to cell death (**6**). To complete the vicious circle, TNF-α may promote further release of eRNA, which may enhance the ongoing cell destruction (**7**). The administration of RNase1 or TACE-inhibitor TAPI will significantly limit or prevent the indicated adverse effects and serve as potent interventional strategies in cardio-protection (**8**).

6. References

Abassi, Z.A., Barac, Y.D., Kostin, S., Roguin, A., Ovcharenko, E., Awad, H., Blank, A., Bar-Am, O., Amit, T., Schaper, J., Youdim, M., Binah, O., 2011. TVP1022 attenuates cardiac remodeling and kidney dysfunction in experimental volume overload-induced congestive heart failure. *Circ Heart Fail.* 4, 463-473.

Abdallah, Y., Wolf, C., Meuter, K., Piper, H.M., Reusch, H.P., Ladilov, Y., 2010. Preconditioning with diazoxide prevents reoxygenation-induced rigor-type hypercontracture. *J Mol Cell Cardiol.* 48, 270-276.

Acharya, A., Baek, S.T., Huang, G., Eskiocak, B., Goetsch, S., Sung, C.Y., Banfi, S., Sauer, M.F., Olsen, G.S., Duffield, J.S., Olson, E.N., Tallquist, M.D., 2012. The bHLH transcription factor Tcf21 is required for lineage-specific EMT of cardiac fibroblast progenitors. *Development.* 139, 2139-2149.

Agullo, L., Garcia-Dorado, D., Escalona, N., Ruiz-Meana, M., Mirabet, M., Inserte, J., Soler-Soler, J., 2005. Membrane association of nitric oxide-sensitive guanylyl cyclase in cardiomyocytes. *Cardiovasc Res.* 68, 65-74.

Antoniak, S., Boltzen, U., Eisenreich, A., Stellbaum, C., Poller, W., Schultheiss, H.P., Rauch, U., 2009. Regulation of cardiomyocyte full-length tissue factor expression and microparticle release under inflammatory conditions in vitro. *J Thromb Haemost.* 7, 871-878.

Bai, Y., Muqier, Murakami, H., Iwasa, M., Sumi, S., Yamada, Y., Ushikoshi, H., Aoyama, T., Nishigaki, K., Takemura, G., Uno, B., Minatoguchi, S., 2011. Cilostazol protects the heart against ischaemia reperfusion injury in a rabbit model of myocardial infarction: focus on adenosine, nitric oxide and mitochondrial ATP-sensitive potassium channels. *Clin Exp Pharmacol Physiol.* 38, 658-665.

Beynon, H.L., Haskard, D.O., Davies, K.A., Haroutunian, R., Walport, M.J., 1993. Combinations of low concentrations of cytokines and acute agonists synergize in increasing the permeability of endothelial monolayers. *Clin Exp. Immunol.* 91, 314-319.

Blobel, C.P., 2005. ADAMS: key components in EGFR signaling and development. *Nat Rev Mol Cell Biol.* 6, 32-43.

Bonner, F., Borg, N., Jacoby, C., Temme, S., Ding, Z., Flogel, U., Schrader, J., 2013. Ecto-5'-nucleotidase on immune cells protects from adverse cardiac remodeling. *Circ Res.* 113, 301-312.

Botker, H.E., Kharbanda, R., Schmidt, M.R., Bottcher, M., Kaltoft, A.K., Terkelsen, C.J., Munk, K., Andersen, N.H., Hansen, T.M., Trautner, S., Lassen, J.F., Christiansen, E.H., Krusell, L.R., Kristensen, S.D., Thuesen, L., Nielsen, S.S., Rehling, M., Sorensen, H.T., Redington, A.N., Nielsen, T.T., 2010. Remote ischaemic conditioning before hospital admission, as a complement to angioplasty, and effect on myocardial salvage in patients with acute myocardial infarction: a randomised trial. *Lancet.* 375, 727-734.

Cabrera-Fuentes, H.A., Aslam, M., Saffarzadeh, M., Kolpakov, A., Zelenikhin, P., Preissner, K.T., Ilinskaya, O.N., 2013. Internalization of Bacillus intermedius ribonuclease (BINASE) induces human alveolar adenocarcinoma cell death. *Toxicon.* 69, 219-226.

Cai, W., Vosschulte, R., Afsah-Hedjri, A., Koltai, S., Kocsis, E., Scholz, D., Kostin, S., Schaper, W., Schaper, J., 2000. Altered balance between extracellular proteolysis and antiproteolysis is associated with adaptive coronary arteriogenesis. *J Mol Cell Cardiol.* 32, 997-1011.

Carpi, A., Menabo, R., Kaludercic, N., Pelicci, P., Di Lisa, F., Giorgio, M., 2009. The cardioprotective effects elicited by p66(Shc) ablation demonstrate the crucial role of mitochondrial ROS formation in ischemia/reperfusion injury. *Biochim Biophys Acta.* 1787, 774-780.

de Vries, H.E., Blom-Roosemalen, M.C.M., van Oosten, M., de Boer, A.G., van Berkel, T.J.C., Breimer, D.D., Kuiper, J., 1996. The influence of cytokines on the integrity of the blood-brain barrier in vitro. *J Neuroimmunol.* 64, 37-43.

Di Lisa, F., Carpi, A., Giorgio, V., Bernardi, P., 2011. The mitochondrial permeability transition pore and cyclophilin D in cardioprotection. *Biochim Biophys Acta.* 1813, 1316-1322.

Di Lisa, F., Kaludercic, N., Carpi, A., Menabo, R., Giorgio, M., 2009. Mitochondria and vascular pathology. *Pharmacol Rep.* 61, 123-130.

Donndorf, P., Kuhn, F., Vollmar, B., Rosner, J., Liebold, A., Gierer, P., Steinhoff, G., Kaminski, A., 2012. Comparing microvascular alterations during minimal extracorporeal circulation and conventional cardiopulmonary bypass in coronary artery bypass graft surgery: a prospective, randomized study. The J *Thorac Cardiovasc Surg.* 144, 677-683.

Ekström, K., Valadi, H., Sjöstrand, M., Malmhäll, C., Bossios, A., Eldh, M., Lötvall, J., 2012. Characterization of mRNA and microRNA in human mast cell-derived exosomes and their transfer to other mast cells and blood CD34 progenitor cells. *J Extracell Vesicles.* 1-12.

Fischer, S., Cabrera-Fuentes, H.A., Noll, T., Preissner, K.T., 2014. Impact of extracellular RNA on endothelial barrier function. Cell and tissue research.

Fischer, S., Gerriets, T., Wessels, C., Walberer, M., Kostin, S., Stolz, E., Zheleva, K., Hocke, A., Hippenstiel, S., Preissner, K.T., 2007. Extracellular RNA mediates endothelial-cell permeability via vascular endothelial growth factor. *Blood.* 110, 2457-2465.

Fischer, S., Gesierich, S., Griemert, B., Schanzer, A., Acker, T., Augustin, H.G., Olsson, A.K., Preissner, K.T., 2013. Extracellular RNA liberates tumor necrosis factor-alpha to promote tumor cell trafficking and progression. *Cancer Res.* 73, 5080-5089.

Fischer, S., Grantzow, T., Pagel, J.-I., Tschernatsch, M., Sperandio, M., Preissner, K.T., Deindl, E., 2012. Extracellular RNA promotes leukocyte recruitment in the vascular system by mobilizing proinflammatory cytokines. *Thromb Haemost.* 108, 730-741.

Fischer, S., Nishio, M., Dadkhahi, S., Gansler, J., Saffarzadeh, M., Shibamiyama, A., Kral, N., Baal, N., Koyama, T., Deindl, E., Preissner, K.T., 2011. Expression and localisation of vascular ribonucleases in endothelial cells. *Thromb Haemost.* 105, 345-355.

Fischer, S., Nishio, M., Peters, S.C., Tschernatsch, M., Walberer, M., Weidemann, S., Heidenreich, R., Couraud, P.O., Weksler, B.B., Romero, I.A., Gerriets, T., Preissner, K.T., 2009. Signaling mechanism of extracellular RNA in endothelial cells. *FASEB.* 23, 2100-2109.

Fischer, S., Preissner, K.T., 2013. Extracellular nucleic acids as novel alarm signals in the vascular system: Mediators of defence and disease. *Hämostaseologie.* 33, 1-6.

Frank, A., Bonney, M., Bonney, S., Weitzel, L., Koeppen, M., Eckle, T., 2012. Myocardial ischemia reperfusion injury: from basic science to clinical bedside. *Semin Cardiothorac Vasc Anesth.* 16, 123-132.

Frias, M.A., Pedretti, S., Hacking, D., Somers, S., Lacerda, L., Opie, L.H., James, R.W., Lecour, S., 2013. HDL protects against ischemia reperfusion injury by preserving mitochondrial integrity. *Atherosclerosis.* 228, 110-116.

Garcia-Dorado, D., Ruiz-Meana, M., Inserte, J., Rodriguez-Sinovas, A., Piper, H.M., 2012. Calcium-mediated cell death during myocardial reperfusion. *Cardiovasc Res.* 94, 168-180.

Gaur, D., Swaminathan, S., Batra, J.K., 2001. Interaction of human pancreatic ribonuclease with human ribonuclease inhibitor: generation of inhibitor-resistant cytotoxic variants. *J Biol Chem.* 276, 24978-24984.

Gedik, N., Heusch, G., Skyschally, A., 2013. Infarct size reduction by cyclosporine A at reperfusion involves inhibition of the mitochondrial permeability transition pore but does not improve mitochondrial respiration. *Arch Med Sci.* 9, 968-975.

Gilles, S., Zahler, S., Welsch, U., Sommerhoff, C.P., Becker, B.F., 2003. Release of TNF-alpha during myocardial reperfusion depends on oxidative stress and is prevented by mast cell stabilizers. *Cardiovasc Res.* 60, 608-616.

Grohe, C., van Eickels, M., Wenzel, S., Meyer, R., Degenhardt, H., Doevendans, P.A., Heinemann, M.P., Ross, G., Schluter, K.D., 2004. Sex-specific differences in ventricular expression and function of parathyroid hormone-related peptide. *Cardiovasc Res*. 61, 307-316.

Halestrap, A.P., 2006. Calcium, mitochondria and reperfusion injury: a pore way to die. *Biochem Soc Trans.* 34, 232-237.

Han, X., Kitamoto, S., Lian, Q., Boisvert, W.A., 2009. Interleukin-10 facilitates both cholesterol uptake and efflux in macrophages. *J Biol Chem.* 284, 32950-32958.

Han, X., Kitamoto, S., Wang, H., Boisvert, W.A., 2010. Interleukin-10 overexpression in macrophages suppresses atherosclerosis in hyperlipidemic mice. *FASEB*. 24, 2869-2880.

Hartman, J., Frishman, W.H., 2014. Inflammation and Atherosclerosis: A Review of the Role of Interleukin-6 in the Development of Atherosclerosis and the Potential for Targeted Drug Therapy. *Cardiology Rev.*

Hausenloy, D.J., Duchen, M.R., Yellon, D.M., 2003. Inhibiting mitochondrial permeability transition pore opening at reperfusion protects against ischaemia-reperfusion injury. *Cardiovasc Res.* 60, 617-625.

Hausenloy, D.J., Yellon, D.M., 2013. Myocardial ischemia-reperfusion injury: a neglected therapeutic target. The Journal of clinical investigation 123, 92-100.

Heusch, G., 2013. Cardioprotection: chances and challenges of its translation to the clinic. *Lancet*. 381, 166-175.

Inoue, T., Croce, K., Morooka, T., Sakuma, M., Node, K., Simon, D.I., 2011. Vascular inflammation and repair: implications for re-endothelialization, restenosis, and stent thrombosis. *JACC Cardiovasc Interv.* 4, 1057-1066.

Inserte, J., Barba, I., Hernando, V., Garcia-Dorado, D., 2009. Delayed recovery of intracellular acidosis during reperfusion prevents calpain activation and determines protection in postconditioned myocardium. *Cardiovasc Res.* 81, 116-122.

Inserte, J., Barba, I., Poncelas-Nozal, M., Hernando, V., Agullo, L., Ruiz-Meana, M., Garcia-Dorado, D., 2011. cGMP/PKG pathway mediates myocardial postconditioning protection in rat hearts by delaying normalization of intracellular acidosis during reperfusion. *J Mol Cell Cardiol.* 50, 903-909.

Javadov, S., Karmazyn, M., Escobales, N., 2009. Mitochondrial permeability transition pore opening as a promising therapeutic target in cardiac diseases. *J Pharmacol Exp Ther.* 330, 670-678.

Kannemeier, C., Shibamiya, A., Nakazawa, F., Trusheim, H., Ruppert, C., Markart, P., Song, Y., Tzima, E., Kennerknecht, E., Niepmann, M., von Bruehl, M.-L., Sedding, D., Massberg, S., Günther, A., Engelmann, B., Preissner, K.T., 2007. Extracellular RNA constitutes a natural procoagulant cofactor in blood coagulation. *Proc Natl Acad Sci U S A.* 104, 6388-6393.

Kleinbongard, P., Heusch, G., Schulz, R., 2010. TNFalpha in atherosclerosis, myocardial ischemia/reperfusion and heart failure. *Pharmacol Ther.* 127, 295-314.

Kleinbongard, P., Schulz, R., Heusch, G., 2011. TNFalpha in myocardial ischemia/reperfusion, remodeling and heart failure. *Heart Fail Rev.* 16, 49-69.

Kopreski, M.S., Benko, F.A., Gocke, C.D., 2001. Circulating RNA as a tumor marker: detection of 5T4 mRNA in breast and lung cancer patient serum. *Ann N Y Acad Sci.* 945, 172-178.

Kopreski, M.S., Benko, F.A., Kwak, L.W., Gocke, C.D., 1999. Detection of tumor messenger RNA in the serum of patients with malignant melanoma. *Clin Cancer Res.* 5, 1961-1965.

Ladilov, Y., Efe, O., Schafer, C., Rother, B., Kasseckert, S., Abdallah, Y., Meuter, K., Dieter Schluter, K., Piper, H.M., 2003. Reoxygenation-induced rigor-type contracture. *J Mol Cell Cardiol.* 35, 1481-1490.

Landre´, J.B.P., Hewett, P.W., Olivot, J.-M., Friedl, P., Y., L., Sachinidis, A., Moenner, M., 2002. Human endothelial cells selectively express large amounts of pancreatic-type ribonuclease (RNase 1). *J Cell Biochem.* 86, 540-552.

Lecour, S., Suleman, N., Deuchar, G.A., Somers, S., Lacerda, L., Huisamen, B., Opie, L.H., 2005. Pharmacological preconditioning with tumor necrosis factor-alpha activates signal transducer and activator of transcription-3 at reperfusion without involving classic prosurvival kinases (Akt and extracellular signal-regulated kinase). *Circulation.* 112, 3911-3918.

Liebold, A., Langhammer, T., Brunger, F., Birnbaum, D.E., 1999. Cardiac interleukin-6 release and myocardial recovery after aortic crossclamping. Crystalloid versus blood cardioplegia. *J Cardiovasc Surg.* 40, 633-636.

Liehn, E.A., Piccinini, A.M., Koenen, R.R., Soehnlein, O., Adage, T., Fatu, R., Curaj, A., Popescu, A., Zernecke, A., Kungl, A.J., Weber, C., 2010. A new monocyte chemotactic protein-1/chemokine CC motif ligand-2 competitor limiting neointima formation and myocardial ischemia/reperfusion injury in mice. *J Am Coll Cardiol.* 56, 1847-1857.

Lucerna, M., Zernecke, A., de Nooijer, R., de Jager, S.C., Bot, I., van der Lans, C., Kholova, I., Liehn, E.A., van Berkel, T.J., Yla-Herttuala, S., Weber, C., Biessen, E.A., 2007. Vascular endothelial growth factor-A induces plaque expansion in ApoE knock-out mice by promoting de novo leukocyte recruitment. *Blood.* 109, 122-129.

Mandel, P., Metais, P., 1947. Les acides nucleíques du plasma sangiun chez l'homme. C. R. Acad. Sci. 112, 16.

Marcus, B.C., Wyble, C.W., Hyner, K.L., Gewertz, B.L., 1996. Cytokine-induced increases in endothelial permeability occur after adhesion molecule expression. *Surgery.* 120, 411-416.

McErlean, E.S., Deluca, S.A., van Lente, F., Peacock, F.t., Rao, J.S., Balog, C.A., Nissen, S.E., 2000. Comparison of troponin T versus creatine kinase-MB in suspected acute coronary syndromes. *Am J Cardiol.* 85, 421-426.

Moenner, M., Hatzi, E., Bader, J., 1997. Secretion of ribonucleases by normal and immortalized cells grown in serum-free culture conditions. *In Vitro Cell Dev Biol Anim.* 33, 553-561.

Moore, K.J., Tabas, I., 2011. Macrophages in the pathogenesis of atherosclerosis. *Cell.* 145, 341-355.

Neu, C., Sedlag, A., Bayer, C., Forster, S., Crauwels, P., Niess, J.H., van Zandbergen, G., Frascaroli, G., Riedel, C.U., 2013. CD14-dependent monocyte isolation enhances phagocytosis of listeria monocytogenes by proinflammatory, GM-CSF-derived macrophages. *PloS One.* 8, e66898.

Ovize, M., Thibault, H., Przyklenk, K., 2013. Myocardial conditioning: opportunities for clinical translation. Circulation research 113, 439-450.

Piper, H.M., Garcia-Dorado, D., Ovize, M., 1998. A fresh look at reperfusion injury. *Cardiovasc Res.* 38, 291-300.

Rhee, S.H., Jones, B.W., Toshchakov, V., Vogel, S.N., Fenton, M.J., 2003. Toll-like receptors 2 and 4 activate STAT1 serine phosphorylation by distinct mechanisms in macrophages. *J Biol Chem.* 278, 22506-22512.

Rodrigo, R., Prieto, J.C., Castillo, R., 2013. Cardioprotection against ischaemia/reperfusion by vitamins C and E plus n-3 fatty acids: molecular mechanisms and potential clinical applications. *Clin Sci.* 124, 1-15.

Rodriguez-Sinovas, A., Abdallah, Y., Piper, H.M., Garcia-Dorado, D., 2007. Reperfusion injury as a therapeutic challenge in patients with acute myocardial infarction. *Heart Fail Rev.* 12, 207-216.

Rohman, M.S., Emoto, N., Takeshima, Y., Yokoyama, M., Matsuo, M., 2003. Decreased mAKAP, ryanodine receptor, and SERCA2a gene expression in mdx hearts. *Biochem Biophys Res Commun.* 310, 228-235.

Rose-John, S., 2013. ADAM17, shedding, TACE as therapeutic targets. *Pharmacol Res.* 71, 19-22.

Ruiz-Meana, M., Abellan, A., Miro-Casas, E., Garcia-Dorado, D., 2007. Opening of mitochondrial permeability transition pore induces hypercontracture in Ca^{2+} overloaded cardiac myocytes. *Basic Res Cardiol.* 102, 542-552.

Ruiz-Meana, M., Garcia-Dorado, D., Julia, M., Inserte, J., Siegmund, B., Ladilov, Y., Piper, M., Tritto, F.P., Gonzalez, M.A., Soler-Soler, J., 2000. Protective effect of HOE642, a selective blocker of Na^+-H^+ exchange, against the development of rigor contracture in rat ventricular myocytes. *Exp Physiol.* 85, 17-25.

Saffarzadeh, M., Juenemann, C., Queisser, M.A., Lochnit, G., Barreto, G., Galuska, S.P., Lohmeyer, J., Preissner, K.T., 2012. Neutrophil extracellular traps directly induce epithelial and endothelial cell death: a predominant role of histones. *PloS One.* 7, e32366.

Santos, E.S., Baltar, V.T., Pereira, M.P., Minuzzo, L., Timerman, A., Avezum, A., 2011. Comparison between cardiac troponin I and CK-MB mass in acute coronary syndrome without st elevation. *Arquiv Brasil Cardiol.* 96, 179-187.

Schafer, C., Ladilov, Y., Inserte, J., Schafer, M., Haffner, S., Garcia-Dorado, D., Piper, H.M., 2001. Role of the reverse mode of the Na^+/Ca^{2+} exchanger in reoxygenation-induced cardiomyocyte injury. *Cardiovasc Res.* 51, 241-250.

Schluter, K.D., Schreiber, D., 2005. Adult ventricular cardiomyocytes: isolation and culture. *Methods Mol Biol.* 290, 305-314.

Schneider, C.A., Rasband, W.S., Eliceiri, K.W., 2012. NIH Image to ImageJ: 25 years of image analysis. *Nat methods.* 9, 671-675.

Schober, A., Manka, D., von Hundelshausen, P., Huo, Y., Hanrath, P., Sarembock, I.J., Ley, K., Weber, C., 2002. Deposition of platelet RANTES triggering monocyte recruitment requires P-selectin and is involved in neointima formation after arterial injury. *Circulation.* 106, 1523-1529.

Sedgwick, J.B., Menon, I., Gern, J.E., Busse, W.W., 2002. Effects of inflammatory cytokines on the permeability of human lung microvascular endothelial cell monolayers and differential eosinophil transmigration. *J Allergy Clin Immunol.* 110, 752-756.

Simsekyilmaz, S., Cabrera-Fuentes, H.A., Meiler, S., Kostin, S., Baumer, Y., Liehn, E.A., Weber, C., Boisvert, W.A., Preissner, K.T., Zernecke, A., 2014. Role of extracellular RNA in atherosclerotic plaque formation in mice. *Circulation.* 129, 598-606.

Skyschally, A., Gres, P., Hoffmann, S., Haude, M., Erbel, R., Schulz, R., Heusch, G., 2007. Bidirectional role of tumor necrosis factor-alpha in coronary microembolization: progressive contractile dysfunction versus delayed protection against infarction. *Circ Res.* 100, 140-146.

Tan, E.M., Schur, P.H., Carr, R.I., Kunkel, H.G., 1966. Deoxybonucleic (DNA) and antibodies to DNA in the serum of patients with systemic lupus erythematosus. *J Clin Invest.* 45, 1732-1740.

Thielmann, M., Kottenberg, E., Kleinbongard, P., Wendt, D., Gedik, N., Pasa, S., Price, V., Tsagakis, K., Neuhauser, M., Peters, J., Jakob, H., Heusch, G., 2013. Cardioprotective and prognostic effects of remote ischaemic preconditioning in patients undergoing coronary artery bypass surgery: a single-centre randomised, double-blind, controlled trial. *Lancet.* 382, 597-604.

Tugal, D., Liao, X., Jain, M.K., 2013. Transcriptional control of macrophage polarization. *Arterioscler Thromb Vasc Biol.* 33, 1135-1144.

Vorderwinkler, K.P., Mair, J., Puschendorf, B., Hempel, A., Schluter, K.D., Piper, H.M., 1996. Cardiac troponin I increases in parallel to cardiac troponin T, creatine kinase and lactate dehydrogenase in effluents from isolated perfused rat hearts after hypoxia-reoxygenation-induced myocardial injury. *Clin Chim Acta.* 251, 113-117.

Wakui, S., Furusato, M., Tanaka, M., Allsbrook, W.C., Jr., Kano, Y., Ushigome, S., 1990. Endothelium and pericyte interdigitation: pathway for epidermal growth factor? *Microvasc Res.* 40, 285-291.

Walberer, M., Tschernatsch, M., Fischer, S., Ritschel, N., Volk, K., Friedrich, C., Bachmann, G., Mueller, C., Kaps, M., Nedelmann, M., Blaes, F., Preissner, K.T., Gerriets, T., 2009. RNase therapy assessed by magnetic resonance imaging reduces cerebral edema and infarction size in acute stroke. *Curr Neurovasc Res.* 6, 12-19.

Wan, S., DeSmet, J.M., Barvais, L., Goldstein, M., Vincent, J.L., LeClerc, J.L., 1996. Myocardium is a major source of proinflammatory cytokines in patients undergoing cardiopulmonary bypass. J Thorac Cardiovasc Surg 112, 806-811.

Wang, T., Town, T., Alexopoulou, L., Anderson, J.F., Fikrig, E., Flavell, R.A., 2004. Toll-like receptor 3 mediates west nile virus entry into the brain causing lethal encephalitis. *Nat Med.* 12, 1366-1373.

Weber, C., Aepfelbacher, M., Haag, H., Ziegler-Heitbrock, H.W., Weber, P.C., 1993. Tumor necrosis factor induces enhanced responses to platelet-activating factor and differentiation in human monocytic Mono Mac 6 cells. *Eur J Immunol.* 23, 852-859.

Weber, C., Noels, H., 2011. Atherosclerosis: current pathogenesis and therapeutic options. *Nat Med.* 17, 1410-1422.

Weber, C., Schober, A., Zernecke, A., 2010. MicroRNAs in arterial remodelling, inflammation and atherosclerosis. *Current Drug Targets.* 11, 950-956.

Wieczorek, A.J., Rhyner, C., Block, L.H., 1985a. Isolation and characterization of an RNA-proteolipid complex assiciated with the malignant state in humans. Proc Natl. Acad. Sci. U.S.A. 82, 3455-3459.

Writing Group, M., Lloyd-Jones, D., Adams, R.J., Brown, T.M., Carnethon, M., Dai, S., De Simone, G., Ferguson, T.B., Ford, E., Furie, K., Gillespie, C., Go, A., Greenlund, K., Haase, N., Hailpern, S., Ho, P.M., Howard, V., Kissela, B., Kittner, S., Lackland, D., Lisabeth, L., Marelli, A., McDermott, M.M., Meigs, J., Mozaffarian, D., Mussolino, M., Nichol, G., Roger, V.L., Rosamond, W., Sacco, R., Sorlie, P., Roger, V.L., Thom, T., Wasserthiel-Smoller, S., Wong, N.D., Wylie-Rosett, J., American Heart Association Statistics, C., Stroke Statistics, S., 2010. Heart disease and stroke statistics--2010 update: a report from the American Heart Association. *Circulation.* 121, e46-e215.

Yellon, D.M., Hausenloy, D.J., 2007. Myocardial reperfusion injury. *New Engl J Med.* 357, 1121-1135.

Zhao, Q., Shao, L., Hu, X., Wu, G., Du, J., Xia, J., Qiu, H., 2013. Lipoxin a4 preconditioning and postconditioning protect myocardial ischemia/reperfusion injury in rats. *Mediators Inflamm.* 2013, 231351.

7. Declaration

I declare that I have completed this dissertation single-handedly without the unauthorized help of a second party and only with the assistance acknowledged therein. I have appropriately acknowledged and referenced all text passages that are derived literally from or are based on the content of published or unpublished work of others, and all information that relates to verbal communications. I have abided by the principles of good scientific conduct laid down in the charter of the Justus Liebig University of Giessen in carrying out the investigations described in the dissertation.

Der Lebenslauf wurde aus der elektronischen Version der Arbeit entfernt.

The curriculum vitae was removed from the electronic version of the paper.

Publications	***Published*** 1) Simsekyilmaz S[#], **Cabrera-Fuentes HA[#],** Meiler S, Kostin S, Baumer Y, Liehn EA, Weber C, Boisvert WA, Preissner KT, Zernecke A. The Role of Extracellular RNA in Atherosclerotic Plaque Formation in Mice. ***Circulation.*** 2014;129:598-606. [#]**Joint First Author.** *IF-15.2* 2) Saffarzadeh M, **Cabrera-Fuentes HA**, Veit F, Jiang D, Scharffetter-Kochanek K, Gille C, Rooijakkers SHM, Hartl D, Preissner KT. Characterization of rapid neutrophil extracellular trap formation and its cooperation with phagocytosis in human neutrophils. ***Discoveries.*** 2014;2(2):e19. DOI:10.15190/d.2014.11 3) Fischer S, **Cabrera-Fuentes HA,** Noll T, Preissner KT. Impact of Extracellular RNA on Endothelial Barrier Function. ***Review. Cell Tissue Res*** – 2014; 255:635-645. *IF-3.6*

Publications	4) Singh I, Metha A, Contreras A, Carraro G, Wheeler M, **Cabrera-Fuentes HA**, Bellusci S, Seeger W, Braun T, Barreto G. Hmga2 is required for canonical WNT signaling during lung development. ***BMC Biology*** – 2014; 12:21. *IF- 6.53* 5) Sanchez-Vega JT[#], **Cabrera-Fuentes HA[#,*],** Romero-Olmedo AJ, Ortiz-Frias JL, Sokolina F, Barreto G.[*] Cyclospora cayetanensis: This emerging protozoan pathogen in Mexico. ***Am J Trop Med Hyg.*** 2014; 90(2):351-353. [#]Joint first author and *Corresponding author. *IF-2.5* 6) Mukhametshina RT, Ruhs A, Singh I, Hasan D, Contreras A, Mehta A, Nikam VS, Ahlbrecht K, Carraro G, **Cabrera-Fuentes HA**, Jiang D, Voswinckel R, Seeger W, Bellusci S, Scharffetter-Kochanek K, Bagaeva TV, Preissner KT, Boettger T, Braun T, Kruger M, Barreto G. 2013. Quantitative proteome analysis of alveolar type II cells revealed a connection of integrin receptor subunits beta 2/6 and WNT signaling. ***J Proteome Res.*** 2013; 12: 5598-5608. *IF-5.0* 7) Ruiz-Rosado A, **Cabrera-Fuentes HA,** Gonzalez-Calixto C, Gonzalez-Lopez L, Cazares-Raga FE, Segura-Alegria B, Lochnit G, de la Cruz Hernandez-Hernandez F, Preissner KT, Jimenez-Estrada I. Influence of chronic food deprivation on structure-function relationship of juvenile rat fast muscles. ***J Muscle Res Cell Motil.*** 2013;34:357-368. *IF-1.8* 8) **Cabrera-Fuentes HA*,** Aslam M, Saffarzadeh M., Kolpakov A, Zelenikhin P, Preissner KT, Ilinskaya ON. Internalization of Bacillus intermedius ribonuclease (BINASE) induces human alveolar adenocarcinoma cell death. ***Toxicon.*** 2013;69:219-226. *Corresponding author. *IF-2.9* 9) **Cabrera-Fuentes HA,** Mukhametshina RT, Zelenikhin PV, Kolpakov AI, Barreto G., Preissner KT, Ilinskaya ON. Binase penetration into alveolar epithelial cells does not induce cell death. Biomed Khim. 2012;58:272-80. [Article in Russian] 10) **Cabrera-Fuentes HA,** Zelenikhin PV, Kolpakov AI, Preissner KT, Ilinskaya ON. Comparative toxicity of Binase towards tumor and normal cells. **Toxicon.** 2012;60:104-109. *IF-2.9* 11) **Cabrera-Fuentes HA,** Fischer S, Schluter KD, Preissner KT. Biphasic extracellular RNA released during cardiac reperfusion Injury. ***J Muscle Res Cell Motil.*** 2012;32:327–333. ***IF-1.8***

Publications	12) **Cabrera-Fuentes H.A.,** Zelenikhin, P.V., Kolpakov, A.I., Ilinskaya, O.N. Antitumor RNase (binase) induces the alteration of cellular permeability. Cellular Transplantation and Tissue Engineering. 2012; 7(3):72 - 76 ***Accepted*** 13) Thrombin selectively induces transcription of genes involved in inflammation and wound healing in human monocytes. Lopéz ML, Deglesne PA, Alvarado-Castillo C, Bruges G, Crespo G, Salazar V, Schneider H, **Cabrera-Fuentes HA,** Schmitz ML, Preissner KT. ***Tromb Haemost*** ***In Revision*** 14) **Cabrera-Fuentes HA,** Ruiz-Meana M, Simsekyilmaz S, Kostin S, Inserte J, Saffarzadeh M, Vijayan V, Barba I, Pedretti S, Barreto G, Adam T, Fischer S, Lochnit G, Ilinskaya ON, Galuska SP, Baumgart-Vogt E, Boening A, Lecour S, Hausenloy DJ, Liehn EA, Garcia-Dorado D, Schluter KD, Preissner KT. The Damaging Interplay Between Extracellular RNA and Tumor-Necrosis-Factor-α Triggers Cardiac Ischemia/Reperfusion Injury: Prevention of Cardiomyocyte Death and Heart Failure by RNase1. ***Science Translational Medicine.*** 15) **Cabrera-Fuentes HA,** Meiler S, Baumer Y, Fischer S, Galuska S, Preissner KT, Boisvert WA. Regulation of Macrophage Polarization by Extracellular RNA: the Role of Sialoadhesin-1. ***Tromb Haemost*** 16) Weber P, Schreckenberg R, **Cabrera-Fuentes HA**, Preissner KT, Ferdinandy P, Czabor P, Schulz R, Schlüter KD. Mechanism and consequences of the cardiac shift in arginine metabolism following ischemia and reperfusion in rats. ***Tromb Haemost*** ***Submitted*** ***17)*** Zimmermann B, Köppert S, Fischer S, **Cabrera-Fuentes HA**, Lefèvre S, Rickert M, Steinmeyer J, Rehart S, Umscheid T, Schönburg S, Müller-Ladner U, Preissner KT, Neumann E. Inflammatory functions of extracellular RNA together with synovial fibroblasts in rheumatoid arthritis. ***J Exp Med.*** 18) *Bacillus intermedius* ribonuclease (BINASE) induces apoptosis in human ovarian cancer cells. Garipov AR, Nesmelov AA, Cabrera-Fuentes HA*, Ilinskaya ON. ***Molecular Oncology.*** *Corresponding author.

Presentations	Talk – March 2014 The damaging nature of extracellular RNA in aterosclerosis DIaMICOM Network Spring School 2014 Heidelberg, Germany Invited Speaker – March 2014 The Hatter Cardiovascular Institute - Lecture Series The Damaging Nature of Extracellular RNA in Atherosclerosis and Cardiovascular Disease UCL Division of Medicine London, UK Invited speaker – February 2014 The Damaging Interplay between Extracellular RNA and Tumor-Necrosis-Factor-α Triggers Cardiac Ischemia/Reperfusion Injury: Prevention of Cardiomyocyte Death and Heart Failure by RNase1 Research Institute Princesa (IP), Research Unit, Hospital of Santa Cristina Madrid, Spain Talk – March 2013 Young Investigator Award The role of the sialic acid-dependent membrane receptor sialoadhesin in cellular inflammation: the contribution of extracellular-RNA Deutsche Gesellschaft für Arteriosklerosеforschung e.V. Talk – February 2013 Induction of ischemia-reperfusion injury by extracellular RNA: a case for tumor necrosis factor (TNF-α) – shedding 57th Annual Congress of Gesellschaft für Thrombose- und Hämostaseforschung (GTH) Poster – August 2012 RNase1 protects against cardiac ischemia/reperfusion injury European Society of Cardiology Congress 2012 – Munich, Germany ***Poster Award*** Talk – August 2012 Extracellular RNA during cardiac ischemia/reperfusion injury Hatter Cardiovascular Institute, University of Cape Town, South Africa, Workshop UK-SA Talk – July 2012 Comparative toxicity of binase towards tumor and normal cells 17th World Congress for the Society on Toxinology Honolulu Hawaii, USA

Presentations	Talk – June 2012 RNase1 Protects Against Cardiac Ischemia/Reperfusion Injury The International Vascular Biology Meeting (IVBM) 2012 Wiesbaden, Germany Talk – September 2011 Biphasic Extracellular RNA Released During Cardiac Reperfusion Injury 40th European Muscle Conference of the European Society for Muscle Research Berllin, Germany Poster- June 2011 Extracellular RNA and RNase1 durig cardiac ischemia/reperfusion injury Symposium of the Excellence Cluster Cardio-Pulmonary System Max-Planck-Institute (MPI) for Heart and Lung Research Bad Nauheim, Germany Talk- December 2010 The role of RNA/RNase system in heart ischemia-reperfusion injury ”Protecting the Heart from Ischemia” – PROMISE retreat Hospital Universitari Vall d'Hebron Barcelona, Spain

9. Acknowledgments

Having come all the way out here, I would like to thank all the following who have made me work stronger whilst writing this thesis, and those who put their trust in me so that I could achieve this rewarding goal.

I would like to express my deep appreciation to my supervisor ***Prof. Dr. Klaus T. Preissner*** who gave me the opportunity to perform my PhD in his laboratory. When I came to Giessen, I was a microbiologist … with an ever so micro knowledge of biology, pipetting and absolutely no experience in working with cardiovascular biology. Thank you, not only for your trust, but also for your friendship, patience and creating a welcoming atmosphere. From you, I learned how to work independently, be flexible and find alternative ways to reach the goals.

Thank you for your support, your constructive criticisms as well as your new ideas.

GRACIAS!!!! СПАСИБО!!! MAHALO!!!

Выражаю благодарность профессору О.Н. Ильинской за консультации и обсуждение моей научной работы.

Moreover, I would like to sincerely thank Prof. Dr. Klaus D. Schlueter who supported, and helped me to perform them in his laboratory. Special thanks too to Herr Peter Volk for his gracious assistance with the many animal experiments.

Sinceramente quiero agradecer enormemente al Prof. Dr. William Boisvert, que me permitió formar parte de su grupo de trabajo en la Universidad de Hawaii, y quien aparte de ser un científico ejemplar, personalmente, se convirtió en una persona muy querida, estimada y principalmente en un gran amigo.

Additionally, I am extremely grateful to all the outstanding scientists that allowed me to learn the techniques, the well-established methods, and the ways of performing my experiments; all of which has led me to this point in my life. I particularly want thank to Dr. Sawa Kostin, Dr. Guillermo Barreto, Prof. Dr. Eveline Baumgart-Vogt, Prof. Dr. Andreas Böning, Prof. Dr. Sandrine Lecour, Dr. Derek J. Hausenloy, Dr. Elisa A. Liehn and Prof. Dr. David Garcia-Dorado, and their working groups.

I am deeply grateful for the help and support of Dr. Mona Saffarzadeh, Dr. Silvia Fischer, Dr. Julia Gansler, Dr. Barbara Griemert, Bärbel Fühler, and Uwe Schubert (most especially at the beginning of my PhD). Thanks for your teaching, ideas, and your constant support.

It is a pleasure to thank my very good friend Mareike Kahl, not only for her constant friendship, but also for suggestions and comments, which have been of great value to me.

I thank Prof. Dr. Günter Lochnit, Dr. Sebastian Galuska, Dr. Laureano de la Vega for their collaboration, and also answering my questions always patiently, which I'm sure was a lot to ask for at times!

Furthermore, I owe my deepest gratitude to the all lab members: Ute Neibergall for her kind assistance since the beginning. I would also thank Jessica Schneider, Susanne Tannert-Otto and Thomas Schmidt-Wöll and other members of the lab who provide a friendly atmosphere in the lab, their friendship and their assistance.

I would like to thank the International Graduate School PROMISE "IRTG-1566, Giessen-Barcelona" for funding my work in Giessen and also giving me the opportunity to attend at the international conferences. Lastly,

I cannot skip my sincere thanks to Pia Jugens and Mary Kromeier, without their help, I would go crazy with the administrative procedures in Germany.

Gracias a Dios y mi amada familia; a mi muy querido Padre Héctor Cabrera Guzmán, mi amada Madre Lucila Fuentes Cruz, a mis hermanos Nancy Guie Niza y Alexis que por años me han dado valor, respaldado mis decisiones y acompañado en todo momento, gracias por todo, los amo.

Une spécial remerciement à Nicole y Claude Vouin, parce ils me sont toujours supporte, aime et confie en moi depuis qu'on s avait connu. Je vous aime comme si vous étaient mes vrai parents, avec tout mon cœur.

Siempre hay una luz al final del camino, y la oportunidad de alcanzarla, ha llegado!!!

édition scientifique
VVB LAUFERSWEILER VERLAG

VVB LAUFERSWEILER VERLAG
STAUFENBERGRING 15
D-35396 GIESSEN

Tel: 0641-5599888 Fax: -5599890
redaktion@doktorverlag.de
www.doktorverlag.de

ISBN: 978-3-8359-6202-6

R

Photo cover: © graphicsdunia4you - istockphoto.com